TRANSPORTATION RESEARCH RECORD 755

Evaluation and Analysis of Flexible Pavement Components and Properties

TRANSPORTATION RESEARCH BOARD

COMMISSION ON SOCIOTECHNICAL SYSTEMS
NATIONAL RESEARCH COUNCIL

NATIONAL ACADEMY OF SCIENCES
WASHINGTON, D.C. 1980

Transportation Research Record 755
Price $4.20
Edited for TRB by Naomi Kassabian

modes
1 highway transportation
4 air transportation

subject area
24 pavement design and performance

Library of Congress Cataloging in Publication Data

National Research Council. Transportation Research Board.
Evaluation and analysis of flexible pavement components and properties.

(Transportation research record; 755)
Reports prepared for the 59th annual meeting of the Transportation Research Board.
1. Pavements, Flexible–Testing–Addresses, essays, lectures. 2. Road materials–Testing–Addresses, essays, lectures. I. Title. II. Series.
TE7.H5 no. 755 [TE250] 625.8'028'7 80-26335
ISBN 0-309-03068-4 ISSN 0361-1981

Sponsorship of the Papers in This Transportation Research Record

GROUP 2–DESIGN AND CONSTRUCTION OF TRANSPORTATION FACILITIES
R. V. LeClerc, Washington State Department of Transportation, chairman

Pavement Design Section
W. Ronald Hudson, University of Texas at Austin, chairman

Committee on Flexible Pavement Design
R. G. Hicks, Oregon State University, chairman
Leon M. Noel, Federal Highway Administration, secretary
Ernest J. Barenberg, Robert A. Crawford, R. N. Doty, W. B. Drake, Fred N. Finn, Wade L. Gramling, William Bryan Greene, R. V. LeClerc, J. W. Lyon, Jr., Frank P. Nichols, Jr., Adrian Pelzner, Dale E. Peterson, William A. Phang, Carl L. Schulten, James A. Sherwood, James F. Shook, Eugene L. Skok, Jr., William T. Stapler, Harvey J. Treybig, Harry H. Ulery, Jr., Loren M. Womack, Richard J. Worch

Committee on Pavement Condition Evaluation
K. H. McGhee, Virginia Highway and Transportation Research Council, chairman
Michael I. Darter, Edwin J. Dudka, Karl H. Dunn, Asif Faiz, Wouter Gulden, Lawrence E. Hart, William H. Highter, W. Ronald Hudson, L. B. R. Hunter, Don H. Kobi, Scott A. Kutz, J. W. Lyon, Jr., Robert L. Novak, R. D. Pavlovich, William A. Phang, Bayard E. Quinn, Freddy L. Roberts Albert F. Sanborn III, Lawrence L. Smith, Paul N. Sonnenburg, Herbert F. Southgate, Elson B. Spangler, Shiraz D. Tayabji, Robert J. Weaver, Loren M. Womack

Committee on Theory of Pavement Systems
Ralph C. G. Haas, University of Waterloo, chairman
G. H. Argue, Yu T. Chou, Santiago Corro Caballero, Michael I. Darter, Paul J. Diethelm, David C. Esch, Fred N. Finn, Per E. Fossberg, W. Ronald Hudson, Lynne H. Irwin, Ali S. Kemahli, William J. Kenis, Ramesh Kher, Robert L. Lytton, Carl L. Monismith, Leon M. Noel, Robert G. Packard, Dale E. Peterson, James F. Shook, William T. Stapler, Ronald L. Terrel, Kornelis Wester

Committee on Strength and Deformation Characteristics of Pavement Sections
Amir N. Hanna, Portland Cement Association, chairman
Richard D. Barksdale, Stephen F. Brown, Gaylord Cumberledge, Jim W. Hall, Jr., R. G. Hicks, Ignat V. Kalcheff, William J. Kenis, Thomas W. Kennedy, Erland Lukanen, Kamran Majidzadeh, Lutfi Raad, J. Brent Rauhut, Quentin L. Robnett, Jatinder Sharma, Gary Wayne Sharpe, James F. Shook, Eugene L. Skok, Jr., T. C. Paul Teng

Lawrence F. Spaine, Transportation Research Board staff

Sponsorship is indicated by a footnote at the end of each report. The organizational units, officers, and members are as of December 31, 1979.

Contents

Authors of the Papers in This Record

Ali, Galal A., Faculty of Engineering, University of Riyadh, Riyadh, Saudi Arabia
Brown, S.F., University of Nottingham, Nottingham NG7 2RD, England
Cowe Falls, Lynne G., Alberta Transportation, Airdrie, Alberta, Canada; formerly with University of Waterloo
D'Amato, Paul A., Ackenheil and Associates, Baltimore, MD 21233; formerly with Department of Civil Engineering, University of Maryland
Goetz, W.H., Department of Civil Engineering, Purdue University, West Lafayette, IN 47901
Gramling, W.L., Pennsylvania Department of Transportation, 1118 State Street, Harrisburg, PA 17120
Haas, Ralph, Department of Civil Engineering, University of Waterloo, Waterloo, Ontario N2L 3G1, Canada
Harr, M.E., Department of Civil Engineering, Purdue University, West Lafayette, IN 47901
Kennedy, Thomas W., Department of Civil Engineering, University of Texas at Austin, Austin, TX 78746
Raad, Lutfi, Department of Civil Engineering, University of Illinois at Urbana-Champaign, Urbana, IL 61801
Roberts, Freddy L., Austin Research Engineers, Inc., 2600 Dellana Lane, Austin, TX 78746
Sharma, Jatinder, Dynatest Consulting, P.O. Box 71, Ojai, CA 93023; formerly with Florida Department of Transportation
Stock, A.F., Department of Civil Engineering, University of Dundee, Dundee DD1 4HN, Scotland
Stubstad, R.N., Dynatest Consulting, P.O. Box 71, Ojai, CA 93023
Wang, M.C., Pennsylvania Transportation Institute, Department of Civil Engineering, Pennsylvania State University, University Park, PA 16802
Witczak, M.W., Department of Civil Engineering, University of Maryland, College Park, MD 20742

Material Properties of Zero-Maintenance Flexible Pavement

FREDDY L. ROBERTS AND THOMAS W. KENNEDY

This study involved models selected as suitable for the prediction of important distresses that have occurred historically in flexible pavements and the determination of material properties that will provide 20 years of satisfactory performance without maintenance and an additional 10-20 years of satisfactory performance with normal maintenance. To accomplish the overall objective, results were used from a previous study that identified the most important distresses occurring in flexible pavements, identified the material properties that affect those distresses, and selected mathematical models to predict those distresses by using the identified material properties. This paper presents the range of values selected for each of the material properties and discusses the distresses predicted by using the selected mathematical models. The distresses selected for study included fatigue cracking, rutting, and low-temperature cracking. The mathematical models selected for the analysis were VESYS for modeling fatigue cracking and rutting and the Shahin-McCullough model for low-temperature cracking. Input values were selected for each of these models, and ranges of the material properties affecting distress were established. The results for each study have been included and discussed, and practical criteria have been cited to evaluate the level of material properties required to provide zero-maintenance performance. The effects of each set of material properties used are identified, and the trade-offs of the effects of material properties on the distresses are discussed.

The Federal Highway Administration (FHWA) has for several years pursued multiple research studies aimed at producing premium pavement structures for heavily traveled highways. The objectives of these various efforts have been to develop pavement-design methodologies and to establish ranges of material properties for pavements so that they will be maintenance free for 20 years and require only routine maintenance for 10-20 years thereafter.

The research reported here had as its goal the identification of material properties that would provide optimal performance in flexible, rigid, and composite premium or zero-maintenance pavements. The portions of the project to be discussed include

1. Review of the analytical models capable of modeling distresses in flexible pavements that were selected to evaluate the effect of material properties on the production of distress,
2. Establishment of ranges of material properties and evaluation of the effects of the material properties on production of distress, and
3. Development of ranges of properties that are most suited to the production of zero-maintenance pavements.

The material properties identified as important in the study of flexible-pavement distress are discussed here and have been reported elsewhere (1).

MODEL SELECTION AND DESCRIPTION

A complete literature survey was conducted to review all analytical models available to predict pavement distress. The models reviewed included those based on linear elasticity, finite-element theory, and elastic-layer theory. These various models were classified and compared with the final model selected (1) for capability of predicting distress. The models used in the study of flexible-pavement distress were VESYS (2,3) for fatigue and rutting and the Shahin-McCullough model (4,5) for low-temperature cracking.

MODEL INPUTS

The models selected for the distress studies outlined above require the development of input values for each variable that occurs in each model. Several categories of input variable are discussed.

Common Inputs

Several categories of factors are common to all pavements and models and are independent of the pavement material properties themselves: the environment in which the pavement occurs, the traffic level to which the pavement is subjected, and the thickness of the pavement layers. Other input factors are dependent on the model used and the pavement type.

Four zones were selected as representative of the United States and are designated wet—freeze, dry—freeze, wet--no-freeze, and dry—no-freeze.

Previously reported traffic data (1,6,7) indicated that most flexible pavements sustain less than 500 000 18-kip (80-kN) equivalent single-axle loads (ESALs) per year. However, to ensure an adequate level of traffic, a design value of 1 million 18-kip ESALs was selected. Initial thicknesses for the flexible-pavement studies were developed by using SAMP6, a computer design procedure based on the procedures of the American Association of State Highway and Transportation Officials (AASHTO) (8). Inputs for SAMP6 were developed by using the traffic and environmental data associated with each zone, available structural and soil data, and 1977 material costs.

Since fatigue cracking, the most prevalent cause of failure in flexible pavements, is not considered directly by SAMP6, an elastic-layer analysis using ELSYM5 was conducted by using the initial layer thicknesses and fatigue relationships developed by Austin Research Engineers (9) and by Finn (10). This analysis indicated that only deep-strength or full-depth asphalt-concrete pavement could be expected to survive the 20 million 18-kip ESALs without fatigue damage.

By using the cost-optimization information based on serviceability, SAMP6, and these fatigue relationships, the minimum cross sections at thicknesses selected for the study of flexible pavements were 13 in (330 mm) of asphalt concrete and 8 in (203 mm) of asphalt-stabilized granular base. The base served primarily as a drainage layer and thus was open graded and asphalt treated for waterproofing, which minimized changes in modulus between seasons and provided constant support to the surface layer.

For the fatigue analysis, additional surface thickness combinations of 18, 16, and 10 in (457, 406, and 254 mm) over an 8-in base were selected.

The basic properties required for the analysis of flexible pavements were fatigue constants, stiffness, permanent deformation characteristics, and low-temperature cracking factors. Values selected for each are discussed below. VESYS IIIA was used for the first three properties; the Shahin-McCullough model was used to study low-temperature cracking.

Material Properties: VESYS IIIA Model

Fatigue Constants

By using information from various reports (11-15), we performed a regression analysis to determine the nature of and correlation coefficients for a relationship between material constants K_1 and K_2 (11). An excellent correlation coefficient and standard error were obtained for

K_2 as a function of K_1 as given below:

$$K_2 = 1.350 - 0.252 \log K_1 \quad (R = 0.95, SE = 0.29) \quad (1)$$

Since the values of K_1 and K_2 vary with temperature, they were modified to reflect the temperature range of each environmental zone by using the techniques presented by Rauhut, O'Quin, and Hudson (2).

Values of K_1 at temperatures other than 70°F (21°C), designated K_1 (T), were obtained by multiplying K_1 (70°F) by a normalizing value for temperature T (2).

Selected values for K_1 spanned the range of reported values, and K_2 was computed by using the equation developed earlier (11). Below are values of the K_1 and K_2 at 70°F selected for the parameter study.

Fatigue Constant	Values Selected			
log K_1	-5	-10	-15	-20
K_2	2.61	3.87	5.13	6.39

The seasonal temperatures for each environmental zone are shown below [t°F = (t°C ÷ 0.55) + 32]:

	Environmental-Zone Temperature (°F)			
Season	Wet--Freeze	Dry--Freeze	Wet--No-Freeze	Dry--No-Freeze
Winter	35	35	75	55
Spring	65	60	95	75
Summer	95	90	105	95
Fall	60	50	95	75

Stiffness

The multipliers used to establish the asphalt-concrete stiffness at each seasonal temperature were developed primarily by using results from the Asphalt Institute (16) and were checked with results from a study by Hudson and Kennedy (17). These data were plotted, and multipliers were selected for each seasonal temperature that was used in this analysis.

Permanent Deformation Parameters

The procedures for calculating permanent deformations at the pavement surface that were used in VESYS IIIA and the derivation of the terms ALPHA and GNU are discussed in detail elsewhere (2). The findings of the more-extensive testing programs conducted to evaluate ALPHA and GNU are also reported elsewhere (2,6,18). ALPHA and GNU are defined by the intercept and slope of the relationship between the logarithm of permanent strain and the logarithm of the number of load applications. ALPHA values that range from 0.7 to 0.9 and GNU values that range from 0.2 to 1.4 were selected by using previous recommendations (2).

The effects of variations in the permanent deformation characteristics of the base and subgrade materials were eliminated by using constant values for ALPHA and GNU of 0.92 and 0.25 for the base and 0.90 and 0.15 for the subgrade, respectively.

Stochastic Parameters

Because of the very heavy traffic and low mileage of zero-maintenance pavements, extraordinarily high quality control of construction was believed to be necessary. The quality-control level selected closely matched that exercised during the construction of the AASHO Road Test pavements. Rauhut has discussed the AASHO Road Test quality control and has presented typical values for the coefficients of variation for the various parameters of strength, stiffness, and permanent deformation (2). The following values were selected to be compatible with the objectives of providing zero-maintenance pavements:

Variable	Description	Input Value
VARCOEF	Coefficient of variation (Cv) in material properties for	
	Surface	0.10
	Base	0.15
	Subgrade	0.15
$COEFK_1$	Cv in K_1	0.20
$COEFK_2$	Cv in K_2	0.04
K_1K_2CORL	Correlation coefficient between K_1 and K_2	-0.9

Material Properties: Shahin-McCullough Model

The asphalt-concrete material properties required for analysis of low-temperature cracking are given below [t°F = (t°C ÷ 0.55) + 32; 1 psi = 6.89 kPa]:

Material Property	Level Low	Level High
Original penetration at 100 g, 5 s, 77°F (mm)	120	50
Original softening point (°F)	115	125
Penetration after thin-film oven test (%)	67	70
Specific gravity	1.040	1.015
Maximum tensile strength (psi)	300	600
Thermal coefficient (x10^{-6}/°F)	11	17

Required material properties include stiffness, tensile strength, and thermal coefficient. The range of stiffness for the parameter study was determined from typical properties for AC-40 and AC-10 asphalt cements. To ensure a proper comparison of cracking and stiffness, the material properties for an asphalt cement that were used to calculate the stiffness were made comparable in terms of temperature susceptibility by producing similar penetration indices. These material properties were established by using previously determined information (19-26).

The values shown above for tensile strength represent the maximum that was expected to occur at a bitumen stiffness of approximately 10 000 psi (68 948 kPa). A range in tensile strength from 300 to 600 psi (2068 to 4136 kPa) was selected for this study. The range in thermal coefficients was derived from Simpson, Griffin, and Miles (22). The values for the thermal coefficient of asphalt concrete were held constant for this analysis even though they do vary with temperature.

Climatological data from selected cities in each environmental zone were used to develop a composite set of data representative of each zone (27). The annual air-temperature range was developed so that the lowest calculated air temperature over the analysis period was approximately the lowest 20-year extreme. The input variables that varied between the zones were from a recent report (28).

DISCUSSION OF RESULTS

Fatigue Cracking

A typical relationship between the percentage of fatigue cracking and time for the wet—freeze environmental zone is shown in Figure 1. The fatigue cracking is the predicted cumulative damage for each season of each year accumulated by using the summation-of-cycle ratios. Since the traffic was assumed to be uniform at 1 million 18-kip ESALs per year, time was used on the abscissa. These

relationships show the percentage of cracking for each K_1, K_2, and thickness combination. Only values for K_1 are shown, since K_2 is a function of K_1. It is quite apparent that surface thickness is the dominant factor that influences fatigue cracking. Until the total thickness exceeded some critical value, a 20-year fatigue life could not be obtained by varying K_1 and K_2 within the range of values reported for currently available materials. For the lowest log K_1 value, which produces the longest value of fatigue life, the 13-in (305-mm) pavement experienced fatigue cracking exceeding tolerable levels in all environmental zones within 5-13 years. No set of material properties investigated met the zero-maintenance criteria for a surface thickness of 13 in over an 8-in (203-mm) base (Table 1).

As the pavement thickness was increased from 13 in to 16 in (406 mm) and 18 in (457 mm), the asphalt concrete began to perform in a manner that would satisfy zero-maintenance requirements. At a log K_1 of -10 for the 18-in surface, the fatigue cracking for all environmental zones was at an acceptable level after 20 years. However, it should be noted that, once fatigue cracking was initiated, only a few years at this very high traffic rate were required for the fatigue cracking to advance to an unacceptable level. It can be seen that zero-maintenance fatigue life could not be obtained solely by increasing the fatigue properties over a range consistent with currently available materials. Only when thicknesses were increased was it possible for several levels of fatigue properties to provide zero-maintenance service.

The development of fatigue cracking occurred in a similar pattern for the wet--freeze, dry--freeze, and dry--no-freeze zones. However, in the wet--no-freeze zone the time required to develop an unacceptable level of class 3 and class 4 fatigue cracking was substantially longer than it was for the other zones. This was attributed to the interaction of the strain-stiffness-fatigue relationship produced by the higher seasonal temperatures and the smaller temperature range between seasons for the wet—no-freeze zone. It should also be noted that the fatigue-life relationships are more closely spaced for the wet--no-freeze zone than for any of the other zones, which indicates that in higher-temperature zones the difference between the fatigue constants is not nearly so important as it is in the lower-temperature zones in which the range of stiffnesses during a year was larger.

Table 1 shows the fatigue life for the wet—freeze zone as a function of one of the accepted fatigue-cracking criteria. The fatigue properties significantly affected the time required to produce 5 percent fatigue cracking, but the more significant effect of thickness is evident. As can be seen in Table 1, the increase in time that was required in the wet--freeze zone to develop unacceptable cracking increased by 460 percent when log K_1 changed from -10 to -20; however, the increase in time produced by increasing the thickness from 13 in to 18 in was 960 percent when log K_1 equaled -10. Similar effects were also observed for the dry--freeze and the dry--no-freeze zones. For the wet—no-freeze zone the effect of thickness was even more dramatic than for the other zones; an increase in thickness for 13 in to either 16 in or 18 in resulted in essentially no class 3 and class 4 fatigue cracking and thus satisfied the zero-maintenance requirements.

For the 18-in pavement, a material with log K_1 less than -10 would meet the requirement for no maintenance during the first 20 years. However, to ensure that the fatigue cracking was not a problem for 25 years or more, a log K_1 equal to or less than -15 is suggested for a surface thickness of 18 in.

In developing criteria for selection of thickness requirements for zero maintenance, the engineer must evaluate the costs and uncertainties associated with the more-stringent material-property requirements as compared with the cost and uncertainty of obtaining a thicker layer and the less-stringent material-property requirements for the thicker layer. These evaluations must be performed for each proposed zero-maintenance project.

Figure 1. Fatigue in flexible pavements for various K_1, K_2 combinations and surface thicknesses: wet—freeze zone.

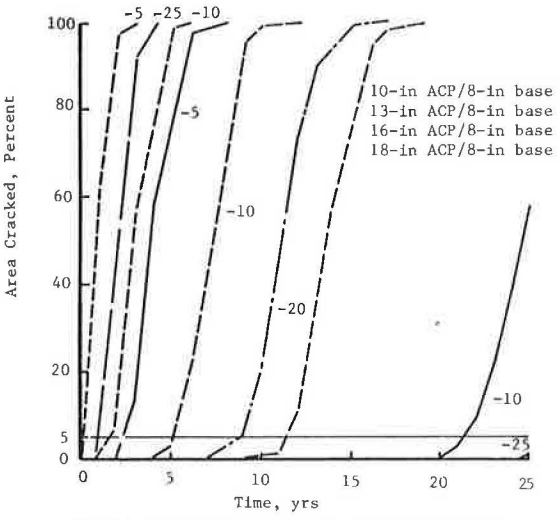

Note: No cracks for log K_1 = -15 and -20 for 16- and 18-in ACP over 8-in base.

Rutting

A typical relationship between cumulative permanent deformation and time for the wet—no-freeze zone and an ALPHA of 0.7 is shown in Figure 2. The relationships for the other environmental zones were similar, and summary information taken from those relationships was included in subsequent analyses.

To establish a limit for rutting, safety considerations have frequently been used. Generally, when rutting is 0.5 in (13 mm) or less, the crossfall of a premium pavement is sufficient to prevent both significant water accumulation in the wheel paths and steering problems associated with moving out of the wheel path. Therefore, any material that provided a combination of permanent deformation parameters (ALPHA and GNU) that produced a rut of 0.5 in or less after 20 million 18-kip ESALs was considered acceptable as a zero-maintenance pavement.

Table 1. Time required (in years) for 5 percent fatigue cracking to occur.

	13-in Thickness				16-in Thickness		18-in Thickness			
	Log K_1				Log K_1		Log K_1			
Zone	-5	-10	-15	-20	-10	-15	-5	-10	-15	-20
Wet—freeze	0.2	2.0	5.2	11.2	8.0	25[a]	22[a]	21.2[a]	25[a]	25[a]
Dry—freeze	0.1	1.4	4.7	11.5	7.5	25[a]	2.2	20.7[a]	25[a]	25[a]
Wet—no-freeze	6.7	7.4	7.4	8.7	25[a]	25[a]	25[a]	25[a]	25[a]	25[a]
Dry—no-freeze	0.5	1.3	2.5	4.8	9.1	24.7	5.1	23.7[a]	25[a]	25[a]

[a]Satisfies zero-maintenance requirements.

As shown in Figure 2, most of the rutting occurs early in the service life of the pavement; at least 50 percent occurred during the first five years. After five years, most combinations of ALPHA and GNU sustained very little additional cumulative permanent deformation.

The time required for a 0.5-in rut to develop was determined for each ALPHA value and each zone; the results are shown in Table 2. Analysis of these results showed that a GNU level of 1.4 was unsatisfactory for ALPHA values less than 0.8. Since most reported ALPHA values are less than 0.9, GNUs of 1.4 or greater are not expected to satisfy the zero-maintenance requirements for rutting. However, for ALPHAs as high as 0.9, all values of GNU met the rutting criterion.

Figure 2. Rutting versus time for ALPHA = 0.7, all GNUs, and 13-in surface: wet—freeze zone.

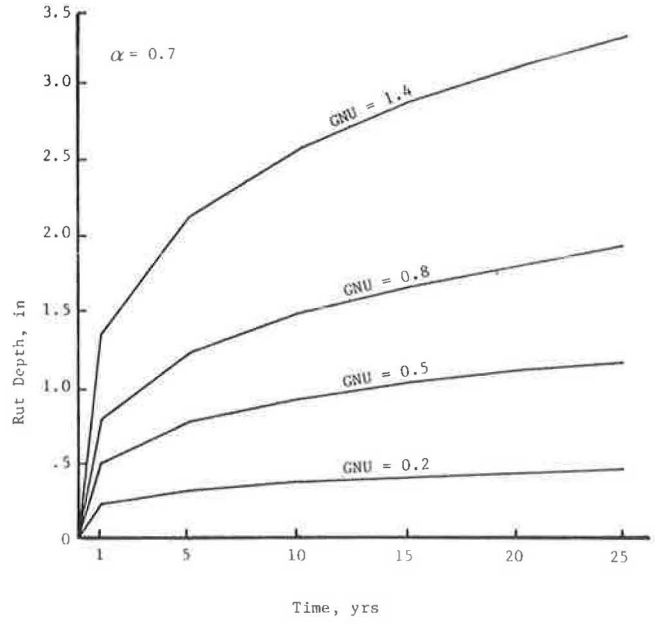

Table 2. Zones in which acceptable rutting performance occurred for both 13- and 18-in surfaces.

Value of GNU	Value of ALPHA		
	0.7	0.8	0.9
0.2	WF, DF, W-NF, D-NF[a]	WF, DF, W-NF, D-NF[a]	WF, DF, W-NF, D-NF[a]
0.5	–	WF, DF, W-NF, D-NF[a]	WF, DF, W-NF, D-NF[a]
0.8	–	WF, DF, D-NF[a]	WF, DF, W-NF, D-NF[a]
1.4	–	–	WF, DF, W-NF, D-NF[a]

Note: WF = wet–freeze zone; DF = dry–freeze zone; W-NF = wet–no-freeze zone; D-NF = dry–no-freeze zone.

[a]Zero-maintenance requirements are satisfied for each environmental zone listed.

The form of the relationship between GNU and time to a 0.5-in rut depth was the same for the wet—freeze, dry—freeze, and dry—no-freeze zones. The interactive effects of temperature and stiffness produced a characteristically different response curve for the wet--no-freeze zone. Again, with the higher temperatures, lower stiffnesses, and increased deflections, the cumulative permanent deformations were more critical in that zone than in any of the other environmental zones.

Table 2 also shows the material combinations of ALPHA and GNU that produced acceptable rutting performance by using the previously cited criteria. The only combination that did not meet the criteria was for ALPHA of 0.8 and GNU of 0.8 in the wet—no-freeze environmental zone. This wet--no-freeze zone was typically very warm and was the only zone where rutting rather than fatigue cracking was the most prevalent distress.

Low-Temperature Cracking

A summary of the results of the low-temperature cracking analysis is presented in Table 3. For each combination of inputs the tabulated values represent the calculated amount of low-temperature cracking.

The AC-40 mixtures experienced greater cracking than did the AC-10 mixtures. These results imply that low-temperature cracking increases as the bitumen stiffness increases in all environmental zones, even though almost no cracking occurred in the no-freeze zones.

Results showed that cracking increased as tensile strength decreased. The model predicted significantly lower cracking as the mixture strength increased from 300 to 600 psi (2068-4136 kPa). In general, changes in strength had a greater effect on cracking than did changes in asphalt type. However, it should be pointed out that significant changes in strength are usually coupled with changes in asphalt type, so that the effects of these two factors cannot be easily separated.

Other results showed that cracking decreased as the thermal coefficient was reduced from 17×10^{-6}/°F (31×10^{-6}/°C) to 11×10^{-6}/°F (20×10^{-6}/°C). The effects of changes in thermal coefficient on cracking are comparable to those of strength but controllable only through aggregate selection.

The asphalt cement that worked best to prevent low-temperature cracking was one that had low stiffness at low temperatures. For a particular grade of asphalt

Table 3. Predicted low-temperature cracking.

Type	Tensile Strength of Mixture (psi)	Thermal Coefficient ($\times 10^{-6}$/°F)	Cracking (ft/1000 ft^2)			
			Wet–Freeze Zone	Dry–Freeze Zone	Wet–No-Freeze Zone	Dry–No-Freeze Zone
AC-10[a]	300	11	15[b]	67	0.2[b]	0.1[b]
		17	63	123	2.9[b]	1.5[b]
	600	11	0.3[b]	4.78[b]	0[b]	0[b]
		17	3.9[b]	33	0.0[b]	0.0[b]
AC-40[c]	300	11	37	138	1.0[b]	0.6[b]
		17	98	167	11[b]	7.0[b]
	600	11	1.3[b]	45	0.0[b]	0.0[b]
		17	14[b]	107	0.2[b]	0.1[b]

Note: 1 psi = 6.89 kPa; t°F = (t°C ÷ 0.55) + 32; 1 ft = 0.3 m.

[a]Properties of AC-10 are penetration value, 120; original penetration temperature, 77°F; ring-and-ball penetration temperature, 115°F; penetration after thin-film oven test, 67 percent; specific gravity, 1.040.

[b]Satisfies zero-maintenance requirements.

[c]Properties of AC-40 are pentration value, 50; original penetration temperature, 77°F; ring-and-ball penetration after thin-film oven test, 70 percent; specific gravity, 1.015.

Figure 3. Low-temperature cracking versus asphalt concrete stiffness.

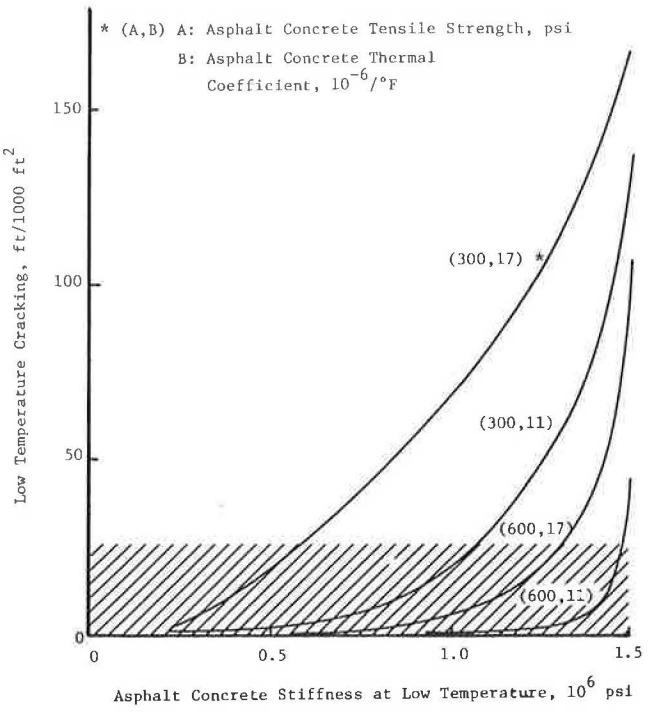

cement, low stiffness at low temperatures can be obtained by means of a high penetration index. The penetration index is a measure of asphalt consistency developed by Shell researchers that is based on measurements of penetration at 77°F and the ring-and-ball softening point.

Figure 3 was prepared for use in selecting material-property levels to minimize low-temperature cracking; the shaded area satisfies zero-maintenance requirements, as in Haas (29). At a mixture stiffness of 500 000 psi (3 447 000 kPa), the predicted cracking was greater than 10 ft/1000 ft² (33 m/1000 m²) for a maximum tensile strength of 300 psi and a thermal coefficient of 17 x 10^{-6}/°F. For these properties, the predicted cracking was approximately 20 ft/1000 ft² (66 m/1000 m²). As can be seen in Figure 3, thermal cracking at a stiffness of 500 000 psi may be eliminated either by decreasing the thermal coefficient or by increasing the tensile strength. After extensive observations in Canada, McLeod (30) recommended a limiting stiffness of 500 000 psi to prevent low-temperature cracking for an expected low temperature of -40°F (-40°C).

Due to the nature and background of the Shahin-McCullough model, the study has several imposed limitations. The most severe was the restriction on the length of the analysis period. The asphalt-cement aging model was a regression model based on data for asphalt cements that had been aged for 10 years or less. No basis exists for extrapolating the results to longer periods of aging. Thus, a 20- or 30-year analysis could not be directly simulated to demonstrate zero-maintenance pavement performance for the material properties under investigation. However, the material properties that minimize low-temperature cracking over a 10-year period were assumed to be applicable for the zero-maintenance time period.

The results show that the amount of cracking predicted was a function of the lowest input temperature. The daily temperature drops for both the wet and dry environmental zones were approximately the same. The greatest amount of cracking was predicted for the wet--freeze zone, in which the low air temperature was -30°F (-34°C). The least amount of cracking was calculated for the dry--no-freeze zone, in which the low air temperature was 8°F (-13°C).

The ideal asphaltic concrete for prevention of low-temperature cracking was determined to be one that has a minimum thermal coefficient of contraction, a high tensile strength, and a minimum stiffness at the expected low temperature. Currently available materials are generally unable to provide this set of properties and at the same time meet the other distress requirements.

It is difficult to infer the low-temperature performance of conventional asphaltic paving materials for zero-maintenance pavement criteria. Although conservative low temperatures were used, the effects of aging were not considered over the required 20-year maintenance-free period. If additional aging is assumed to have no effect, the results obtained in this analysis can be applied to longer analysis periods.

SUMMARY

Permanent Deformation

Permanent deformation parameters used in VESYS were not related to any other material properties, and the values suggested in Table 2 should be used for the environmental zones indicated. No significant interaction was observed between pavement thickness and predicted rutting for the permanent deformation parameters included in this analysis. However, if the full-depth asphalt-concrete thickness exceeds 18 in (457 mm), additional rutting calculations should be performed to ensure that excessive rutting is not predicted. To establish the rutting potential of an asphalt-concrete mixture that has been proposed for use in a zero-maintenance pavement, laboratory testing should be performed to determine the values of ALPHA and GNU for each mixture; Kenis (3) has proposed testing procedures for measuring these values. VESYS IIIA showed that rutting was a very significant problem for the wet--no-freeze zone but that it was not a significant problem for the other zones, especially the freeze zones.

Fatigue Cracking

Zero-maintenance fatigue cracking criteria were satisfied by several of the material-property combinations included in the study. Adequate fatigue life could not be achieved by using material properties that were included in this study for the 13-in (330-mm) surface over an 8-in (203-mm) base for any environmental zone. Even when the log K_1 was increased to -25, which corresponds to a material similar to an excellent sulfur asphalt, the improvement in material property was not sufficient to overcome the effects of strain in the thinner 10-in (250-mm) and 13-in pavements. However, when the thickness was increased to 16 in (406 mm), the better material-property values began to produce performance compatible with zero-maintenance requirements, as shown in Figure 1 and as summarized in Table 1. As the pavement thickness was increased to 18 in, more than 75 percent of the material combinations met the zero-maintenance fatigue criterion.

Low-Temperature Cracking

As can be observed in Table 3, low-temperature cracking for the no-freeze zones was minimal. It should be noted that the Shahin-McCullough model does predict cracking for the combinations of high thermal coefficient and low tensile strength of the mixture; the predicted crack spacing is about 80 ft (24 m). In the freeze zones, the model results indicate that the high tensile strength and low thermal coefficient would be satisfactory for an AC-10 but that a crack spacing of about 20 ft (6 m) would result for the AC-40 from the same mixture characteristics. For the freeze zones, the AC-10 with high tensile strength and low thermal coefficient served best to minimize or to prevent formation of low-temperature cracking.

Techniques considered to prevent low-temperature

cracking and to keep fatigue life high and rutting low work at cross-purposes. To minimize low-temperature cracking, the stiffness should be low at the design low temperature; thus a low-viscosity asphalt is required. A low-viscosity asphalt, however, also produces a low stiffness during the warmer seasons; the result is that the stresses and strains in the pavement structure increase and produce a reduction in fatigue life and an increase in rutting. Increasing stiffness at higher temperatures to enhance resistance to fatigue damage also increases the stiffness at low temperature. It should be noted that reasonable stiffnesses at higher temperatures can be obtained by using the high-tensile-strength materials.

McLeod has suggested values of stiffness versus temperature that should eliminate low-temperature cracking (30). These stiffnesses are for loading times of 20 000 s but can be shifted to other loading times and temperatures by using techniques described in the literature (30).

Haas (29) has suggested that a maximum cracking index of 12.5 for primary roads will ensure adequate performance. This cracking-index value transforms to a transverse crack spacing of approximately 30 ft (9 m). Haas also indicated that results from the Ste. Anne road test showed that increasing the thickness of the asphalt-concrete layer from 4 in (102 mm) to 10 in (254 mm) produced a 50 percent reduction in the cracking frequency. As a result, a suggested criterion for low-temperature cracking of 30 ft/1000 ft² (98 m/1000 m²) was included in Figure 3 and adopted for use in this analysis.

One other consideration in relation to low-temperature cracking is that the type of subgrade influences the effect of the low-temperature cracking on performance and maintenance. Studies by Haas have shown that if the subgrade has a very low swell potential the low-temperature cracking will have little effect on performance and subsequent maintenance. However, if the subgrade soil is a clay, the designer should carefully consider paving materials that will prevent formation of low-temperature cracking. Water infiltration through the low-temperature cracks will produce subsequent movements in the subgrade soil either through swelling or frost action and reduce the maintenance-free life of the pavement structure.

CONCLUSIONS

It has been demonstrated that, within the limits of the models selected, zero-maintenance pavements can be constructed; however, these pavements are very thick. In addition, the trade-offs of effects of properties on the various distresses must be carefully considered in order to provide pavements that will serve traffic for 20 years with no structural maintenance.

Combinations of material properties and necessary structural characteristics have been summarized. It should be noted that special emphasis must be given to provision of quality control and adequate thickness if conventional materials are used in the designs.

There is a need for additional materials research to develop, refine, and adapt new materials that can produce thinner surfacing layers for flexible pavements to provide zero-maintenance performance. The reductions in layer thickness can be used to offset the cost of producing these superior materials.

ACKNOWLEDGMENT

The work presented in this paper was accomplished by a team that included Thomas W. Kennedy, Freddy L. Roberts, Gary E. Elkins, J. Brent Rauhut, Fred N. Finn, Ralph Haas, James Ma, and Lee Jane Ream. We wish to thank Carl L. Monismith for his ideas on the models and for his review and discussion of distresses and material properties. Support for the project was provided by the Office of Research and Development of the Federal Highway Administration. We are grateful for the technical coordination provided by Ken Clear and William Kenis.

REFERENCES

1. J.B. Rauhut, F.L. Roberts, and T.W. Kennedy. Models and Significant Material Properties for Predicting Distresses in Zero-Maintenance Pavements. Federal Highway Administration, U.S. Department of Transportation, Rept. FHWA-RD-78-84, Sept. 1978.
2. J.B. Rauhut, J.C. O'Quin, and W.R. Hudson. Sensitivity Analysis of FHWA Structural Model VESYS II. Federal Highway Administration, U.S. Department of Transportation, Rept. FHWA-RD-76-24, March 1976.
3. W.J. Kenis. Predicted Design Procedures—A Design Method for Flexible Pavements Using the VESYS Structural Subsystem. Proc., 4th International Conference on Structural Design of Asphalt Pavements, Univ. of Michigan, Ann Arbor, Vol. 1, Aug. 1977.
4. M.Y. Shahin. Prediction of Low-Temperature and Thermal Fatigue Cracking of Bituminous Pavements. Univ. of Texas, Austin, Ph.D. dissertation, Aug. 1972.
5. M.Y. Shahin. Design System for Minimizing Asphalt Concrete Thermal Cracking. Proc., 4th International Conference on Structural Design of Asphalt Pavements. Univ. of Michigan, Ann Arbor, Aug. 1977.
6. J.B. Rauhut and P.R. Jordahl. Effects on Flexible Highways of Increased Legal Vehicle Weights Using VESYS IIM. Federal Highway Administration, U.S. Department of Transportation, Final Rept. FHWA-RD-77-134, Jan. 1978.
7. M.I. Darter and E.J. Barenberg. Zero-Maintenance Pavement Requirements and Capabilities of Conventional Pavement Systems. Federal Highway Administration, U.S. Department of Transportation, Interim Rept. FHWA-RD-76-105, April 1976.
8. R.L. Lytton, W.F. McFarland, and D.L. Schaefer. Flexible Pavement Design and Management: Systems Approach Implementation. NCHRP, Rept. 160, 1975.
9. H.J. Treybig, B.F. McCullough, P. Smith, and H. Von Quintus. Overlay Design and Reflection Cracking Analysis for Rigid Pavements: Volume 1--Development of New Design Criteria. Federal Highway Administration, U.S. Department of Transportation, Final Rept. FHWA-RD-77-66, Jan. 1978.
10. F.N. Finn, C. Saraf, R. Kulkarni, K. Nair, W. Smith, and A. Abdullah. Development of Pavement Structural Subsystems. NCHRP, Project 1-10B, Final Rept., Feb. 1977.
11. A.S. Adelimila and T.W. Kennedy. Fatigue and Resilient Characteristics of Asphalt Mixtures by Repeated-Load Indirect Tensile Test. Center for Highway Research, Univ. of Texas, Austin, CFHR Res. Rept. 183-5, Aug. 1975.
12. C.L. Monismith, J.A. Epps, D.A. Kasianchuk, and D.B. McLean. Asphalt Mixture Behavior in Repeated Flexure. Office of Research Services, Univ. of California, Berkeley, Rept. TE-70-5, Dec. 1970.
13. B.F. Kallas and V.P. Puzinauskas. Flexural Fatigue Tests on Asphalt Paving Mixtures. ASTM Special Tech. Publ. 508, 1972, pp. 47-65.
14. P.S. Pell and K.E. Cooper. The Effect of Testing and Mix Variables on the Fatigue Performance of Bituminous Materials. Proc., AAPT, Vol. 44, 1975.
15. D. Navarro and T.W. Kennedy. Fatigue and Repeated-Load Elastic Characteristics in In-Service Asphalt-Treated Materials. Center for Highway Research, Univ. of Texas, Austin, CFHR Res. Rept. 183-2, Jan. 1975.
16. M.W. Witczak. Development of Regression Models for Asphalt Concrete Modulus for Use in MS-1 Study. Asphalt Institute, College Park, MD, Jan. 1978.
17. W.R. Hudson and T.W. Kennedy. An Indirect Tensile Test for Stabilized Materials. Center for Highway

Research, Univ. of Texas, Austin, CFHR Res. Rept. 98-1, Jan. 1968.
18. J.F. Shook and B.F. Kallas. Factors Influencing Dynamic Modulus of Asphalt Concrete. Proc., AAPT, Vol. 38, 1969.
19. W.H. Gotolski, S.K. Ciesielski, and L.N. Heagy. Progress Report on Changing Asphalt Properties of In-Service Pavements in Pennsylvania. Proc., AAPT, Vol. 33, Feb. 1964, pp. 285-319.
20. W.J. Kenis. Progress Report on Changes in Asphaltic Concrete in Service. HRB, Bull. 333, 1962, pp. 39-65.
21. W.J. Liddle, G.M. Jones, and D.E. Peterson. Use of Synthetic Rubber-in-Asphalt Pavement to Determine Mixture Behavior and Pavement Performance. Materials and Tests Division, Utah State Highway Department, Interim Rept. Utah Project HPR 1 (8), BPR Studies 10 and 14; State Studies 903 and 910, Dec. 1979.
22. W.E. Simpson, R.L. Griffin, and T.K. Miles. Correlation of the Microfilm Durability Test with Field Hardening Observed in the Zaca-Wigmore Experiment Project. Symposium on Paving Materials, ASTM Special Tech. Publ. 277, 1959, pp. 52-63.
23. J. Skog. Results of Cooperative Test Series on Asphalts from the Zaca-Wigmore Experimental Project. Symposium on Paving Materials, ASTM Special Tech. Publ. 277, 1959, pp. 46-51.
24. E. Zube and J. Skog. Final Report on the Zaca-Wigmore Asphalt Test Road. Materials and Research Department, Division of Highways, California Department of Transportation, Sacramento, 1959.
25. L.W. Corbett and R.E. Merz. Asphalt Binder Hardening in the Michigan Test Road After 18 Years of Service. TRB, Transportation Research Record 544, 1975, pp. 27-34.
26. R.J. Schmidt. Use of ASTM Tests to Predict Low-Temperature Stiffness of Asphalt Mixes. TRB, Transportation Research Record 544, 1975, pp. 46-55.
27. Local Climatological Data: Annual Summaries for 1977. National Oceanic and Atmospheric Administration, Rockville, MD, 1978.
28. F.L. Roberts, T.W. Kennedy, and G.E. Elkins. Material Properties to Minimize Distress in Zero-Maintenance Pavements. Federal Highway Administration, U.S. Department of Transportation, Draft Final Rept., Aug. 1979.
29. R.C.G. Haas. A Method for Designing Asphalt Pavements to Minimize Low-Temperature Shrinkage Cracking. Asphalt Institute, College Park, MD, Res. Rept. 73-1, Jan. 1973.
30. N.W. McLeod. Prepared Discussion on Ste. Anne Test Road. Proc., Canadian Technical Asphalt Association, 1969.

Publication of this paper sponsored by Committee on Flexible Pavement Design.

Distress Behavior of Flexible Pavements That Contain Stabilized Base Courses

M. C. WANG AND W. L. GRAMLING

The distress behavior of full-scale experimental pavements is analyzed and discussed. The pavements contained five different base-course materials, namely, bituminous concrete, aggregate cement, aggregate-lime-pozzolan, aggregate bituminous, and crushed stone. Three types of aggregate—limestone, slag, and gravel—were used in the aggregate-cement base. Distress behavior discussed includes rutting, surface roughness, and cracking. Distress behavior observed is related to the pavement response, which was analyzed by using the BISAR computer program. The critical responses analyzed are maximum tensile strain at the bottom of the base course and maximum compressive strain at the top of the subgrade. Various equations relating distress and response are established that permit prediction of the amount of rutting, roughness, and cracking, and allowable subgrade compressive strains to limit different distress modes within specified levels are also established. Field distress data are also related to the present-serviceability-index (PSI) values of each test pavement. From these relationships, various levels of each mode of distress manifestation are established for each level of PSI drop. Results obtained from this study may be useful in selecting allowable distress levels and allowable subgrade compressive strain for pavement design and can also be helpful in developing the relationship between distress and performance.

Distress is related to structural defects that result from a variety of traffic- and environment-related causes; it may affect pavement performance directly or indirectly. In general, distress takes one of three forms—fracture, distortion, or disintegration. The distress mechanisms that contribute most significantly to a reduction in pavement serviceability, according to Finn (1), are fatigue cracking, rutting and slope variance, and cracking caused by shrinkage or by changes in temperature and subgrade moisture.

To design a pavement structure that will be maintenance-free within a design period of normally 20 years requires a thorough understanding of distress behavior and an ability to predict the degree of various distress manifestations. To date, a number of mathematical distress models have been developed for flexible pavements. An extensive list of these models is given by Rauhut, Roberts, and Kennedy (2). Some models capable of predicting rutting, fatigue cracking, and low-temperature cracking are VESYS A (3), PDMAP (4), the Shell method (5), and WATMODE (6). Some of these models were developed from statistical analysis of field data and thus require modification for use under other loading, environmental, and material conditions. Others were developed with assumptions to simplify loading and structure conditions and require field data for calibration and validation.

This paper discusses the distress behavior of several types of pavements studied at the Pennsylvania Transportation Research Facility, and various equations that relate distress and response variables are developed. These equations permit prediction of the degree of different distress manifestations and also provide data useful for relating distress and performance.

EXPERIMENTAL PAVEMENTS

The Pennsylvania Transportation Research Facility is a 1.6-km (1-mile), one-lane, 3.7-m (12-ft) wide test road that was constructed in the summer of 1972. The original facility consisted of 17 sections; each section contained either different base-course materials with the same layer thicknesses or one type of base-course material with

different layer thicknesses. In the fall of 1975, one section (section 8) was overlaid, and four sections (sections 10-13) were replaced by eight shorter sections, as shown in Figure 1.

The wearing surface was an ID-2A bituminous concrete. The subbase material was a crushed limestone. The subgrade soil was a silty clay that had classifications from A-4 to A-7. The base-course materials were bituminous concrete, aggregate cement, aggregate-lime-pozzolan, aggregate bituminous, and crushed stone. Three types of aggregate were used in the aggregate-cement base--limestone, slag, and gravel. Although three different base thicknesses were available for the aggregate-lime-pozzolan base, the pavements with bases that were 10.1 cm (4 in) and 15.2 cm (6 in) thick, i.e., sections F and G, were unable to cure properly due to cold weather during construction. Thus, these two sections were excluded from this analysis.

The traffic on the facility was provided by a conventional truck tractor pulling a semitrailer and one or two full trailers. The pavements constructed in 1972 had been subjected to about 2.4 million applications of 80-kN (18-kip) equivalent single-axle loads (EALs), whereas the pavements constructed in 1975 had received about 1.3 million EALs by the end of May 1978. Complete information on design, construction, and traffic operation is documented elsewhere (7,8).

FIELD TESTING

Rut depth was measured biweekly every 12.2 m (40 ft) in both wheel paths by using an A-frame that was attached to a base channel 2.1 m (7 ft) long. Surface cracking was surveyed and mapped biweekly. Surface roughness was measured in both wheel paths by using a MacBeth profilograph. The roughness factors obtained from the profilograph data were converted into the present serviceability index (PSI) of the pavement by using the following equations:

$$PSI = 11.33 - 4.06(\log RF) - 0.01\sqrt{C + P} - 0.21\overline{RD}^2 \quad (1)$$

$$RF = 63.267 + 0.686R \quad (2)$$

where

RF = Mays road-meter roughness factor,
C = area of cracking (m^2/1000 m^2),
P = area of patching (m^2/1000 m^2),
$\overline{RD}$ = average rut depth (cm), and
R = profilograph readings (cm/km).

Figure 1. Plan view and longitudinal profile of test track.

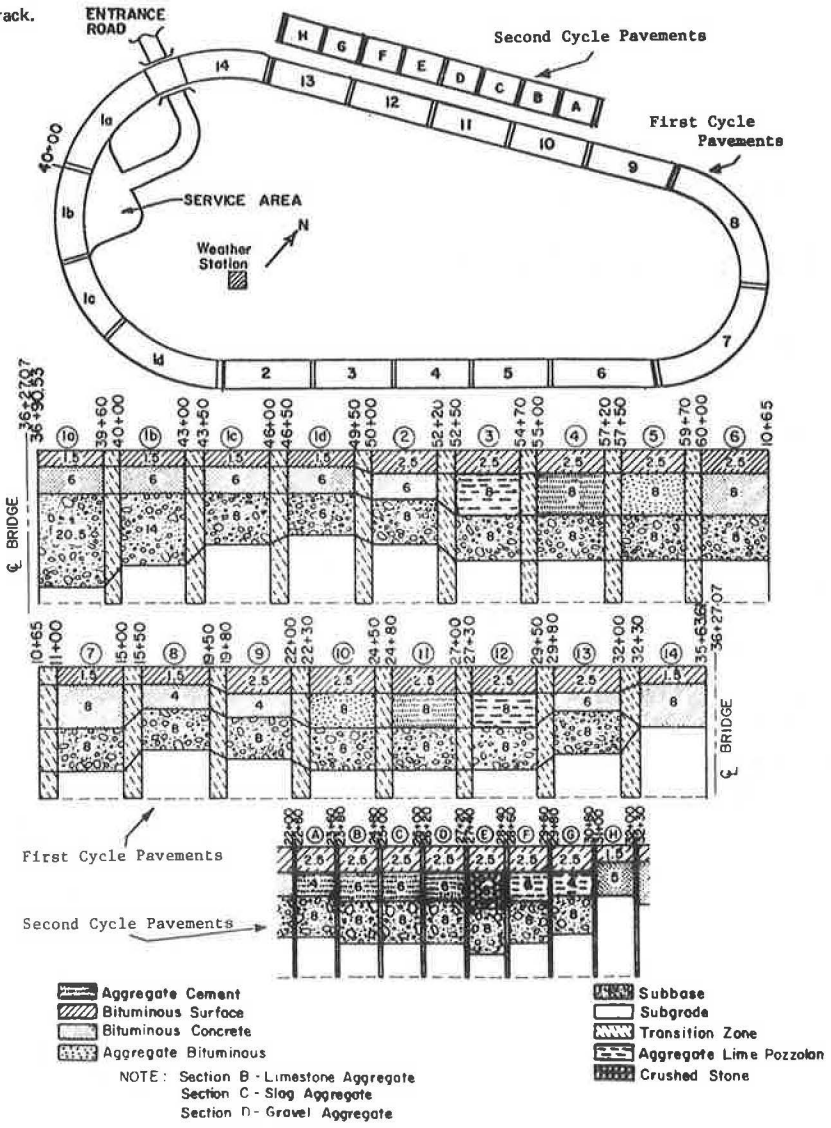

Table 1. Elastic constants and fatigue properties of pavement materials for spring weather conditions.

Layer	Material	Elastic Modulus (MPa)	Poisson's Ratio	Fatigue Constants K_1	Fatigue Constants K_2
Surface	Bituminous concrete	966	0.40	4.66×10^{-7}	3.61
Base	Bituminous concrete	2 207	0.35	1.06×10^{-6}	3.14
	Limestone aggregate cement	24 828	0.20	6.56×10^{-21}	6.05
	Slag aggregate cement	22 069	0.20	4.48×10^{-9}	3.08
	Gravel aggregate cement	17 241	0.20	1.83×10^{-8}	2.93
	Aggregate-lime-pozzolan	16 552	0.15	2.80×10^{-4}	2.17
	Aggregate bituminous	690	0.35	–	–
Subbase	Crushed limestone	331	0.40	–	–
Subgrade	Silty clay	55	0.45	–	–

Notes: 1 MPa = 145 lbf/in^2. Fatigue equation: $N_i = K_1(1/\epsilon)^{K_2}$.

These two equations were developed by Hopkins (9) of the Pennsylvania Department of Transportation.

In addition, surface deflections were measured in the wheel paths by using the Benkelman beam and the road rater. Pavement temperature profile and subgrade moisture distribution were measured by using thermocouples and moisture cells. Also, two frost-depth indicators were installed at the research facility to measure the depth of frost penetration. Weather data such as wind velocity, precipitation, and temperature were collected by using various meteorological gages.

MATERIAL PROPERTIES

The composition, gradation, and index properties of the constituent material of each pavement are documented in a research report (7). The modulus of elasticity of each layer was determined by using laboratory repeated-load tests on laboratory-compacted test specimens. The specimens had a diameter of 15.2 cm (6 in) and a height of 25.4 cm (10 in). The repeated load had a frequency of 20 cycles/min and a duration of 0.1 s. The modulus values obtained for the spring weather conditions are summarized in Table 1. In the spring season, the average pavement temperature was approximately 15.6°C (60°F), and the average subgrade moisture content was about 23 percent.

Data on the change of modulus values with the number of axle-load applications are required for determination of the variation in pavement response during the pavement's service life. For this purpose, regression analyses were performed for the Benkelman-beam deflection data. Results of the analyses were equations that related deflection with influential factors such as the number of EALs, pavement temperature, and subgrade moisture. The complete deflection equations can be found elsewhere (10). These deflection equations permit calculation of spring season deflections at any time for all experimental pavements except sections 1a, F, and G. On the basis of the computed spring season deflections, the modulus of elasticity of the combined surface and base layer at any number of axle-load applications was determined by using the bitumen-structures-analysis-in-roads (BISAR) computer program. In the determination, an assumption was made that the subgrade and subbase moduli remained constant through the entire service life of the experimental pavements. This assumption was also adopted in a previous study (11).

Fatigue properties of the surface and base-course materials were determined by conducting fatigue tests on laboratory-compacted beam specimens. The repeated loading had the same frequency and duration as that used in the testing of the resilient modulus. The test results are included in Table 1. Note that, because of the difficulty in preparing aggregate-bituminous test specimens, no fatigue data for this base-course material are given. Also contained in Table 1 is Poisson's ratio for each pavement constituent material. These ratios were obtained from other studies (12-14).

PAVEMENT RESPONSE

The response of the test pavements to traffic loading was analyzed by using the BISAR computer program and the material properties described previously. The traffic loading used had an 80-kN dual-wheel single-axle load and a 55-kPa (80-lbf/in^2) tire pressure. The analysis was made for spring weather conditions only. In the analysis for tensile strain variation with EAL, the surface and base courses were combined into one layer. For the analysis of initial pavement conditions, the surface and base layers were treated individually.

The critical responses analyzed were maximum tensile strain at the bottom of the base layer and maximum vertical compressive strain in the subgrade. The critical responses analyzed for initial pavement conditions were later related to the distress and performance data collected from the research facility.

RUTTING BEHAVIOR

As expected, rut depth increased with increasing number of 80-kN EAL applications. The rate of increase varies with many factors, such as base-course material, layer thickness, and axle-load applications. For the same base-course material, the pavement with a thick base course displays less rutting, as would be expected. Figure 2 shows the rut data for different base-course materials with the same 15.2-cm thickness. It can be seen that in the early stage the amount of rutting increases with the type of base-course material in the following order: aggregate cement, aggregate-lime-pozzolan, bituminous concrete, aggregate bituminous, and crushed stone. After about 1.2 million EALs, however, rutting in the aggregate-lime-pozzolan pavement surpasses that in other stabilized base pavements. A possible reason for this observation will be discussed.

Rutting is primarily a result of permanent deformation of each pavement constituent layer and the subgrade soil. Among the four stabilized base-course materials studied, aggregate cement and aggregate-lime-pozzolan are more rigid and brittle than bituminous-concrete and aggregate-bituminous base courses. The brittle nature gives smaller permanent deformations in the aggregate cement and aggregate-lime-pozzolan base courses, and the greater rigidity results in a smaller compressive stress at the top of the subgrade. The lower compressive stress on the top of the subgrade induces a smaller permanent deformation in the subgrade. As a consequence, both aggregate-cement and aggregate-lime-pozzolan pavements undergo less rutting than bituminous-concrete and aggregate-bituminous pavements while the pavements are in a structurally sound condition. The cracking data presented later indicate that, after about 2.4 million EALs, (a) surface cracking developed in both wheel paths throughout the entire aggregate-lime-pozzolan pavements, (b) the intensity of surface cracking in the aggregate bituminous pavement was much less, (c) only slight class 1 cracking developed in the aggregate-cement pavement, and (d) no apparent surface cracking was observed in the bituminous-concrete pavement. Because of the intensive cracking in the aggregate-lime-pozzolan

pavements, the stiffness of the surface and base layers decreased and the compressive stress in the subgrade increased. Consequently, rutting in the aggregate-lime-pozzolan pavement increased fastest among the four stabilized base pavements during the later stage of their service life.

Also shown in Figure 2 are seasons within which the rut-depth data were taken. No clear indication is seen that rutting varied significantly with season, as reported by Saraf, Smith, and Finn (15).

The rut-depth data for the three pavements that contained a 15.2-cm aggregate-cement base indicate that, among the three types of aggregate studied, limestone has the greatest resistance to rutting, slag has an intermediate level, and gravel has the least. This is probably due to the difference in the resilient modulus, which is greatest for limestone, intermediate for slag, and least for gravel, as shown in Table 1. A detailed discussion of the rutting behavior of the three types of aggregate can be found elsewhere (16).

The relationship between rut depth and the number of EALs was formulated by using the curve-fitting process. Results of the analysis give the following equation:

$$\overline{RD} = 2.54c_1(N)^{c_2} \quad (3)$$

where N = the number of 80-kN EALs (000 000s) and c_1, c_2 = coefficients. Coefficients c_1 and c_2 are given in Table 2 for all test pavements except section 1a. This section is not included because it was disturbed by the construction of the bridge and was overloaded by the equipment used for the bridge testing. Both c_1 and c_2 can be expressed in terms of the maximum compressive strain on the top of the subgrade (ε_V) as follows.

For bituminous-concrete and aggregate-bituminous pavements: $\log c_1 = 260\,\varepsilon_V^2 - 1.137$, $\log c_2 = 0.028\sqrt{\varepsilon_V} - 0.474$.
For limestone-aggregate cement and aggregate-lime-pozzolan pavements: $\log c_1 = 1020\,\varepsilon_V^2 - 1.076$, $\log c_2 = 0.028\sqrt{\varepsilon_V} - 0.274$.
For gravel and slag aggregate-cement pavements: $\log c_1 = 1080\,\varepsilon_V^2 - 0.754$, $\log c_2 = 0.028\sqrt{\varepsilon_V} - 0.274$.

Because more data points for pavements that contain bituminous-concrete base-course material are available for the development of the preceding equations, the first two calculations may provide better relations than others. A fairly good agreement between the calculations and the field data is shown in Figure 2.

The number of 80-kN EALs required to produce a rut depth is related to the initial maximum compressive strain on the top of the subgrade in Figure 3. It is interesting to note that the data points for the aggregate-bituminous pavement fall within the group of data points for the bituminous-concrete pavements, while those of the aggregate-lime-pozzolan pavements are located inside the group of the aggregate-cement pavements. The figure indicates the values of allowable maximum compressive strain so that rutting will not exceed any specified limit. For example, to limit rutting within 6.4 mm (0.25 in) after 1 million EALs, the allowable maximum compressive strain equals about 180 μm/m for the gravel-aggregate cement, slag-aggregate cement, and aggregate-lime-pozzolan pavements and approximately 230 μm/m for the limestone-aggregate cement pavements. For the bituminous-concrete and aggregate-bituminous pavements, the maximum compressive strain required to limit rutting within 6.4, 12.8, and 17.2 mm (0.25, 0.50, and 0.75 in) with 1 million EALs is 450, 550, and 600 μm/m, respectively. These allowable maximum compressive strains constitute a strain criterion for preventing excessive rutting in a newly designed pavement.

Figure 2. Rut depth versus EAL for different base-course materials.

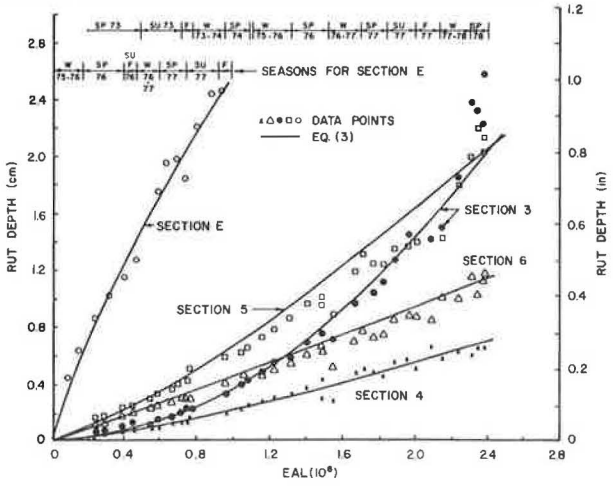

ROUGHNESS BEHAVIOR

Surface roughness, which is measured in terms of profilograph readings, increases with increasing number of EALs, as would be expected. Figure 4 compares the change of roughness with EALs for the different base-course

Table 2. Coefficients of rut depth and roughness equations.

Base	Section	Maximum Compressive Strain (μm/m)	Coefficients			
			c_1	c_2	m_1	m_2
Bituminous concrete	1b	294.2	0.12	1.41	78.97	0.23
	1c	426.6	0.16	1.41	64.96	0.23
	1d	483.0	0.22	1.41	74.48	0.31
	2	383.6	0.14	1.25	46.28	0.22
	6	291.6	0.18	1.05	69.43	0.22
	7	322.4	0.18	1.05	75.31	0.38
	8	594.0	0.57	1.62	103.88	0.47
	9	525.8	0.50	1.25	46.53	0.78
	H	884.8	8.10	2.50	107.77	0.42
	14	390.9	0.17	2.32	132.42	0.22
Aggregate cement	4	107.5	0.09	1.30	30.98	0.68
	A	288.0	0.50	1.37	62.26	1.04
	B	171.5	0.19	0.95	207.43	1.51
	C	185.5	0.43	1.35	50.65	1.23
	D	216.0	0.55	1.70	100.29	1.23
Aggregate-lime-pozzolan	3	142.8	0.18	1.77	56.12	1.12
Aggregate bituminous	5	403.0	0.27	1.26	44.20	0.46
Crushed stone	E	575.4	1.00	0.80	43.29	1.05

Note: 1 μm/m = 1 × 10^{-6} in/in.

materials studied. In general, the difference in roughness behavior among the various base-course materials and aggregate types studied is similar to that of rutting behavior. Meanwhile, no significant variation in surface roughness between seasons has been observed for the pavements under investigation.

Figure 5 shows the relation between the maximum compressive strain on the top of the subgrade and the number of EALs required to produce a certain level of surface roughness. According to this figure, the maximum allowable compressive strains to limit surface roughness at 1 million EALs within 15.8, 31.6, and 57.3 cm/km (10, 20, and 30 in/mile) are roughly 140, 170, and 190 μm/m, respectively, for the aggregate-cement and aggregate-lime-pozzolan pavements. For the bituminous-concrete and aggregate-bituminous pavements, the allowable maximum compressive strains are approximately 330, 400, and 460 μm/m, respectively, for 15.8, 31.6, and 57.3 cm/km with 1 million EALs.

Typical relationships between surface roughness and rutting are shown in Figure 6. The well-defined linear relation in the logarithmic scale suggests the following equation:

$$R = m_1(\overline{RD})^{m_2} \quad (4)$$

where R = surface roughness (cm/km) and m_1, m_2 = coefficients. The values of coefficients m_1 and m_2 are tabulated with the coefficients of Equation 3 in Table 2. The table reveals that both m_1 and m_2 increase with an increase in the compressive strain.

CRACKING BEHAVIOR

Transverse shrinkage cracking developed across the entire width in all aggregate-cement pavements except section 11, which contained a 20.3-cm (8-in) limestone-aggregate cement base course and was removed after about 1.1 million EALs. This shrinkage cracking was observed earlier than load-associated cracking. In most cases, the presence of shrinkage cracking aided, in varying degrees, the growth of load-associated cracking. More detailed information on cracking in the aggregate-cement pavements is available elsewhere (16). Transverse temperature cracking appeared

Figure 3. Initial maximum compressive strain versus EAL at different rut depths.

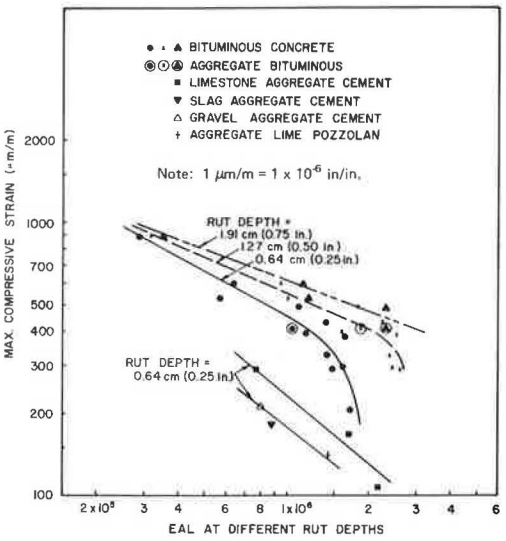

Figure 4. Roughness versus EALs for different base-course materials.

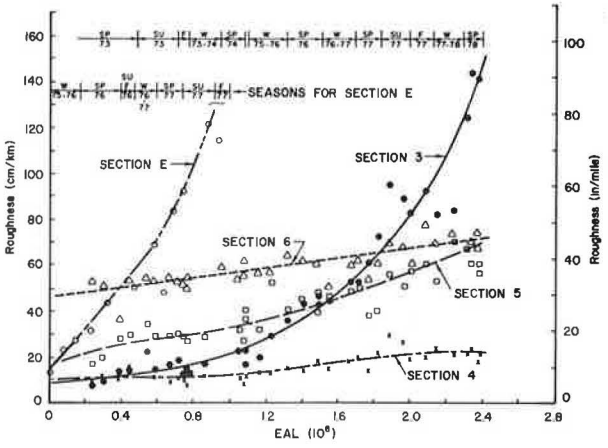

Figure 5. Initial maximum compressive strain versus EALs for various levels of roughness.

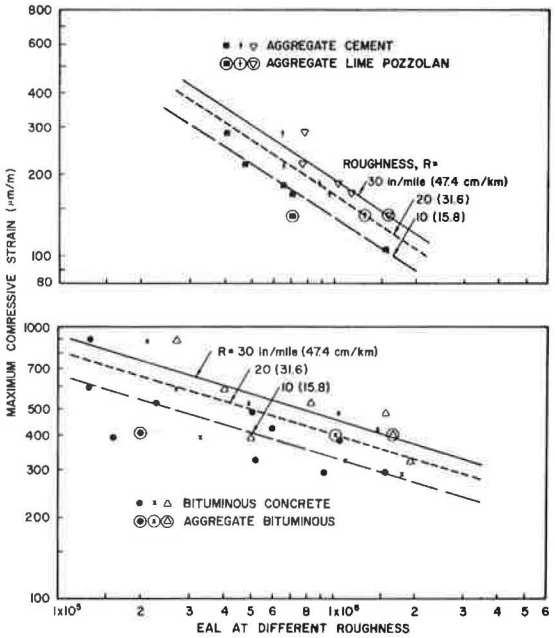

Figure 6. Relationship between rut depth and roughness.

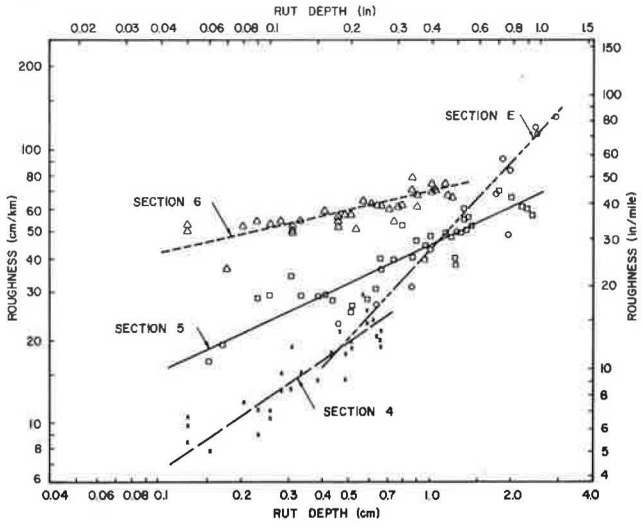

in 6 of 12 bituminous-concrete pavements, which included sections 1a, 1b, 1c, 1d, 8, and 9; however, no such type of cracking was observed in the pavements containing a crushed-stone, aggregate-lime-pozzolan, or aggregate-bituminous base. Among the many test pavements, potholes developed only in the aggregate-lime-pozzolan pavement. Details on the development of potholes have already been reported (17).

Class 2 and class 3 cracking developed in most test pavements. Previous papers (16,17) have described in detail the development and growth of surface cracking in the aggregate-cement, aggregate-lime-pozzolan, and crushed-stone pavements. Table 3 summarizes the number of EALs at 10 m^2/1000 m^2 of the entire pavement surface area, the number of EALs at crack initiation at the bottom of the base course, the number of EALs for crack propagation from the bottom of the base course to the top of the surface course, and the initial maximum tensile strain at the bottom of the base course for all cracked test pavements.

The rate of growth of the cracked area given in Table 3 was estimated by fitting the field data. Since the rate of growth in most cases is slow at the initial stage and increases at a greater rate, the values given are approximate average rates of crack propagation. The number of EALs at crack initiation was evaluated in the following way. First, the tensile strain at the bottom of the base course was computed by using the BISAR computer program together with the elastic moduli already determined for the spring conditions. The computed tensile strain varied with the number of EALs in a shape that resembles the variation of Benkelman-beam spring-season deflection. Second, the fatigue line of each base-course material was plotted. Finally, the approximate number of EALs for crack initiation at the bottom of the base course was obtained from the intersection of each fatigue line and the corresponding tensile-strain curve.

The difference between the number of EALs at crack initiation and that at a crack area of 10 m^2/1000 m^2 equals approximately the rate of crack propagation from the bottom of the base course to the top of the surface layer. The crack area of 10 m^2/1000 m^2 of entire pavement surface area was chosen arbitrarily. This amount of cracking corresponds to a PSI drop of about 0.6, as will be shown later. Relating the rate of crack propagation to the combined thickness of the base and surface layers yields the following approximate equation for rate of crack propagation:

$$(dC_l)/(dN) \cong 95.3 \exp(0.75\ N) \quad (5)$$

where C_l = the crack length (mm) and N = the number of EALs (000 000s). Note that Equation 5 was formulated by using the crack data obtained from the pavements that contained bituminous-concrete base only. Because the bituminous concrete in the base course is different from that in the surface layer and the surface-layer thickness varies at two different levels, 3.8 cm (1.5 in) and 6.4 cm (2.5 in), Equation 5 provides only a rough approximation of the average crack propagation through two different layers.

For the bituminous-concrete pavements, the rate of growth of the cracked area can be related to the maximum tensile strain at the bottom of the base course as follows:

$$(dC_a)/(dN) \cong 9.88 \times 10^{-12}\ \epsilon_t^{5.3} \quad (6)$$

where C_a = area of class 2 and class 3 cracking (m^2/1000 m^2) and ϵ_t = maximum tensile strain at the bottom of the base course (μm/m); thus,

Section 1d = 0.6×10^{-4},
Section 8 = 1.3×10^{-4},
Section 9 = 2.1×10^{-4},
Section H = 17.8×10^{-4},
Section 14 = 1.8×10^{-4},
Section A = 7.6×10^{-4},
Section C = 10.8×10^{-4},
Section D = 33.3×10^{-4},
Section 3 = 8.5×10^{-4},
Section 5 = 1.4×10^{-4}, and
Section E = 50.0×10^{-4}.

Therefore, it would be possible to estimate the degree of surface cracking at any time for the bituminous-concrete pavements by using Equations 5 and 6.

PAVEMENT PERFORMANCE

The PSI decreased with increasing number of EALs; the rate of decrease varied with such factors as base-course material, layer thickness, and EAL. In general, the shape of the performance curve followed the power function that was originally proposed by the American Association of State Highway Officials (18). As in the case of distress behavior, no significant variation in PSI between seasons was observed for the pavements studied. More detailed information on the change in PSI with EALs is given elsewhere (16,17,19).

Because the initial PSI values are generally low and vary considerably among pavements, this analysis considers only the difference in PSI that occurred after the initial measurements. Figure 7 presents the relationship between the maximum compressive strain on the top of the subgrade with the number of EALs for three levels of PSI drop, namely, ΔPSI = 0.5, 1.0, and 1.5. This figure indicates that a maximum value of compressive strain exists, so that the PSI drop after certain repetitions of EALs will not exceed any specified value. For the pavements that contain

Table 3. Crack data.

Section	Maximum Tensile Strain (μm/m)	Number of EALs at Crack Initiation (N_i) (000 000s)	Number of EALs at Crack Area of 10 m^2/1000 m^2 (N) (000 000s)	$N-N_i$ (000 000s)
1d	109.5	0.93	1.80	0.87
8	139.0	0.24	0.39	0.15
9	122.7	0.76	1.04	0.28
H	209.1	0.034	0.36	0.33
14	118.0	0.30	1.00	0.70
A	65.0	0.29	1.13	0.84
C	46.1	0.06	1.21	1.15
D	54.4	0.04	0.75	0.71
3	41.1	0.98	1.26	0.28
5	165.0	–	2.40	–
E	279.0	–	0.61	–

Note: 1 μm/m = 1×10^{-6} in/in; 1 m^2/1000 m^2 = 1 $yard^2$/1000 $yards^2$.

Figure 7. Initial maximum compressive strain versus EALs for various levels of PSI drop.

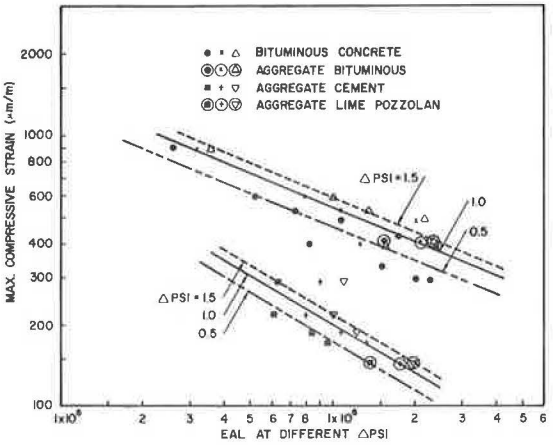

Figure 8. Rut depth versus PSI drop.

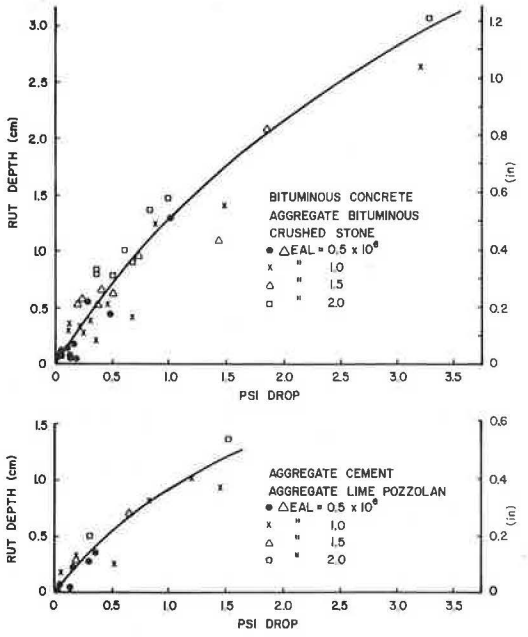

Figure 9. Surface roughness versus PSI drop.

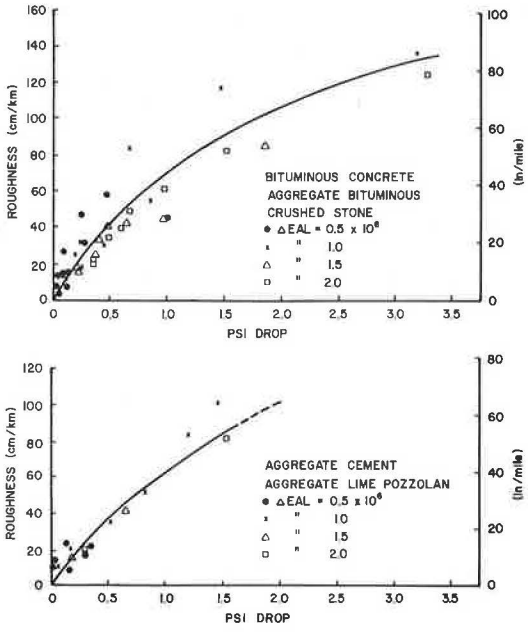

bituminous-concrete and aggregate-bituminous bases, the maximum compressive strains for ΔPSI = 0.5, 1.0, and 1.5 are approximately 460, 540, and 590 μm/m, respectively, at 1 million EALs. For aggregate-cement and aggregate-lime-pozzolan pavements, the maximum compressive strains are approximately 170, 200, and 240 μm/m for ΔPSI = 0.5, 1.0, and 1.5, respectively.

The PSI drops (ΔPSI) at 0.5, 1.0, 1.5, and 2.0 million EALs are related to the corresponding increases in rut depth (Figure 8), surface roughness (Figure 9), and area of surface cracking (Figure 10). Figures 8 and 9 demonstrate that the rate of increase with increasing ΔPSI for both rut depth and roughness becomes smaller at higher levels of ΔPSI. The reason for this is that, at higher ΔPSI values, cracking becomes more important in the determination of PSI, as depicted by Figure 10.

Figure 10. Area of surface cracking versus PSI drop.

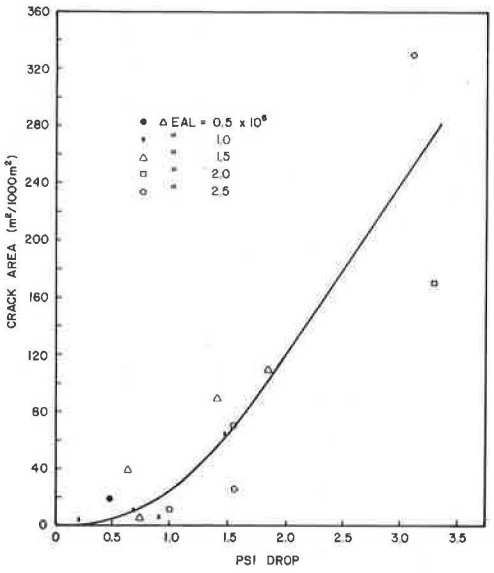

According to Figure 8, under the same levels of PSI drop, pavements whose bases contain bituminous concrete, aggregate bituminous, and crushed stone undergo greater rutting than do pavements whose bases contain aggregate cement and aggregate lime pozzolan. For the pavement bases that contain bituminous concrete, aggregate bituminous, and crushed stone, rut depths equal 0.71, 1.30, 1.78, and 2.16 cm (0.28, 0.51, 0.70, and 0.85 in), respectively, for ΔPSI = 0.5, 1.0, 1.5, and 2.0. Rut depths corresponding to the same levels of ΔPSI are 0.56, 0.91, 1.19, and 1.47 cm (0.22, 0.36, 0.47, and 0.58 in) for the pavement bases that contain aggregate cement and aggregate lime pozzolan. It is noteworthy that the rut depth at ΔPSI = 0.5 is very close to 6.4 mm (0.25 in) for all test pavements. This particular level of rutting has been widely used as an allowable rut depth in the design of high-quality highway pavements (20,21).

Figure 9 demonstrates that roughness changes for ΔPSI = 0.5, 1.0, and 1.5 are almost equal, regardless of the type of base-course material. The values of roughness are approximately 39.5, 71.0, and 94.7 cm/km (25, 45, and 60 in/mile) for ΔPSI = 0.5, 1.0, and 1.5, respectively. Based on Figure 10, the areas of surface cracking corresponding to ΔPSI = 0.5, 1.0, 1.5, and 2.0 are approximately 5, 25, 65, and 120 $m^2/1000\ m^2$ in terms of the entire pavement surface area, respectively. These levels of various distress manifestations and various levels of PSI drop might be used as a guide for selecting allowable distress levels for pavement design.

SUMMARY AND CONCLUSIONS

Rutting, roughness, and surface cracking of flexible pavements that contain five different base-course materials were discussed. The distress behavior was related to pavement response, which was analyzed by using the BISAR computer program. The distress behavior was also related to PSI values to establish the level of each mode of distress manifestation that corresponded to each level of PSI drop.

From this study, various equations that permit prediction of pavement distress from pavement response were developed. Also, allowable subgrade compressive strains to limit different distress modes within specific levels were established. The results of this study may be useful in selecting allowable distress levels and strain criteria for pavement design and also may be helpful in developing the relationship between distress and performance.

ACKNOWLEDGMENT

The study presented here is a part of a research project sponsored by the Pennsylvania Department of Transportation in cooperation with the Federal Highway Administration, U.S. Department of Transportation. Their support is gratefully acknowledged. The field data reported here were collected and reduced with the assistance of W. P. Kilareski, S. A. Kutz, B. A. Anani, R. P. Anderson, and P. J. Kersavage. This paper represents our views and does not necessarily reflect those of the Pennsylvania Department of Transportation or the Federal Highway Administration.

REFERENCES

1. F. N. Finn. Observation of Distress in Full-Scale Pavements. In Structural Design of Asphalt Concrete Pavement Systems, HRB, Special Rept. 126, 1971, pp. 86-90.
2. J. B. Rauhut, F. L. Roberts, and T. W. Kennedy. Response and Distress Models for Pavement Studies. TRB, Transportation Research Record 715, 1979, pp. 7-14.
3. J. B. Rauhut and P. R. Jordahl. Effects on Flexible Highways of Increased Legal Vehicle Weights Using VESYS IIM. Federal Highway Administration, U.S. Department of Transportation, Final Rept. FHWA-RD-77-134, Jan. 1978.
4. F. N. Finn, C. Saraf, R. Kulkarni, K. Nair, W. Smith, and A. Abdullah. Development of Pavement Structural Subsystems. NCHRP Project 1-10B, Final Rept., Feb. 1977.
5. A. I. M. Claessen, J. M. Edwards, P. Sommer, and P. Ugé. Asphalt Pavement Design—The Shell Method. Proc., 4th International Conference on Structural Design of Asphalt Pavements, Univ. of Michigan, Ann Arbor, Aug. 1977, pp. 39-74.
6. F. R. P. Meyer, A. Cheetham, and R. C. G. Haas. A Coordinated Method for Structural Distress Predictions in Asphalt Pavements. Presented at Annual Meeting, AAPT, Lake Buena Vista, FL, Feb. 1978.
7. E. S. Lindow, W. P. Kilareski, G. Q. Bass, and T. D. Larson. Construction, Instrumentation, and Operation. Pennsylvania Transportation Institute, Pennsylvania State Univ., University Park, Interim Rept. PTI 7504, Vol. 2, Feb. 1973.
8. W. P. Kilareski, S. A. Kutz, and G. Cumberledge. Modification, Construction, and Instrumentation of an Experimental Highway. Pennsylvania Transportation Institute, Pennsylvania State Univ., University Park, Interim Rept. PTI 7607, April 1976.
9. J. G. Hopkins. Pavement Roughness and Serviceability. Bureau of Materials, Testing, and Research, Pennsylvania Department of Transportation, Final Rept., Aug. 1975.
10. W. P. Kilareski, B. Anani, R. P. Anderson, M. C. Wang, and T. D. Larson. Remaining Life and Overlay Thickness Design for Modified Flexible Pavements. Pennsylvania Transportation Institute, Pennsylvania State Univ., University Park, Interim Rept. PTI 7905, Jan. 1979.
11. M. C. Wang, T. D. Larson, A. C. Bhajandas, and G. Cumberledge. Use of Road-Rater Deflections in Pavement Evaluation. TRB, Transportation Research Record 666, 1978, pp. 32-39.
12. K. Nair, W. S. Smith, and C. Y. Chang. Characterization of Asphalt Concrete and Cement-Treated Granular Base Course. Federal Highway Administration, U.S. Department of Transportation; Materials Research and Development, Inc., Oakland, CA, Final Rept., Feb. 1972.
13. S. Kolias and R. I. T. Williams. Cement-Bound Road Materials: Strength and Elastic Properties Measured in the Laboratory. Transport and Road Research Laboratory, Crowthorne, Berkshire, England, TRRL Supplementary Rept. 344, 1978.
14. Lime-Fly Ash-Stabilized Bases and Subbases. NCHRP, Synthesis of Highway Practice 37, 1976.
15. C. L. Saraf, W. S. Smith, and F. N. Finn. Rut Depth Perception. TRB, Transportation Research Record 616, 1976, pp. 9-14.
16. M. C. Wang and W. P. Kilareski. Behavior and Performance of Aggregate-Cement Pavements. TRB, Transportation Research Record 725, 1979, pp. 67-73.
17. M. C. Wang and W. P. Kilareski. Field Performance of Aggregate-Lime-Pozzolan Base Materials. TRB, Transportation Research Record 725, 1979, pp. 74-80.
18. The AASHO Road Test: Report 5—Pavement Research. HRB, Special Rept. 61E, 1962.
19. M. C. Wang and T. D. Larson. Evaluation of Structural Coefficients of Stabilized Base-Course Materials. TRB, Transportation Research Record 725, 1979, pp. 58-67.
20. C. L. Monismith and D. B. McLean. Structural Design Considerations. Proc., AAPT, Vol. 41, 1972, pp. 258-305.
21. G. M. Dormon and T. Metcalf. Design Curves for Flexible Pavements Based on Layered System Theory. HRB, Highway Research Record 71, 1965, pp. 69-84.

Publication of this paper sponsored by Committee on Flexible Pavement Design.

Nonlinear Characterization of Granular Materials for Asphalt Pavement Design

A. F. STOCK AND S. F. BROWN

In view of the well-established nonlinear resilient properties of unbound granular materials, analytically based pavement-design procedures should take proper account of this characteristic. The importance of including a failure criterion in the nonlinear model is demonstrated; the potentially high modulus of granular materials is not being realized in situ because of the unfavorable stress conditions that develop. The nonlinear model that has been written into the pavement-design computer program ADEM is described, and typical results are presented and compared with those based entirely on linear-elastic analysis. The results show that the thickness and quality of granular material have only a minor influence on the required thickness of asphalt but that, for accurate design, nonlinear analysis is required.

The development of a computer program for the design of asphalt pavements by using analytical techniques has been reported (1). This program, ADEM, assumed all layers to be

linear elastic and estimated the modulus of the granular layer by assuming that the modular ratio between the granular material and the subgrade was 2.5. However, extensive evidence was available from materials testing that showed granular materials to be markedly nonlinear, and a nonlinear model was incorporated into the further development of ADEM. This allowed for a more-accurate representation of the granular layer so that its structural role could be better assessed under various conditions and also provided results that could be compared with those obtained by using simple linear elasticity.

The general conclusion that can be drawn from the literature on laboratory studies of unbound granular materials is that under load they exhibit stress-stiffening behavior. This conclusion has been reinforced by measurements in test pavements.

The most common form of relationship reported is

$$E = K_1\lambda^{K_2} \quad (1)$$

where

E = resilient modulus,
λ = stress function, and
K_1, K_2 = material constants.

Various stress functions have been used, including the normal stress ($\theta = \sigma_1 + \sigma_2 + \sigma_3$) as proposed by Hicks (2) and the mean value of the mean normal stress for any stress path as proposed by Boyce, Brown, and Pell (3) (mean normal stress $p = \theta/3$). Since Hicks (2) studied a variety of materials and his stress function is a simple one, the modulus relationship that he proposed was adopted for this work:

$$E = K_1\theta^{K_2} \quad (2)$$

Smith (4) used this model to derive equivalent moduli for the granular layer as functions of the asphalt thickness and stiffness, the subgrade modulus, and the constant K_1. These equivalent moduli give the same tensile strain in the asphalt and vertical strain on the subgrade as would be obtained in a nonlinear analysis. While this simplification is very useful, it was not adopted for this work since no failure criterion for the granular material was included in its derivation. Furthermore, use of such simplifications is only valid within the limits of their derivation and, since the ADEM design program is highly versatile, the restrictions imposed by Smith's simplification were considered unacceptable.

DEVELOPMENT OF THE NONLINEAR MODEL

The philosophy of the approach was similar to that originally proposed by Monismith and others (5), which involved used of linear-elastic-layer theory in an iterative procedure designed to obtain compatibility between the calculated stresses and the associated values of modulus for the nonlinear granular layer.

Initial attempts to produce a convergent iteration procedure by means of weightless layers failed; it was thus necessary to investigate methods for determining self-weight stresses.

Preliminary applications of the modulus iteration procedure indicated that unacceptably large tensile stresses were experienced within the granular layer, and further investigation was therefore undertaken with respect to development and incorporation of a failure criterion.

Determination of Self-Weight Stresses

Vertical stresses can be dealt with quite simply by considering the thickness and density of the layer. However, horizontal stresses are less straightforward; the usual method for their calculation is to multiply the vertical stresses by the coefficient of earth pressure at rest (K_0), which, for a linear-elastic system, is given by

$$K_0 = \nu/(1 - \nu) \quad (3)$$

where ν = vertical stress. However, it was felt that this approach was incompatible with a nonlinear system. Brooker and Ireland (6) relate K_0 to the results of materials testing by the equation

$$K_0 = 1 - \sin\phi' \quad (4)$$

where ϕ' = angle of shearing resistance for cohesionless soil. For overconsolidated clays, values greater than unity occur, and it was considered that the effect of compaction equipment on the granular layer produced the same type of effect. Hence, the procedure for estimating K_0 from the overconsolidation ratio (7) was adopted.

To implement this approach, the stress history of granular layers during compaction was estimated. From these estimates and the calculation of vertical self-weight stresses, a relationship between the overconsolidation ratio and depth was developed. This relationship in conjunction with that between K_0 and the overconsolidation ratio (7) provided the data from which K_0 could be expressed as a function of depth for various thicknesses of granular layer. For the purpose of the material model, the granular layer was divided into four sublayers. Average K_0 values for each of these sublayers in a granular layer, which varied in thickness between 100 mm and 700 mm, were estimated from the K_0-depth relationship and are shown in Figure 1.

Failure Criterion

Preliminary analyses with the iterative procedure indicated that unacceptably large tensile stresses could develop in the granular material. Barker of the U.S. Army Engineer Waterways Experiment Station, in attempting finite-element analyses of pavement systems, had observed a similar phenomenon and overcame it by including a failure criterion in the form of a limiting σ_1/σ_3 ratio (where σ_1 and σ_3 are the major and minor principal stresses, respectively). Boyce (8) undertook tests to failure by following several stress paths and noted that the σ_1/σ_3 ratio at which his specimens failed was a function of the stress path. However, when his results were expressed as a ratio of the stress invariants q/p, a value close to 2.2 applied for all cases. In general,

$$q = (1/\sqrt{2})[(\sigma_1 - \sigma_2)^2 + (\sigma_2 - \sigma_3)^2 + (\sigma_3 - \sigma_1)^2]^{1/2} \quad (5)$$

Results reported by Maree (9), when similarly expressed, produce a failure ratio of q/p = 2.3, which, in view of the fact that the two studies were totally independent and carried out on materials from widely different sources, adds considerably to confidence in applying this failure criterion.

For the purpose of pavement analysis, if the limiting q/p ratio of 2.2 was exceeded in the granular layer, an arbitrarily low value of modulus (3 MPa) was inserted into the calculation procedure. Since it was not considered to be physically possible for the stiffness of the granular material to reduce abruptly when failure occurs, the failure criterion included a modulus reduction routine as failure was approached. A lower limit of stress ratio q/p = 1 was set and, between this value and q/p = 2.2, the modulus was obtained by interpolating between the value appropriate to the stress conditions given by Equation 2 and the failure modulus, according to the distance across the zone bounded by q/p = 1 and q/p = 2.2. Figure 2 is a general plot in p–q stress space that shows the three zones in which the model operates and the appropriate formulas for modulus derivation. The lower limit of q/p = 1 for applicability of Equation 1 was selected after consideration of the experimental evidence, which suggests that it is only appropriate for stresses well below failure (2,3).

Figure 1. K_o values as a function of granular layer thickness.

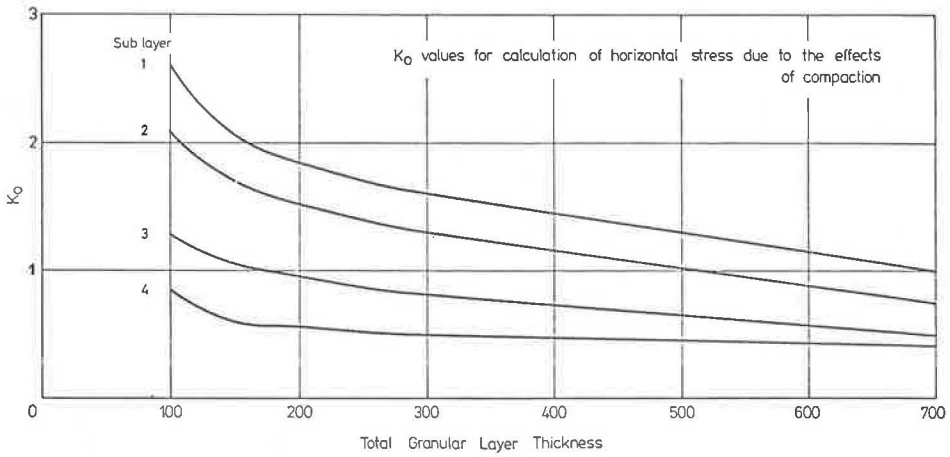

Figure 2. Derivation of granular material modulus for the three stress zones.

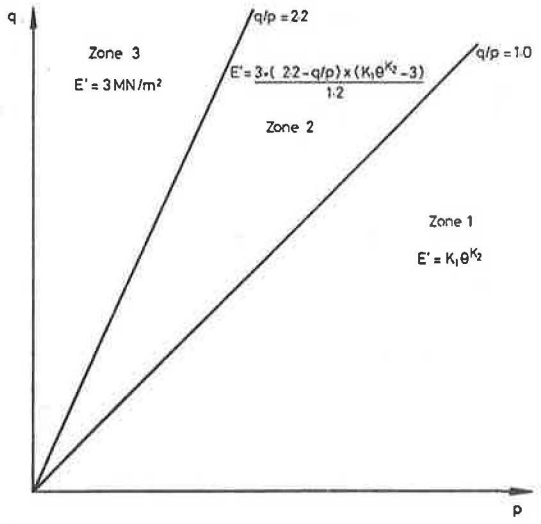

Figure 3. Flowchart for the modulus iteration procedure.

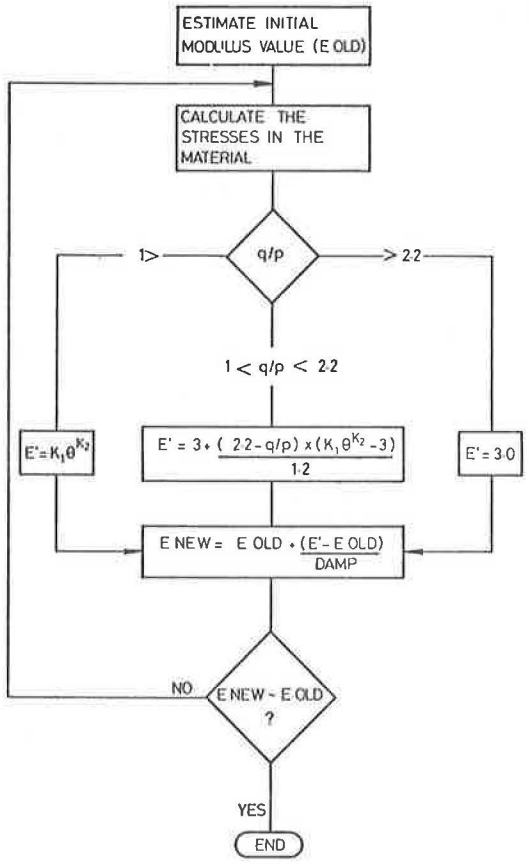

The Nonlinear Model

The nonlinear model finally incorporated into the ADEM pavement-design program was developed around the BISTRO (10) program produced by Shell. In this system, the full vehicle load is applied to the structure through dual wheels. The granular layer is divided into four sublayers, and an iteration procedure that starts with assumed moduli for each sublayer is followed until two consecutive modulus iterations agree to within 5 percent or 3 MPa, whichever is greater, for all four layers.

Stresses for the iterative procedure are calculated on the axis of symmetry of the dual-wheel-load configuration at the center of each sublayer. No attempt is made to consider horizontal variation in the modulus. To speed convergence, the iteration procedure is damped, as indicated in the flowchart of Figure 3; the damping factor ranges from 2 to 5.

EFFECT OF FAILURE CRITERIA

Stress Distribution

Figures 4 and 5 are p-q plots of the stress distribution within the granular layer for structures with 50 mm and 200 mm of asphalt surfacing that has a stiffness of 7000 MPa. Three thicknesses of granular layer (h_2) have been considered--200, 450, and 700 mm. As would be expected, the most highly stressed granular layer is in the structure that has only 50 mm of asphalt surfacing. It can be seen clearly that, in this structure (Figure 4), q is high and p is low; this combination gives a failure condition throughout the layer. Within this structure the failure criterion has the effect of both reducing q and increasing p to bring the layer within zone 2 of the model (Figure 2), although it remains close to failure.

Figure 5 shows that with a 200-mm asphalt surfacing the stress in the granular layer is much reduced. With the exception of the bottom sublayer in the 200-mm granular layer, the q/p stress ratio does not exceed 2.2. However, in this structure the failure criterion still has a significant

Figure 4. Stress distribution within the granular layer for a structure with 50 mm of asphalt surfacing.

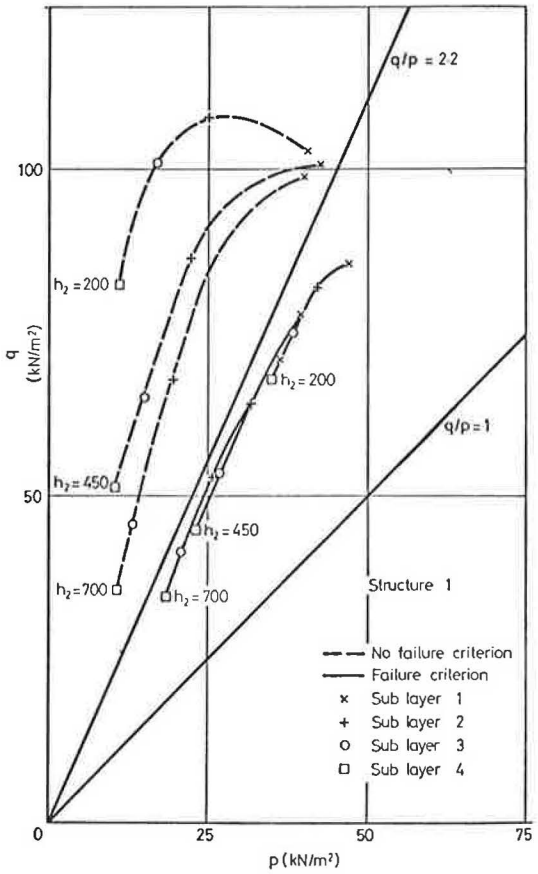

Figure 5. Stress distribution within the granular layer for a structure with 200 mm of asphalt surfacing.

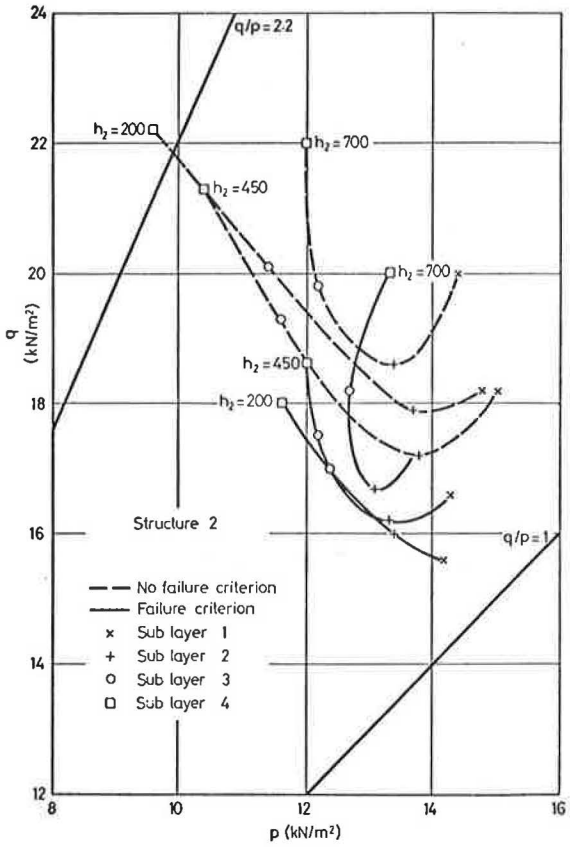

effect on the stress distribution, mainly by reducing q.

It should be noted that the stress distributions in the granular layer for the two surfacing thicknesses are quite different. For 50-mm surfacing both p and q decrease from the top sublayer (sublayer 1) to the bottom (Figure 4). However, when the layer is surfaced with 200 mm of asphalt (Figure 5), the variation in stress with depth is less consistent, although generally p decreases and q increases. This results in a stress distribution that becomes more severe with depth, the q/p ratio generally increasing with depth. Thus, although under 50-mm surfacing the entire granular layer is near failure because it lies along a line of approximately constant q/p, for 200-mm surfacing the stress distribution (q/p ratio) becomes more severe with depth.

Figures 6 and 7 show the derived moduli for the four sublayers for each structure. The effect of the failure criterion is particularly significant for pavements with only 50 mm of surfacing (Figure 6), in which the derived moduli for nearly all sublayers is less than the subgrade modulus and in all cases less than half the modulus derived without regard to failure. For the structures surfaced with 200 mm of asphalt (Figure 7), the effect of the failure criterion is much reduced, as would be expected from the stress distribution (Figure 5), but the use of the failure criterion still indicates a reduction in the derived modulus.

Primary Response Parameters

The effect of the failure criterion on primary response parameters is shown in Figures 8 and 9 as a function of granular layer thickness for the two asphalt-surfacing thicknesses. Structure 1 is surfaced with 50 mm of asphalt, and structure 2 is surfaced with 200 mm. The two parameters chosen—vertical strain on the subgrade and tensile strain at the bottom of the asphalt layer—are commonly used as design criteria in flexible-pavement design and are included as such in ADEM.

It is clear that for a thin asphalt surfacing there is a significant difference between the results obtained by the linear and nonlinear systems; the nonlinear analysis, as would be expected from the lower derived moduli, always gives the greater strain. It is also important to note that, although asphalt strain decreases as the granular layer thickness increases if potential failure is ignored, it increases as the granular layer thickness increases when failure is considered.

It was therefore concluded that it is essential to consider material failure in a nonlinear model for granular layers. Accordingly, the failure criterion was included in the model for granular layers incorporated in the ADEM design program used to produce the results discussed in the following section.

EFFECT OF NONLINEAR MODEL ON DESIGN THICKNESS

Having developed a system for nonlinear characterization of granular layers, we investigated the effect of using this model on the design thickness of an asphalt pavement. To do this, the nonlinear model was incorporated as an option in the ADEM design program, so that pavements could be designed on the basis of linear or nonlinear characterization of the granular layer. For the linear designs a modular ratio of 2.5 was used between the granular layer and subgrade.

It is not the purpose of this paper to discuss ADEM, but a brief description of the program is given since it was used to derive these results. ADEM produces the required thickness of the asphalt layer for a given design life by analyzing a trial structure and adjusting the asphalt-layer thickness to ensure that the design criteria are satisfied. Two performance parameters are used: (a) tensile strain in the

Figure 6. Derived moduli for the granular sublayers for a structure with 50 mm of asphalt surfacing.

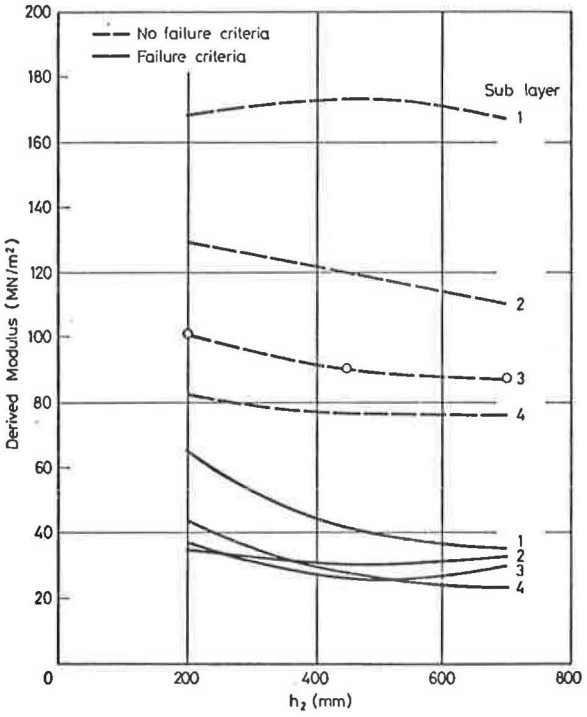

Figure 7. Derived moduli for the granular sublayers for a structure with 200 mm of asphalt surfacing.

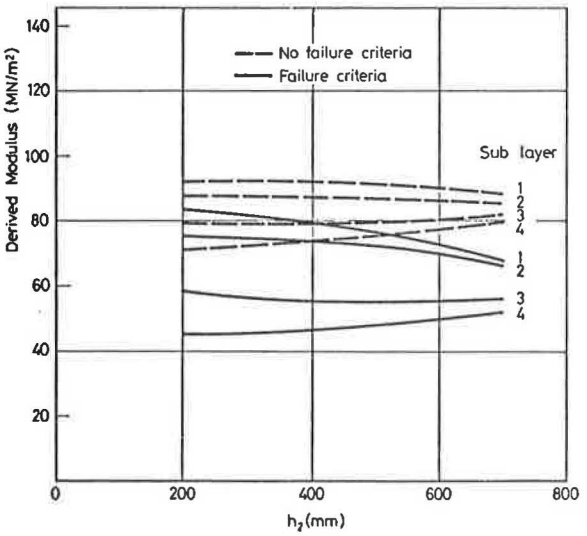

asphalt layer to design against asphalt fatigue failure and (b) vertical strain on the subgrade to design against overall deformation failure. Limiting values of these strains are obtained within the program from knowledge of the strain-life relationships and are used as criteria for the design process. Designs have been produced for assessing the effect of nonlinear modeling of the granular layer for a wide range of parameters. The variables studied were subgrade modulus (E_S), granular material quality characterized by variation in K_1 (Equation 1), granular layer thickness (h_2), and bitumen content and void content of the asphalt mix. Design life, traffic speed, bitumen grade, and temperature have been held constant throughout

Figure 8. Effect of the failure criterion on asphalt strain.

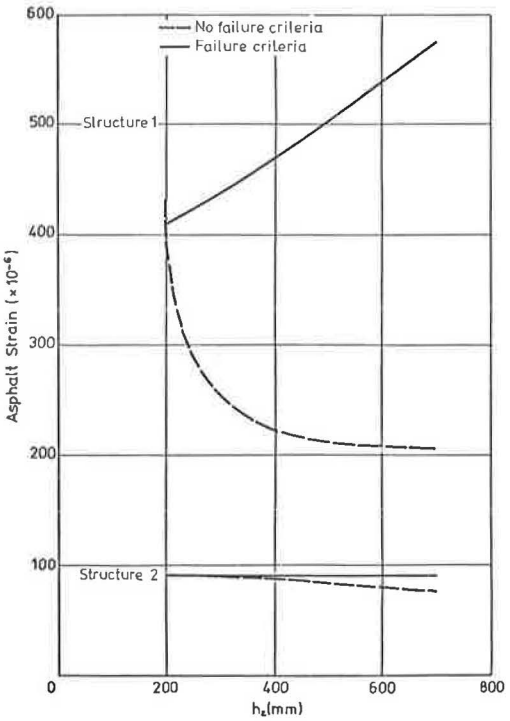

Figure 9. Effect of the failure criterion on subgrade strain.

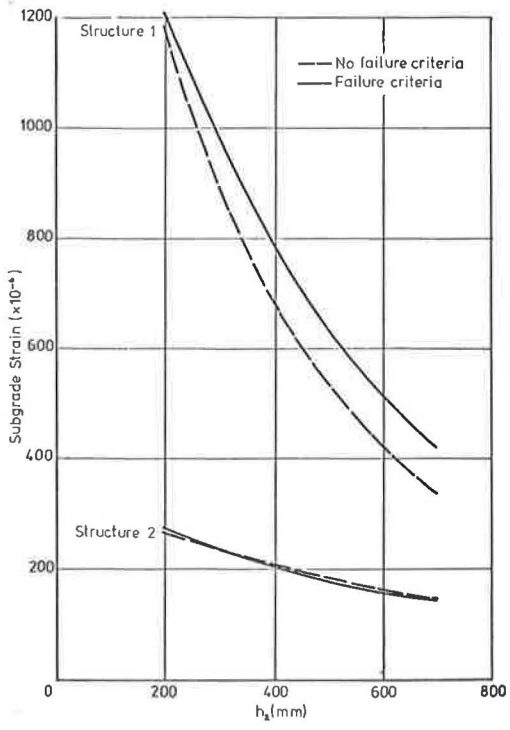

the study at 50 million standard axles, 80 km/h, penetration value of 100, and 15°C, respectively.

Figure 10 shows design thicknesses as a function of granular layer thickness for three values of subgrade modulus and granular material quality (K_1). The effect of variation in K_1 is very small, so a constant value of 400 was used for subsequent studies. For the lowest subgrade modulus (E_S = 20 MPa), linear and nonlinear characterization

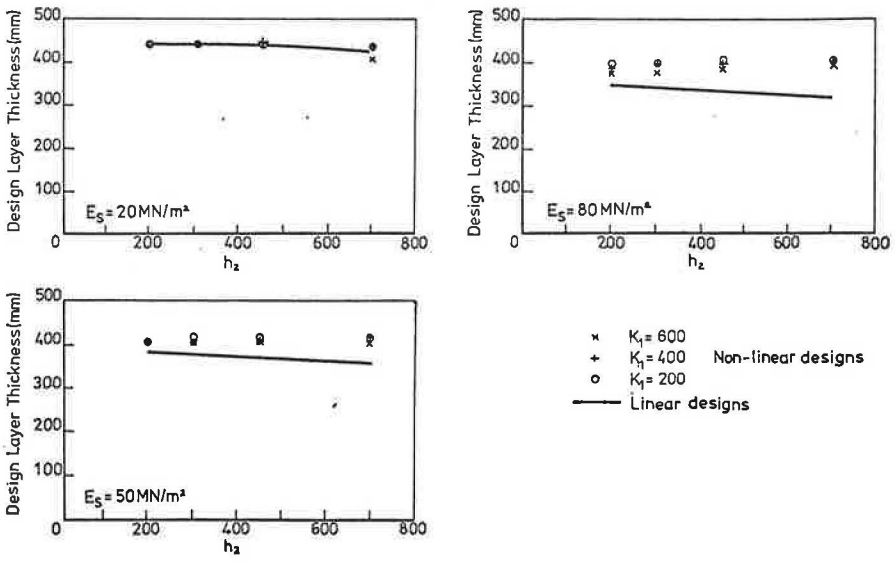

Figure 10. Design thicknesses as a function of granular layer thickness.

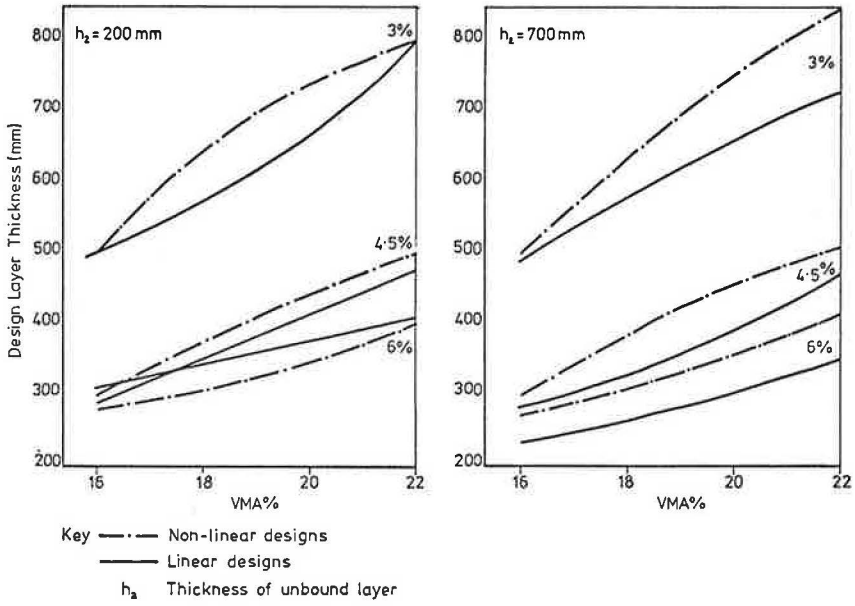

Figure 11. Design thicknesses as a function of VMA and binder content.

produced identical design thicknesses. As the subgrade modulus increases, the two methods of treating the granular layer start to give different answers; the thickness requirement by using the nonlinear system is greater than that for the linear system. The differences between the two systems are greatest on the stiffest subgrade (E_S = 80 MPa) and for thick granular layers (h_2 = 700 mm), but the differences are still not large. It is interesting to note that the granular layer thickness does not greatly affect the asphalt thickness, but designs produced with the nonlinear option are less sensitive to variation in granular layer thickness than those produced by means of the simple linear option.

The parameter termed "voids in mixed aggregates" (VMA) has been introduced to study the effect of mix variables since it is a useful parameter for describing a bituminous mix, particularly with regard to its state of compaction (11). Recent research has indicated that for U.K. mixes and conditions, VMA values of 16, 19, and 22 percent may be taken as approximately representative of good, average, and poor compaction, respectively. In order to examine a range of mixes, bitumen contents of 3, 4.5, and 6 percent by mass were assumed; the calculated void contents for the various combinations of VMA and bitumen content are given below:

	Binder Contents (%)		
VMA (%)	3	4.5	6
16	9.1	5.5	1.8
19	12.4	10.0	5.3
22	15.6	12.3	8.8

Figure 11 shows design thicknesses as a function of VMA and binder content; designs produced by both linear and nonlinear options are compared for two thicknesses of granular layer and a subgrade modulus of 50 MPa.

In all but one case, the design thicknesses of asphalt based on nonlinear analysis are greater than those based on linear analysis. It is therefore evident that significant differences in design-thickness requirements can be obtained if the granular layer is characterized as nonlinear rather than linear elastic.

It was concluded from this design study that linear-elastic characterization of granular layers may be

adequate for comparative design studies but, if a pavement design is required for a highway project, nonlinear characterization of the granular layer is highly desirable. The findings generally confirm those obtained by Dehlen and Monismith (12).

It is not the purpose here to discuss the implications for asphalt-mix design of the results plotted in Figure 11, but we feel that an explanation for the decrease in design thickness with increase in bitumen content is required. Increasing the bitumen content in a mix decreases the stiffness of that mix and increases its fatigue resistance. Reduced mix stiffness means that the tensile strain developed in the bottom of the asphalt will increase, and an increased design thickness may therefore be expected in order to compensate for this. However, for the case illustrated in Figure 11, the improvement in fatigue performance and thus the increased allowable strain is much more significant than is the stiffness loss; hence a reduced layer thickness results. It must be emphasized that reduction in thickness with increased binder content will only be achieved for structures in which fatigue is the critical parameter and will not necessarily be achieved for all these structures.

SUMMARY AND CONCLUSIONS

1. It is essential to include a failure criterion in a system for nonlinear analysis of granular materials.
2. In conventional pavement structures the potentially high modulus of a granular material generally cannot be realized because, when it is highly stressed, the material approaches a failure stress state with a consequent reduction in modulus.
3. Nonlinear characterization of unbound granular layers is required for accurate designs, particularly when thin asphalt surfacings are contemplated.
4. In pavement structures that have asphalt layers of about 300 mm, the required thickness of the asphalt layer is not greatly affected by the thickness of the granular layer.

ACKNOWLEDGMENT

The work on which this paper is based was conducted at the University of Nottingham during a period when one of us (A.F. Stock) was employed as a senior research assistant. The project was undertaken as part of a contract with the Asphalt and Coated Macadam Association. We are grateful for the advice of P. S. Pell and the provision of facilities by R. C. Coates. The assistance of the staff of the Cripps Computing Centre is also gratefully acknowledged.

REFERENCES

1. S. F. Brown, P. S. Pell, and A. F. Stock. Application of Simplified Fundamental Design Procedures for Flexible Pavements. Proc., 4th International Conference on the Structural Design of Asphalt Pavements, Univ. of Michigan, Ann Arbor, Vol. 1, 1977, pp. 327-341.
2. R. G. Hicks. Factors Influencing the Resilient Response of Granular Materials. Univ. of California, Ph.D. thesis, 1970.
3. J. R. Boyce, S. F. Brown, and P. S. Pell. Resilient Behaviour of a Granular Material Under Repeated Loading. Proc., Australian Road Research Board, Vol. 8, 1976, pp. 8-9.
4. E. Smith. Prediction of Equivalent Granular Base Moduli Incorporating Stress Dependent Behavior in Flexible Pavements. Univ. of Maryland, College Park, M.S. thesis, 1977.
5. C. L. Monismith, H. B. Seed, F. G. Mitry, and C. K. Chan. Predictions of Pavement Deflections from Laboratory Repeated Load Tests. Proc., 2d International Conference on the Structural Design of Asphalt Pavements, Univ. of Michigan, Ann Arbor, 1967, pp. 109-140.
6. E. W. Brooker and H. O. Ireland. Earth Pressures at Rest Related to Stress History. Canadian Geotechnical Journal, Vol. 2, No. 1, Feb. 1965, pp. 1-15.
7. T. W. Lambe and R. V. Whitman. Soil Mechanics. Wiley, New York, 1969.
8. J. R. Boyce. Behaviour of a Granular Material Under Repeated Loading. Univ. of Nottingham, Ph.D. thesis, 1976.
9. J. H. Maree. Discussion of paper, South African Mechaniste Pavement Design Procedure, by R. N. Walker, W. D. O. Paterson, C. R. Freeme, and C. P. Marais. Proc., 4th International Conference on the Structural Design of Asphalt Pavements, Univ. of Michigan, Ann Arbor, 1977.
10. M. G. F. Peutz, H. P. M. Van Kempen, and A. Jones. Layered Systems Under Normal Surface Loads. HRB, Highway Research Record 228, 1968, pp. 34-45.
11. D. Leech and W. D. Powell. Levels of Compaction of Dense Coated Macadam Achieved During Pavement Construction. U. K. Transport and Road Research Laboratory, Crowthorne, Berkshire, England, TRRL Rept. 619, 1974.
12. G. L. Dehlen and C. L. Monismith. Effect of Nonlinear Material Response on the Behavior of Pavements Under Traffic. HRB, Highway Research Record 310, 1970, pp. 1-16.

Publication of this paper sponsored by Committee on Flexible Pavement Design.

Analysis of In Situ Granular-Layer Modulus from Dynamic Road-Rater Deflections

PAUL A. D'AMATO AND MATTHEW W. WITCZAK

The major objective of this study was to investigate the ability of elastic-layer theory coupled with nonlinear dynamic modulus tests to predict pavement deflections in a way comparable to dynamic road-rater deflection measurements on three highway sections in Maryland. It was found that theoretically predicted deflections were two to four times the measured road-rater deflections for all three pavement sections studied at all four road-rater sensor locations and for all times throughout the year in which road-rater deflections were made. To obtain equality between predicted and measured deflections, the granular-layer modulus was adjusted by using a K_1-factor. A linear log-log relationship was evident when the K_1-adjustment factor was plotted versus measured surface deflections. It was concluded that the current laboratory method of modulus characterization underestimates the modulus of a granu-

lar material and that an increase in surface deflection results in a decrease of the granular-layer modulus. An investigation was undertaken to determine whether the effect of shear strain was responsible for the decrease in granular-layer modulus. It was found that the granular-layer modulus decreases with increasing shear strain and that shear strain is proportional to surface deflection. The former finding substantiates other research dealing with the dynamic response of granular soils. The study of the K_1-factor and modulus adjustment also led to the development of equations that relate measured surface deflection to in situ granular-layer modulus. For two of the pavements analyzed, predicted granular-layer modulus showed very good agreement with the modulus required for equal computed and measured deflections.

The use of nondestructive deflection measurements has long been recognized as a valuable indicator of a pavement's structural characteristics. Early test-road studies that investigated flexible pavements include the WASHO Road Test (1) in 1952 and the AASHO Road Test (2) begun in 1958. Both these road tests developed correlations of Benkelman-beam deflections with pavement performance.

In recent years, research efforts have also been directed toward the development of deflection-based procedures that could be used to determine in situ moduli of pavement component layers. Determination of layer moduli allows critical stresses and strains to be evaluated by multilayer theoretical approaches. From these critical parameters, estimates by various techniques of remaining pavement life can be used for overlay and rehabilitation purposes.

STUDY OBJECTIVE

This study, part of an overall study of remaining life of flexible pavements, examined three Maryland highway sections in detail (3). Samples of each of the component layer materials were obtained for all of these flexible pavements, and appropriate routine and dynamic laboratory modulus tests were conducted (4,5). In addition, surface-deflection basin measurements on the same pavement sections were determined by means of a road-rater loading device by the Maryland State Highway Administration (MSHA).

The first objective of this study was to assess how well theoretically predicted deflections that used laboratory-determined dynamic moduli along with multilayer theory compared with observed measured deflections obtained from road-rater measurements. Inherent to the multilayer analysis, nonlinear behavior of both granular material (base, subbase) and fine-grained subgrade soils was accounted for. The results of this comparison showed that the computed deflections for the pavement model were not in agreement with observed behavior.

The second consideration hence involved adjusting the pavement model so that the pavement structure, elastic theory, and road-rater deflection measurements agreed. The modulus of the granular base layer was selected for this adjustment because the results of previous research indicated that this was possible (6-8). Relationships for the determination of in situ granular-layer modulus were developed by using the adjusted granular-layer modulus and corresponding road-rater deflections.

Table 1. Input for pavement routes in elastic-layer study.

Pavement Section	Layer	Thickness (cm)	Modulus Relationship (M_R)
US-1	Asphalt concrete		
	Surface	3.1	
	Binder	4.8	
	Base	5.3	
	Granular base		$4\,886\theta^{0.239}$
	1	13.5	
	2	13.5	
	3	13.7	
	Subbase		$2\,632\theta^{0.426}$
	1	31.8	
	2	31.8	
	Subgrade		$57\,962\sigma_d^{-0.696}$
MD-97, section 1	Asphalt concrete		
	Surface	3.8	
	Base	7.9	
	Granular base		$8\,787\theta^{0.365}$
	1	12.4	
	2	12.7	
	3	12.7	
	Subgrade		
	A		$16\,333\sigma_d^{-0.345}$
	B		$13\,035\sigma_d^{-0.180}$
MD-97, section 2	Asphalt concrete		
	Surface	3.8	
	Base	7.9	
	Granular base		$8\,787\theta^{0.365}$
	1	12.4	
	2	12.7	
	3	12.7	
	Subgrade B		$13\,035\sigma_d^{-0.180}$
I-695	Asphalt concrete		
	Surface	6.6	
	Base	19.8	
	Subbase		
	1	9.9	$3\,378\theta^{0.520}$
	2	12.7	$3\,683\theta^{0.517}$
	3A-E	24.5[a]	$4\,856\theta^{0.487}$
	Subgrade		$25\,925\sigma_d^{-0.309}$

Notes: 1 cm = 0.39 in.
Regression equations developed in U.S. customary units (1 lbf/in² = 0.145 kPa).
[a]Five layers, each 24.5 cm thick.

METHOD OF ANALYSIS

The study was conducted on pavement sections of MD-97, I-695, and US-1. For each of these pavement sections, layer thicknesses, material type, and modulus characterizations were ascertained in the remaining-damage portion of the research (4). Table 1 summarizes the required pavement input necessary for the theoretical study of elastic layers. The asphalt modulus relationships were obtained from Shell nomographs and are functions of pavement temperature and load frequency. The temperature within each asphalt layer for each road-rater test date was evaluated from temperature measurements of the pavement surface and relationships developed by Southgate (9). In addition, all unbound granular and subbase and the subgrade soils for all pavements were characterized by the nonlinear (stress-dependent) resilient modulus tests.

Figure 1 illustrates the actual road-rater loading and measuring system and the equivalent system used in the theoretical analysis. The equivalent systems were necessary because the elastic-layer program used is based on circular loads rather than on the actual rectangular foot pads on the road rater. The road rater applies a static preload of 6.0 kN (1350 lbf) and has a variable peak-to-peak dynamic load capability (formulated in U.S. customary units) defined by:

$$F_{p\text{-}p} = 32.704f^2D \quad (1)$$

where

$F_{p\text{-}p}$ = peak-to-peak dynamic force (lbf),
f = load frequency (Hz), and
D = peak-to-peak dynamic displacement or amplitude (in).

The load and contact pressure used in the theoretical study for the equivalent-circular-area loading condition (Figure 1) for the various combinations of f and D used by MSHA to obtain measured road-rater deflections are shown in Table 2.

The theoretical elastic-layer model used in the analysis was the Chevron NLAYER program. Because this program is capable only of solving for states of stress, strain, and deflection due to a single wheel load, superposition principles for total deflection at each sensor location were used.

Road-rater deflections were measured on six test dates for each pavement section under investigation. These measurements were made in 1975 and 1976 and encompassed all seasons. For each test date, deflection measurements

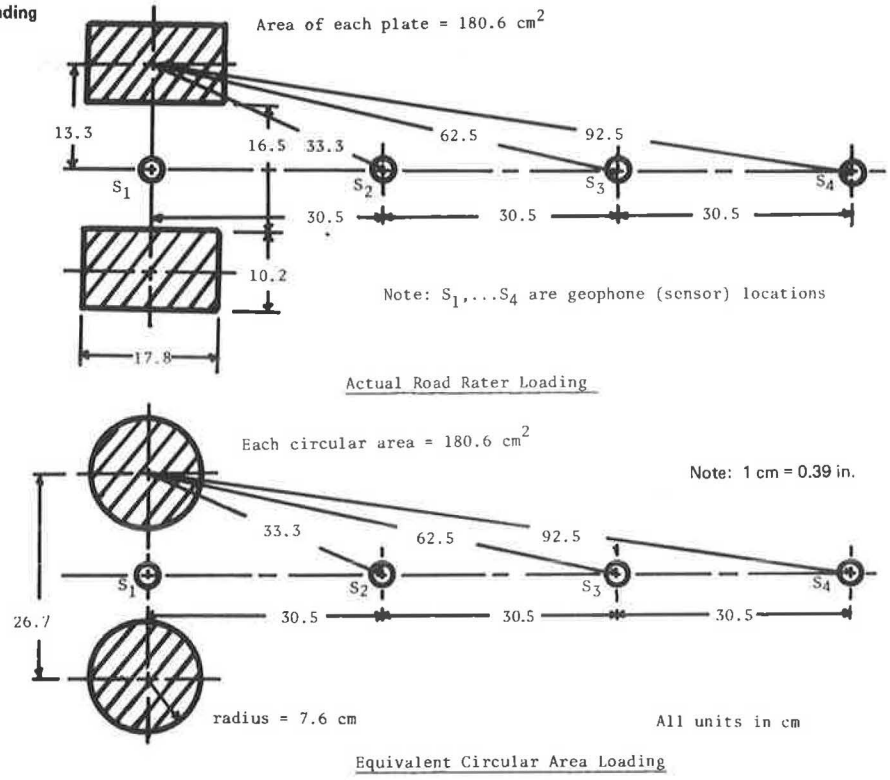

Figure 1. Actual and equivalent road-rater loading geometry.

Table 2. Road-rater dynamic-load summary.

Frequency (Hz)	D (mm)	F_{p-p} (kN)	F_{p-p} Each Circular Load (kN)	Contact Pressure (kPa)
16	1.47	2.16	1.08	59.8
25	1.47	5.27	2.64	146.1
25	0.96	3.45	1.73	95.7
25	1.98	7.09	3.55	196.4

Note: 1 mm = 0.04 in; 1 kN = 224.8 lbf; 1 kPa = 0.145 psi.

were recorded at 161-m (0.1-mile) intervals. The length of each pavement test section ranged from 427 m (1400 ft) to 610 m (2000 ft).

SUBGRADE-LAYER STUDY

Before the main deflection comparison study was undertaken, several preliminary studies were conducted to establish the sensitivity of these items to the overall predictive deflection analysis. One such consideration was an analysis to determine the minimum number of subgrade layers necessary to model each pavement section. This was necessary because the moduli of the subgrades were characterized by nonlinear models. Thus, as the stress induced by the road rater decreases with depth into the subgrade, the modulus constantly changes. As a result, a study was undertaken to establish how many sublayers within the subgrade, if any, were necessary before an equilibrium deflection was reached.

The results of this analysis are summarized as the percentage of change in predicted deflection between three-layer and one-layer subgrade systems.

	Percentage Change for Sensor Locations				
Highway Route	S1	S2	S3	S4	Avg
US-1	0.3	0.5	0.8	3.3	1.2
MD-97					
Section 1	1.8	2.3	3.6	5.4	3.3
Section 2	3.0	3.8	6.7	9.8	5.8
I-695	7.6	5.5	4.6	6.8	6.1
Avg	3.2	3.0	3.9	6.3	4.1

Three 30.5-cm (12-in) sublayers were used within the subgrade in the three-layer system. As can be seen, the percentage of change due to subdividing the subgrade into three layers is quite small, especially at sensor locations 1, 2, and 3. For all combinations considered, the average percentage of change is less than 5 percent. As a result of this study, it was concluded that a one-layer subgrade system was sufficiently accurate to predict deflections with the road-rater-induced loads (stresses) and that it was not necessary to subdivide the subgrade layer for the deflection analysis.

STATIC PRELOAD STUDY

Research by the U.S. Army Engineer Waterways Experiment Station (10) that used large road vibrators, 22.25-89.0 kN (5 000-20 000 lbf), has shown that dynamic stiffness of a pavement (ratio of dynamic load to deflection) is dependent on the magnitude of the applied dynamic and static loads. As the static load of the vibrator is increased, the measured deflections due to the dynamic load have been found to decrease. Whether or not the computed surface deflections would decrease significantly on the inclusion of the 6.0-kN (1350-lbf) static load of the road rater was unknown.

To determine whether θ (bulk stress) due to static preload should be included in the deflection study, an analysis was conducted. Pavement deflections were computed for each pavement section after solving for stress-dependent layer moduli (by trial-and-error iteration) with and without the static preload.

Figure 2. Comparison of predicted pavement deflections and mean measured road-rater deflections by sensor location.

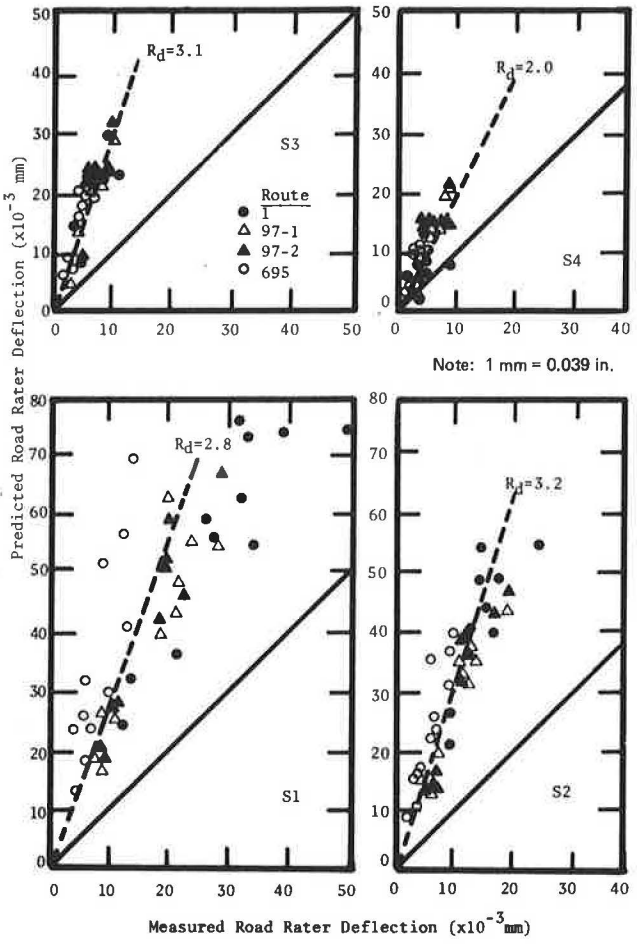

Figure 3. Comparison of predicted to measured deflections.

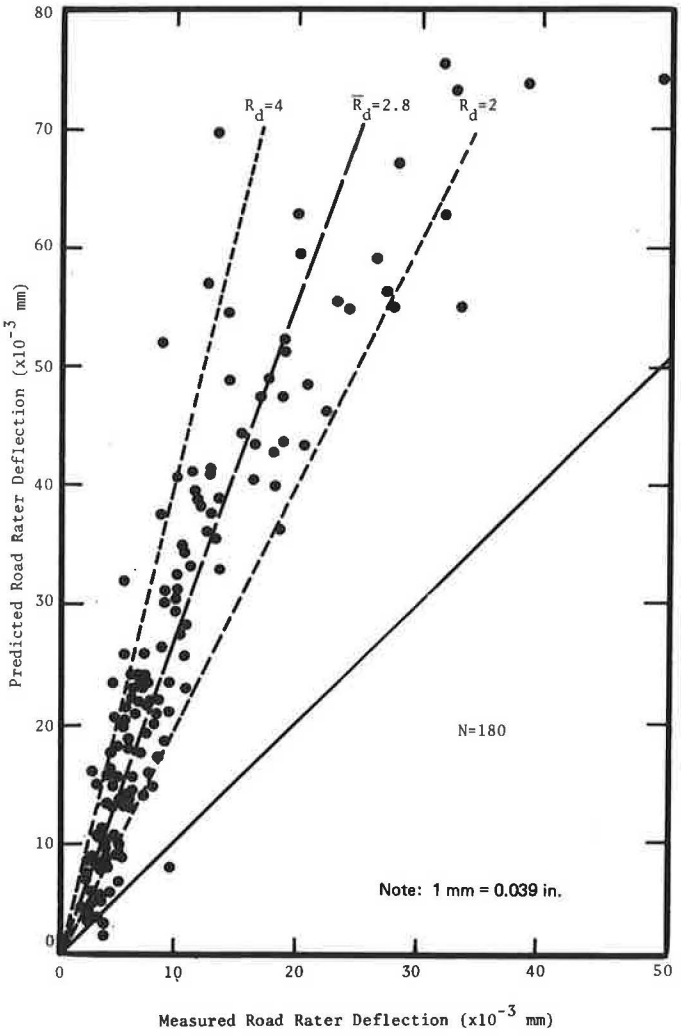

A summary of these results is shown below:

Highway Route	Percentage Change for Sensor Locations S1	S2	S3	S4	Avg
US-1	3.2	3.5	3.8	3.7	3.6
MD-97					
Section 1	5.0	5.3	3.3	0.0	3.4
Section 2	5.1	4.8	4.3	4.5	4.7
I-695	5.1	5.8	6.0	3.2	5.0
Avg	4.6	4.9	4.4	2.9	4.2

As shown, the percentage of change in deflections with and without the static preload bulk stresses is quite insignificant and again averages less than 5 percent. Accordingly, it was concluded that the influence on predicted deflections of incorporating the additional bulk stress increment due to the static preload of the road rater is negligible and for all practical purposes can be ignored.

DEFLECTION COMPARISON

In the theoretical deflection study, a total of 180 separate deflection predictions were made for each measured (road-rater) combination of pavement section, test date, and sensor location (3,5). In this analysis, the mean measured deflections (within a test section) were used together with the mean values of pavement layer thicknesses and mean layer modulus properties for the theoretical study. Hence all comparisons shown are between average measured deflections and average predicted deflections.

Figure 2 summarizes the comparisons between predicted (δ_p) and measured (δ_m) deflections by sensor locations. Figure 3 is a summary of the 180 data points investigated. The R_d value shown on these diagrams is the deflection ratio of predicted to measured deflections: $R_d = \delta_p/\delta_m$.

Based on this study, it is quite obvious that the deflections predicted by multilayer elastic theory (within a nonlinear iterative approach to layer modulus evaluation) are generally two to four times as large as those measured by the road rater. In general, it also appears that the deflection ratios for the thick asphalt pavement (I-695) were slightly higher than those for US-1 and MD-97, which are composed of more-conventional flexible-pavement [thin asphalt concrete (AC) and granular-base] structures.

K_1-INVESTIGATIVE STUDY

A study was then conducted to see whether the difference between predicted and measured deflections could be explained in a rational and logical manner. Assuming that the model selection of multilayer elastic theory is not the salient reason for the discrepancy, it is apparent that for the predicted (theoretical) deflections to be greater than the measured deflections the elastic modulus of a layer (or layers) characterized by laboratory tests and used as input into the theoretical model must be less than the in situ or apparent field-modulus response.

In a study conducted by Jones and Witczak (8) on San Diego test-road sections, computed pavement deflections

determined by means of laboratory-modulus relationships and multilayer theory were also found to be larger than measured surface deflections. In this study, two important conclusions were reached:

1. For test sections made of asphalt-treated base materials, the mean deflection-derived subgrade modulus of 13 728 kPa (20 000 psi) agreed well with the mean value of modulus predicted from the regression models developed from direct laboratory testing of field samples.
2. In the derivation of the subgrade modulus from deflection measurements, for the granular-base test sections, the comparison between the derived moduli and those determined from direct laboratory testing on field cores was very poor. For these types of bases, the stress-dependent function for the modulus of the base, determined from laboratory tests, tended to underpredict the in situ response of the granular material.

In essence, the results of this study suggest that it is the manner in which the unbound granular materials are characterized rather than the subgrade that may be responsible for the difference between predicted and measured deflections. Because of the similarities in relative results between the two studies, it was decided to investigate the granular material and its corresponding resilient-modulus characterization test (in the laboratory) to help explain the deflection deviations observed in the road-rater study.

In dynamic laboratory testing of unbound granular materials, the nonlinear constitutive equation for resilient modulus is given by

$$M_R = k_1\theta^{k_2} \quad (2)$$

where k_1 and k_2 are laboratory-derived regression constants reflecting material type and physical properties and θ represents the first stress invariant (bulk stress), defined by the sum of the three normal stresses at a point (triaxial element).

Recalling that $\delta_p > \delta_m$, the above modulus expression can be adjusted by a factor, termed the K_1-factor, so that a new modular expression of the form shown below is introduced:

$$M_R = K_1k_1\theta^{k_2} \quad (3)$$

The unique K_1-factor required for $\delta_p = \delta_m$ ($R_d = 1.0$) was termed the K_1-factor at a 1.0 deflection ratio or $K_1(R_d = 1.0)$. The technique used to find $K_1(R_d = 1.0)$ for each measured deflection value (δ_m) was to repeat the theoretical study by using assumed values of K_1 and iterative stress solutions until the condition of $\delta_p = \delta_m$ was observed for each measured deflection value. For deflection values measured by sensors 2, 3, and 4, the deflection ratio (R_d) remained greater than unity even when a K_1-factor of 100 was tried. For these measured deflections, the study was terminated and $K_1(R_d = 1.0)$ remained undefined. Considering that $K_1(R_d = 1.0)$ was found for all sensor-1 deflections and that the Jones-Witczak study used deflections measured at the loading point (Benkelman beam), it was decided to consider only $K_1(R_d = 1.0)$ values derived from sensor-1 deflections for the remainder of the study.

In the Jones-Witczak study on the San Diego test sections, a linear relationship between log $K_1(R_d = 1.0)$ and log δ_m (measured deflection) was obtained from eight different flexible-pavement cross sections. In order to see whether the same analytical model was valid for this study, the relationship of the log of $K_1(R_d = 1.0)$ versus the log of δ_m was developed. Figure 4 shows the results of this study for the sensor-1 location. The correlation coefficients $r^2 = 0.26$ are obviously indicative of a poor fit when all three routes are analyzed together. Two separate relationships are shown on the plot. It should be recognized that the equation for the f = 25-Hz data is indicative of a road-rater load of 5.3 kN (1185 lbf), whereas the f = 16-Hz data are for a 2.16-kN (485-lbf) load. As such, although the correlations are poor, the data strongly suggest separation by magnitude of applied dynamic load. A further study of the data in Figure 4 showed that the I-695 data were significantly divergent from the US-1 and MD-97 relationship.

Figure 5 is the relationship developed for the same data shown in Figure 4 with the exception that the I-695 data (full-depth AC section) have been deleted from the analysis. The tremendous increase in the r^2-values from 0.26 to 0.87 and 0.90 signifies that a linear relationship between log $k_1(R_d = 1.0)$ and log δ_m is indeed valid from the flexible (granular-base) sections of US-1 and MD-97 identical to that found from the San Diego road test analysis. Because I-695 is a relatively thick asphalt-stabilized pavement, it appears that the results are not applicable to this pavement type based on the limited data available. However, at this time it cannot be unequivocally stated that a difference occurs between conventional flexible and thick stabilized sections. It must be noted that, because of the relatively thick asphalt section, a small error in the elastic modulus of the asphalt layer would have a significant effect on the theoretically predicted deflection initially computed.

Because the relationships developed appeared to be valid for pavement cross sections similar to the San Diego sections, this prompted a study of how the results of Figure 5 compared with the relationship developed from the Jones-Witczak San Diego study. Figure 6 illustrates these results. It is quite obvious that the results between studies are consistent, and this suggests that there is a family of log $K_1(R_d = 1.0)$-log δ_m lines that are functions of the applied load. By using Figure 6, Figure 7 was developed, which is assumed to be valid for flexible pavements (conventional granular base) and maximum deflection condition and warrants considerably more research because it may result in an extremely important development that would link theoretical to measured pavement deflections.

If Figure 7 was indeed found to be valid for all deflection combinations measured by load (P, δ_m), the required K_1-adjustment factor (for laboratory to field conditions) could be determined simply by using the measured road-rater deflection for a given road-rater load (frequency and amplitude).

The final interesting trend that was found from the K_1-investigation is shown in Figure 8. In this plot, log $K_1(R_d = 1.0)$ is seen to have an excellent correlation with the mean granular base modulus required to achieve a deflection ratio of $R_d = 1.0$. This relationship appears to be valid for all three routes studied (US-1, MD-97, and I-695) at both frequencies of the road rater as well as for the eight sections of the San Diego test road analyzed by Jones (8).

SHEAR STRAIN INVESTIGATION

Recent studies directed toward developing a better understanding of soil response under dynamic loading conditions have indicated that the shear modulus (G) of a granular soil is dependent on the level of shear strain. Idealized relationships have been developed that show that the shear modulus of a granular soil decreases with increasing shear strain (6), as shown in Figure 9. Of particular note in Figure 9 is the K_2-factor in the equation

$$G = 1000K_2(\sigma_m')^{1/2} \quad (4)$$

A similar equation would result if the elastic modulus (E) were substituted for the shear modulus. If the substitution is made, it becomes evident that the K_2-factor in the above equation is very similar in concept to the K_1-factor used in this study. Because of this important tie to dynamic response, it was decided to investigate the effect of shear strain on the $K_1(R_d = 1.0)$ values developed for US-1, MD-97, I-695, and the San Diego test-road sections.

Figure 4. K_1-factor at 1.0 deflection ratio versus mean surface deflection for all routes, sensor 1.

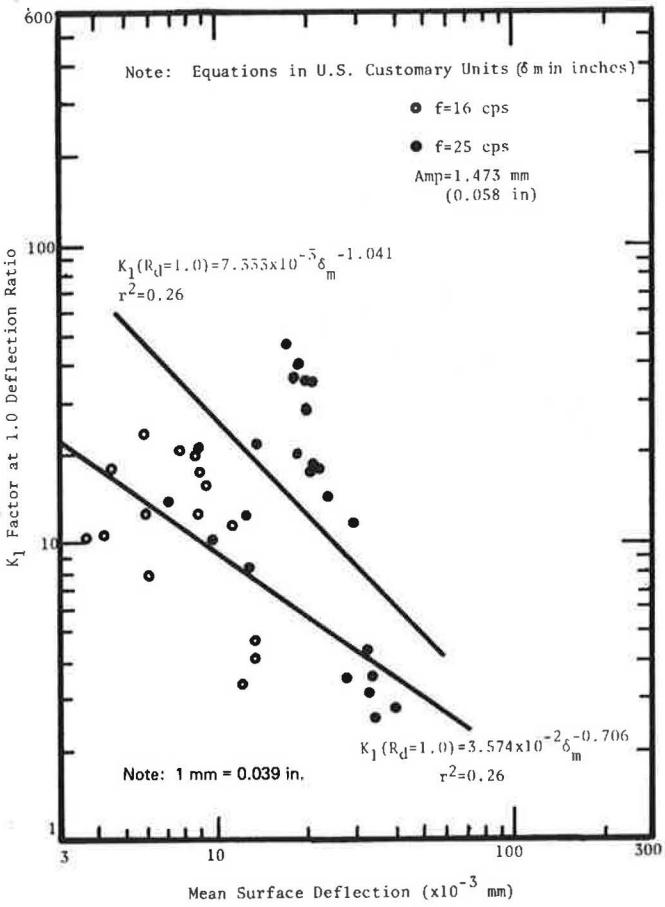

Figure 5. K_1-factor at 1.0 deflection ratio versus mean surface deflection for US-1 and MD-97, sensor 1.

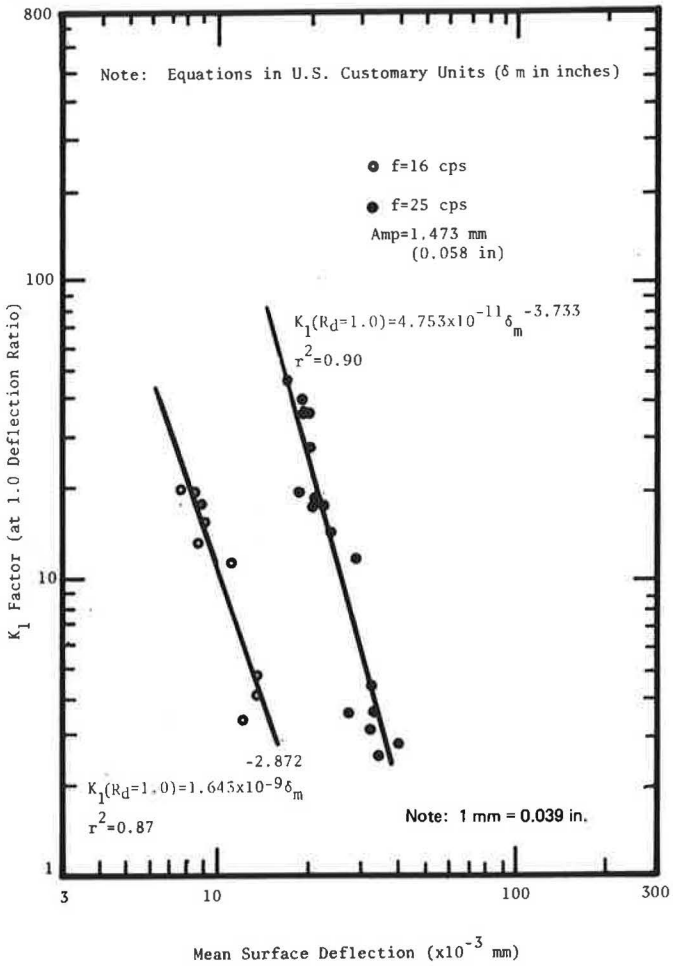

Figure 6. K_1-factor at 1.0 deflection ratio versus mean surface deflection for US-1, MD-97, and San Diego test-road sections.

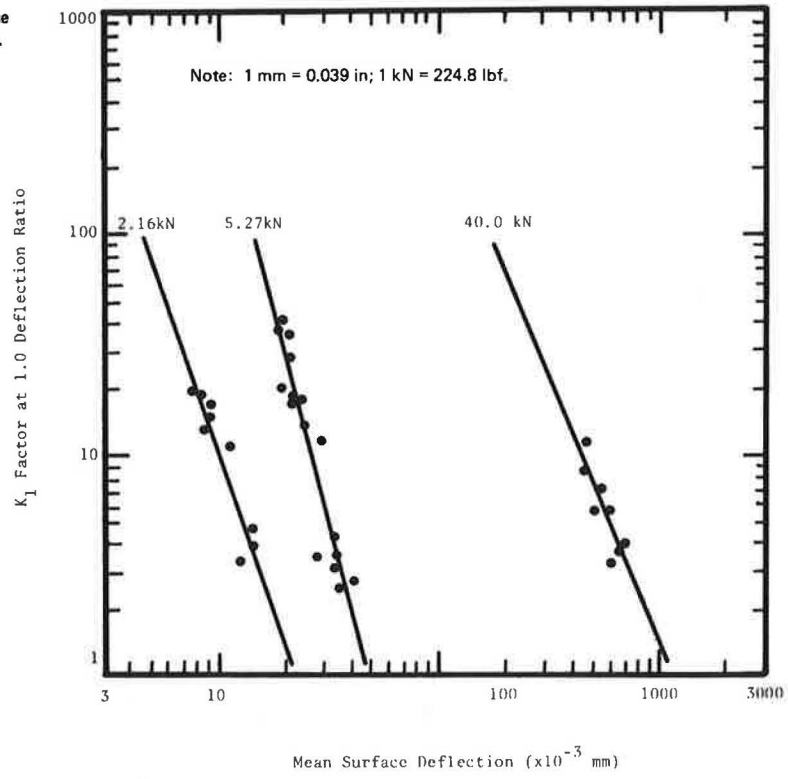

The theoretically predicted maximum shear strain for each adjusted pavement model ($\delta_p = \delta_m$) was determined in the following manner:

1. The modulus values of all pavement layers required for $R_d = 1.0$ were input into the NLAYER program. The granular layer was modeled as a single layer with an average modulus.
2. Strains computed by the NLAYER program and Mohr circle-of-strain relationships were used to evaluate

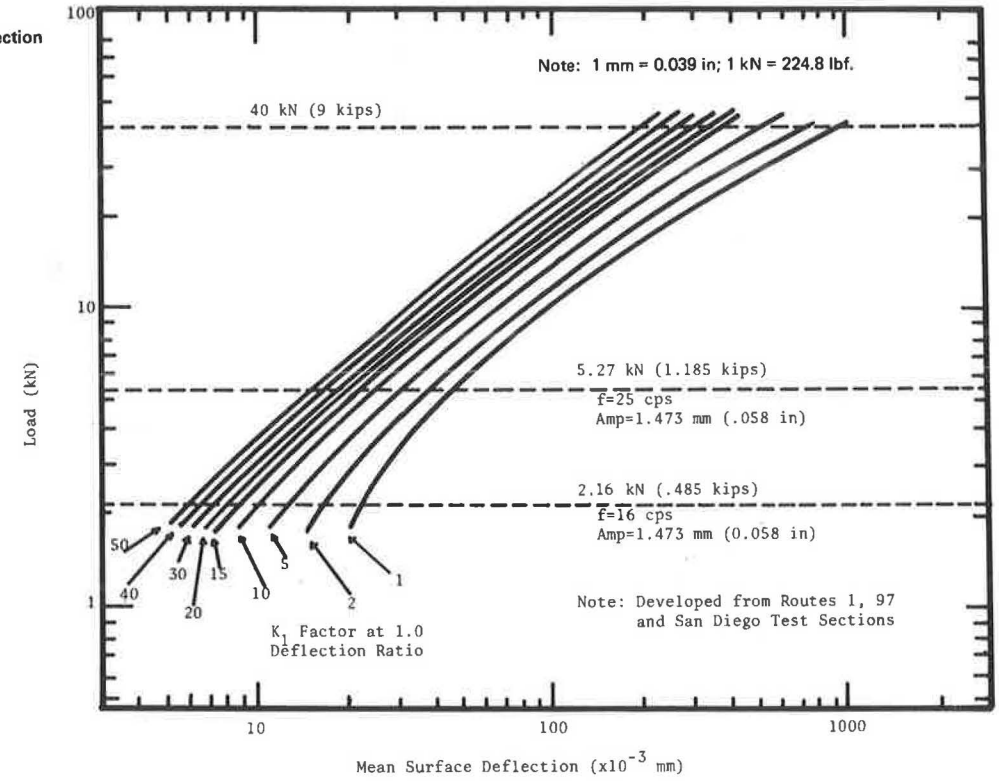

Figure 7. Load versus mean surface deflection for K_1-factors at 1.0 deflection ratio.

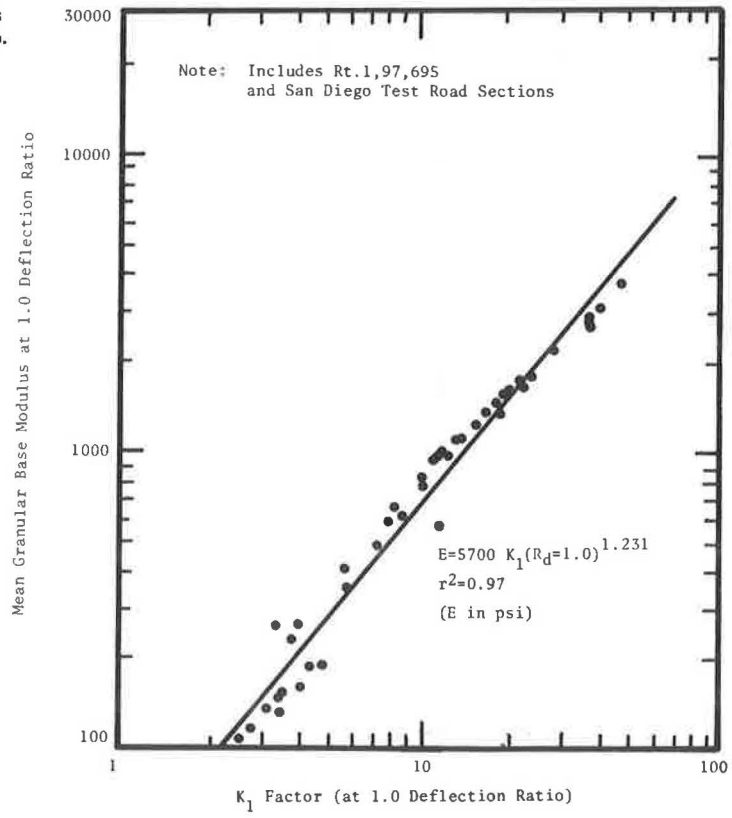

Figure 8. Mean granular base modulus versus K_1-factor at 1.0 deflection ratio.

the maximum shear strain at the middle of the granular layer.

The results of this study were used to develop the relationships shown in Figure 10. For each pavement loading, it can be seen that the $K_1(R_d = 1.0)$ value decreases with increasing shear strain. If we recall that $M_r = K_1 k_1 \theta^{k_2}$, an increase in shear strain [and corresponding decrease in $K_1(R_d = 1.0)$] would result in a decrease in the granular-base elastic modulus. This finding was considered to conceptually support previous findings that demonstrate a decrease in granular-soil shear modulus that results from increasing shear strain (Figure 9).

By comparing relationships shown in Figures 6 and 10, it is evident that the $K_1(R_d = 1.0)$ value decreases with respect to both increasing mean surface deflection and maximum shear strain. This would imply that maximum shear strain is proportional to mean surface deflection. A plot of maximum shear strain versus mean surface deflection is shown in Figure 11. A linear log-log relationship with a squared correlation coefficient of 0.97 results if the data points for I-695 are excluded from the analysis. For I-695, smaller shear strains occur at a particular surface deflection because of the relatively thick asphalt layer.

Figure 9. Shear moduli of sands at different relative densities.

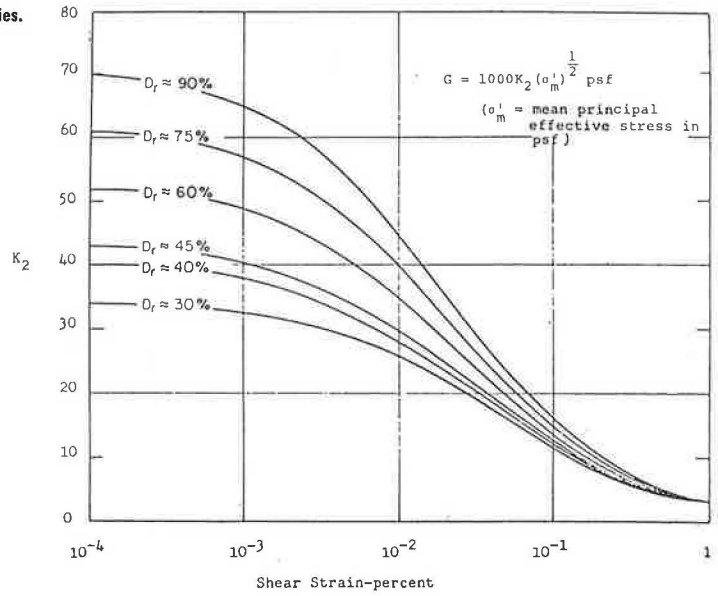

Figure 10. K_1-factor at 1.0 deflection ratio versus maximum computed shear strain.

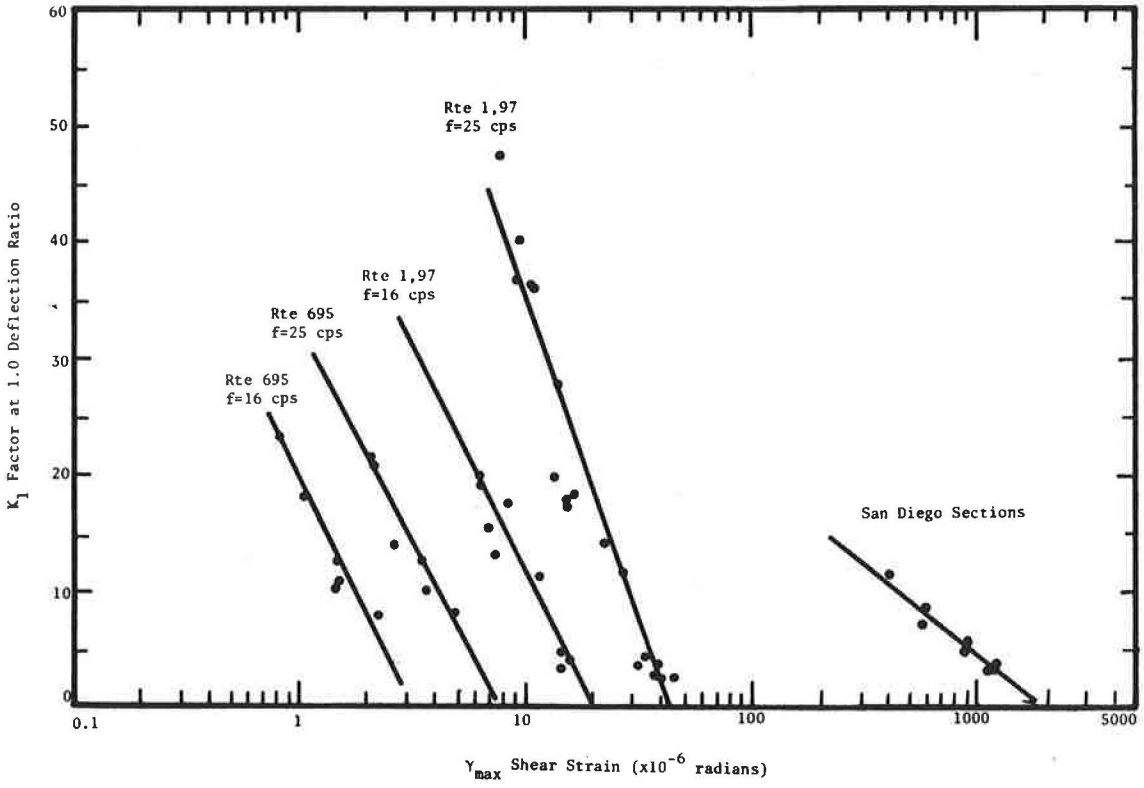

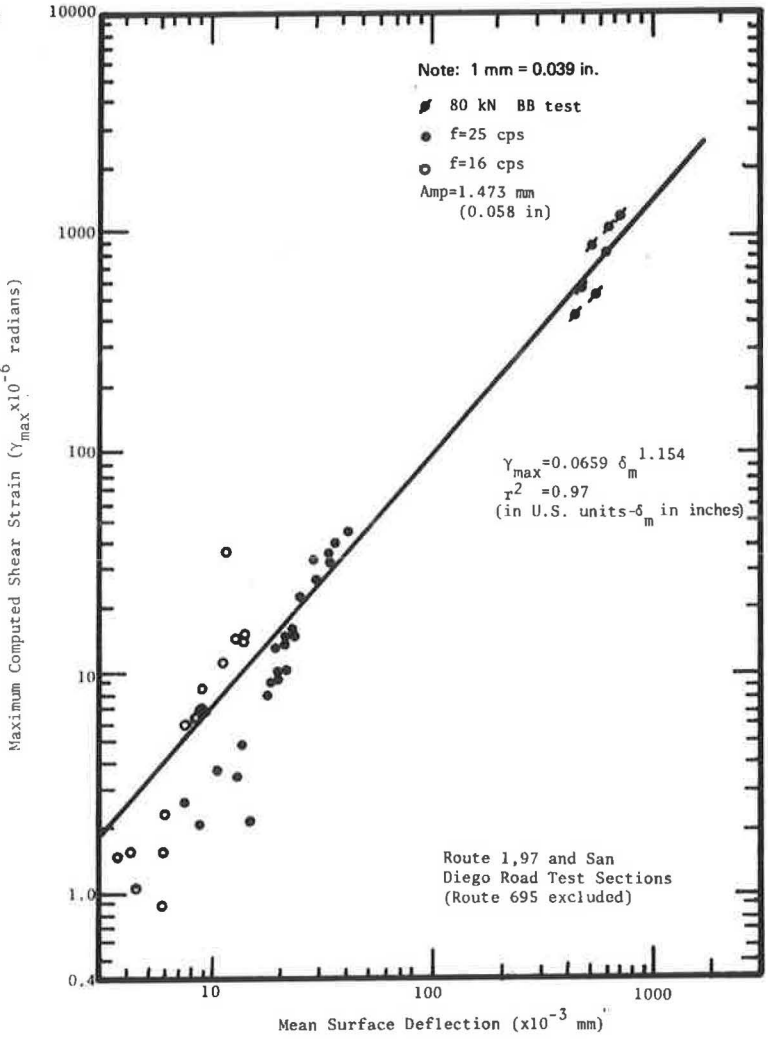

Figure 11. Maximum computed shear strain versus mean surface deflection.

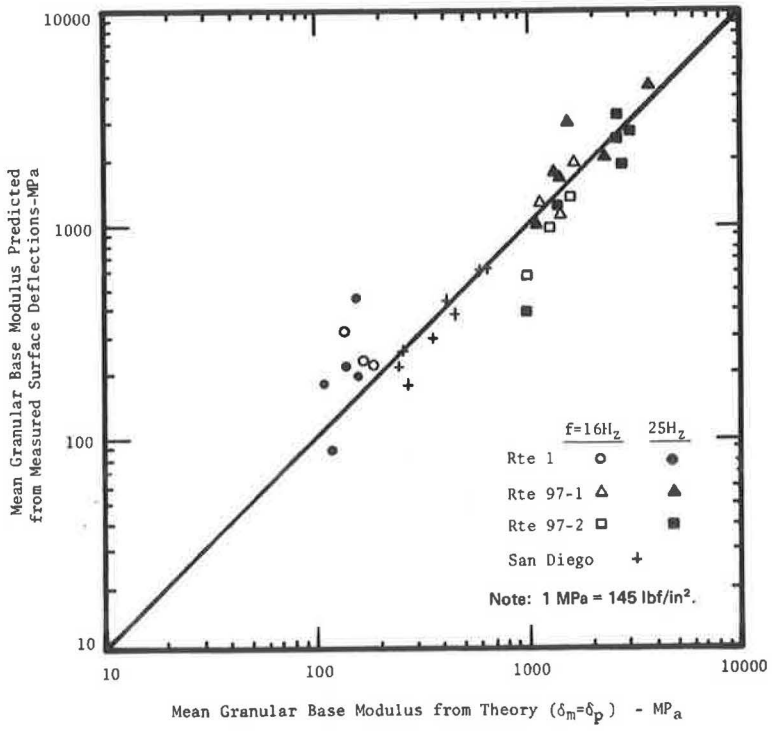

Figure 12. Relationship between mean granular base moduli predicted from measured deflections and moduli computed from theory.

Relationships shown in Figures 10 and 11 can be used to formulate a possible explanation for the decreased $K_1(R_d = 1.0)$ with increased surface deflection. Increased surface deflection implies an increased level of shear strain (Figure 11) and therefore decreased in situ granular-base modulus. This decreasing in situ modulus occurs simultaneously with increasing bulk stress. Hence, the K_1-factor necessary to characterize that modulus must also decrease.

ESTIMATE OF IN SITU MODULUS

The results shown in Figures 6 and 8 were grouped together to formulate a provisional procedure that can be used to estimate the in situ granular-base modulus from measured pavement deflections. From Figure 6, it can be observed that the relationship for a given load (P) is of the form

$$K_1(R_d = 1.0) = A_i \delta_m^{B_i} \quad (5)$$

where A_i and B_i are regression constants that depend on the load magnitude. For the three loads shown in Figure 6 the values of A_i and B_i are (1 kN = 224.8 lbf):

P(kN)	A_i	B_i
2.16	1.645×10^{-9}	-2.872
5.27	4.753×10^{-11}	-3.773
40.00	5.577×10^{-4}	-2.390

From Figure 8, the regression equation relating $K_1(R_d = 1.0)$ to mean granular-base modulus ($\bar{E}_{gb}$) is

$$\bar{E}_{gb} = CK_1(R_d = 1.0)^D \quad (6)$$

where $C = 5700$ and $D = 1.231$. Since $K_1(R_d = 1.0)$ is predicted by the measured deflection (δ_m) and $\bar{E}_{gb}$ is predicted by $K_1(R_d = 1.0)$, $\bar{E}_{gb}$ may be predicted directly from δ_m by

$$\bar{E}_{gb} = C(A_i \delta_m^{B_i})^D \quad (7)$$

Figure 12 is a summary comparison between the predicted $\bar{E}_{gb}$ found from the iterative-layer-theory solution and the computer program for deflection results of US-1, MD-97, and the San Diego test-road sections. The average percentage of error between modulus values was found to be 65 percent and 25 percent, respectively, for US-1 and MD-97 and 13 percent for the San Diego test-road sections. Although the general agreement is not perfect, the relationship is apparent, and further research should certainly develop a more accurate and applicable system. If this is accomplished, it is believed that a very significant step will have been taken toward the use of measured dynamic deflection data to predict the moduli of the subgrade layer. Such an objective is the major utility of eventually employing nondestructive testing devices for overlay and rehabilitation problems.

CONCLUSIONS

The following conclusions are presented, based on the data obtained in this study.

1. For small dynamic loadings (road rater), flexible-pavement models with a one-layer subgrade condition were found to be sufficient for accurate surface-deflection computations when the nonlinear subgrade response was incorporated into the analysis. Only a minor decrease in computed surface deflection was found when the subgrade was subdivided into three layers for the stress-dependent pavement study.
2. The 6.0-kN static preload of the road rater need not be considered for accurate modeling of the loading methodology. Results of the static preload study have shown that the inclusion of the static preload will reduce computed deflections by only a minor degree (4 percent).
3. Based on the comparison of computed and measured surface deflections for US-1 and pavement sections of MD-97 and I-695, deflections computed with elastic-layer theory, laboratory dynamic modulus testing, and a nonlinear iteration approach for both granular and subgrade layers are larger (by a factor of 2 to 4) than measured surface deflections from the road rater. Results of this study support previous research, which indicates that the major factor contributing to this discrepancy lies in the present characterization procedure for the resilient modulus of granular materials (i.e., $M_R = k_1 \theta^{k2}$).
4. It was found that the log $K_1(R_d = 1.0)$ versus log measured-surface-deflection (δ_m) relationship reported by Jones (8) for the San Diego test-road sections could also be applied to pavements analyzed in this study. This relationship was found valid for US-1 and MD-97, both of which have pavement cross sections similar to those studied by Jones [asphalt surface layer 7.5-13 cm (3-5 in) thick and conventional granular base].
5. The linear relationship between log in situ granular-layer modulus and log $K_1(R_d = 1.0)$ demonstrated by Figure 8 was observed for all pavement sections analyzed, regardless of dynamic load magnitude and asphalt layer thickness. This and the $K_1(R_d = 1.0)$ versus δ_m relationship were used to develop a provisional procedure for estimating in situ granular-layer modulus from dynamic road-rater deflections. It is concluded that this procedure has promise and that further research should certainly allow development of a more accurate and applicable system.
6. The resilient modulus of the granular layer was found to decrease with increasing level of shear strain. This finding was demonstrated by the linear log-log relationship of $K_1(R_d = 1.0)$ versus maximum shear strain (Figure 10) and substantiates other recent research dealing with the dynamic response of granular soils.
7. The effect of shear strain on the granular-layer modulus (theoretical model) is believed responsible for the increase in $K_1(R_d = 1.0)$ with increase in surface deflection. Increased surface deflection was found to increase the level of shear strain, thus decreasing the in situ modulus. This decreasing in situ modulus occurs simultaneously with increasing bulk stress (θ). Since $\delta_p > \delta_m$ and M_R is proportional to θ (i.e., $M_R = K_1 k_1 \theta k2$), the $K_1(R_d = 1.0)$ value must decrease as δ_m increases.

Although the results of this study demonstrate a problem in laboratory modulus characterization of granular materials, it should also be recognized that further research that involves a larger number of pavement sections and dynamic loads between those of the road rater and an 80-kN axle load needs to be conducted before final conclusions and a rational explanation of this phenomenon can be stated.

ACKNOWLEDGMENT

We are indebted to the Maryland State Highway Administration for providing financial and technical assistance necessary for this study.

REFERENCES

1. The WASHO Road Test: Part 1. HRB, Special Rept. 18, 1962.
2. The AASHO Road Test: Report 5—Pavement Research. HRB, Special Rept. 61E, 1962.
3. P.A. D'Amato. Analysis of In Situ Granular Layer Modulus from Dynamic Road Rater Deflections. Univ. of Maryland, College Park, M.S. thesis, 1977.
4. M.W. Witczak and K.R. Bell. Remaining-Life Analysis of Flexible Pavements. Proc., AAPT, Vol. 47, 1978.
5. M.W. Witczak. Determination of Remaining Flexible Pavement Life, Volume 1: Executive Summary. State Highway Administration, Maryland Department of

Transportation, Brooklandville, FHWA-MD-R-79-1, Oct. 1978. NTIS: PB-296562/2ST.
6. Seismic Analysis of Structures and Equipment for Nuclear Power Plants. Bechtel Power Corporation, San Francisco, CA, Rept. BC-TOP—4-A, Revision 3, Nov. 1974.
7. S.F. Brown. Repeated Load Testing of a Granular Material. Geotechnical Engineering Journal of ASCE, Vol. 100, No. GT7, July 1974, pp. 825-841.
8. M.P. Jones and M.W. Witczak. Subgrade Modulus on the San Diego Test Road. TRB, Transportation Research Record 641, 1977, pp. 1-6.
9. H.F. Southgate. An Evaluation of Temperature Distribution Within Asphalt Pavements and Its Relationship to Pavement Deflections. Kentucky Department of Transportation, Frankfort, Rept. HPR-1(3), Part 2, 1968.
10. J.W. Hall, Jr. Nondestructive Pavement Evaluation Machine. U.S. Army Engineer Waterways Experiment Station, Vicksburg, MS, Prelim. Rept., July 1973.

Publication of this paper sponsored by Committee on Pavement Condition Evaluation.

Pavement Design for Permafrost Conditions: Structural and Thermal Requirements

LYNNE G. COWÉ FALLS AND RALPH HAAS

The existing Arctic road network is made up almost completely of gravel-surfaced secondary roads for which design, construction, and maintenance procedures are adequate. Proposed reconstruction and paving of the Alaska Highway in the next decade has raised several questions about the adequacy of pavement-design technology for permafrost areas. Because of the nature of permafrost terrain the problems of pavement design are twofold: provision of a structurally sound, smooth pavement to allow safe passage of vehicles during critical thaw periods and prevention of thermal degradation of the subgrade and right-of-way. Recent research has concentrated on the evaluation of new materials and design configurations that minimize subgrade thaw settlement. Research into the structural performance of pavements on permafrost has been minimal. Identification of the structural and thermal bases for pavement design in permafrost areas is a key requirement for the development of a design technology that includes economic analysis and evaluation. This paper examines the effects of environment, materials, and loading on the thermal and structural responses of insulated and conventional pavement designs on discontinuous permafrost. The vertical temperature and stress distribution for a range of feasible designs was analyzed by means of two computer programs. Dynamic traffic loading of the structures investigated did not produce excessive subgrade strains. However, the dead load of the structure contributed greatly to thaw consolidation of the subgrade. None of the designs completely prevented subgrade thaw. A trade-off between dead load of the structure and thermal protection of the subgrade was identified. This conclusion provides a new justification for the use of low-density insulating layers in pavements on unstable permafrost.

With the increased emphasis on northern construction, such as the jointly financed Canadian-U.S. project to reconstruct and pave the Alaska Highway, pavement-design technology needs to be able to consider permafrost conditions.

On continuous permafrost where the depth of annual thaw is shallow, paved surfaces have been constructed with reasonable success by using conventional design technology. However, the scale of the Alaska Highway project and the instability of the terrain that it traverses bring into serious question the adequacy of southern pavement-design methods applied to discontinuous permafrost. Although equilibrium with the subgrade has been reached in the 35-year existence of the Alaska Highway, differential settlements can be expected when additional construction (and in many cases realignment) again upsets the thermal balance. Although these settlements would be relatively easy to correct if the highway were to remain a gravel surface, patching and padding on an asphalt surface will be much more expensive. Current annual maintenance costs for the gravel-surfaced highway are about $6500/km (1). The annual maintenance cost of a badly distorted and cracked paved surface would be substantially higher.

The general purpose of this paper is to consider the design interaction between thermal and structural requirements for pavements on permafrost by using the Alaska Highway as a case history. There are three main objectives:

1. Review of the general design problems associated with discontinuous permafrost, the applicability of current design technology, and the use of experimental pavement designs;
2. Fundamentally based analysis of the structural and thermal responses of a range of feasible designs for a variety of environmental, loading, material, and other conditions; and
3. Evaluation of the boundaries within which structural and thermal trade-offs can be made within the factor space of 2.

Some of the terms used in this paper are defined as follows:

1. Permafrost: Soil or rock (or both) that has a mean annual ground temperature at or below 0°C for several years;
2. Active layer: Depth below the surface at which annual temperature fluctuations are not felt, i.e., depth of maximum thaw;
3. Continuous permafrost: Permafrost that has a mean annual ground temperature below -4°C--frozen ground is continuous (i.e., there are no breaks) and the active layer is shallow; and
4. Discontinuous permafrost: Permafrost that has a mean annual ground temperature between 0° and -4°C--the active layer is very deep and the existence of permafrost is widespread; vegetation and topography dictate the presence or absence of frozen ground.

DESIGN PROBLEMS, CURRENT TECHNOLOGY, AND EXPERIMENTAL DESIGNS

Problems of Pavement Design in Discontinuous Permafrost

In permafrost zones, where the mean annual ground temperature is at or below 0°C, thaw penetration has a greater effect on a pavement structure than does frost penetration. Because of the ice-rich nature of permafrost silts, clays, and organic soils, alteration of the surface characteristics causes an increase in the equilibrium ground temperature and a deepening of the active layer. Over the

long term, increasing the mean ground temperature raises the bottom of the permafrost table. Both events will cause thawing of frozen groundwater, either interstitial or massive lens ice, and severe loss of strength (Figure 1).

Beneath a road embankment, thawed permafrost can cause substantial settlement, rotational sliding of the embankment, or massive heaving when freezeback occurs. All these render the structure either impassably rough or structurally unsound and result in premature loss of serviceability. This one-way causal link between subgrade thaw and loss of structural strength has long been known. However, not much work has been directed at the possibility of a causal link that operates in the opposite direction, i.e., that structural loading, either dynamically or statically, may affect thaw consolidation of the subgrade soil. Similarly, little research has been done on identification of areas where trade-offs can be made between thermal protection of the subgrade and structural performance of the pavement. Understanding this trade-off is a key requirement in the economic analysis of alternative design types. Not only will this knowledge help in the analysis of design strategies, but also it will provide a mechanism for the generation of alternative pavement designs.

Existing Design Technology

A review of current design technology (2) has used three procedures as examples—those of the U.S. Army Corps of Engineers, the state of Alaska, and the USSR.

Although these procedures represent a working technology and the efforts of highly capable engineers and scientists, they have a number of limitations. First, they do not provide for estimating performance (i.e., the serviceability-age relationship). Second, because experience with pavements on permafrost is considerably less than that for southern conditions, design errors are much more likely to occur, and little verification of the design methods has been conducted. Third, the concurrent requirements for structural adequacy and thermal protection are not considered in a fundamentally based and integrated manner.

Experimental Pavement Designs

Several experimental pavements have been built and tested on permafrost. Most of the test designs incorporate an insulating layer to retard penetration of the thaw front, although passive methods, such as by painting the asphalt white or by using chemical additives, have also been used.

Esch (3) has described a test road in Fairbanks, Alaska, which is in a warm permafrost zone (mean annual air temperature, -2.8°C; active layer, 0.4-0.5 m). Three sections were constructed—control (gravel), 51 mm of Styrofoam, and 102 mm of Styrofoam. The results indicated that both insulation thicknesses were effective in retarding thaw, although the more economical solution would be to use the thinner section whenever possible.

Figure 1. Effect of terrain disturbance on thermal profile of permafrost.

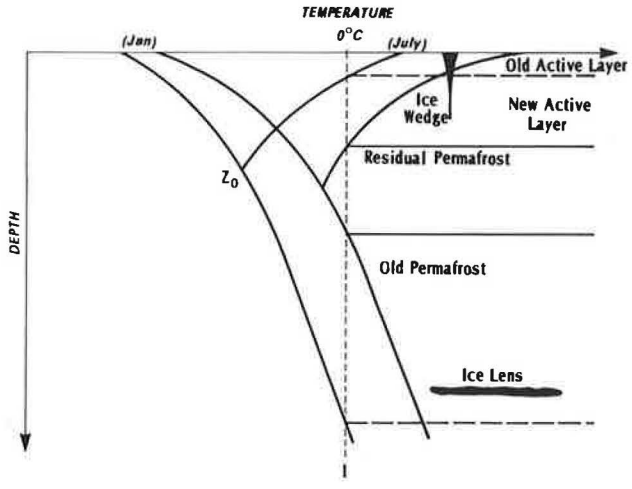

Smith, Berg, and Muller (4) used polyurethane as a surface insulation and wearing course on a temporary haul road in northern Alaska. Varying thicknesses of two densities of polyurethane were foamed on a wood-chip leveling course and covered with a thin layer (150 mm) of gravel and aluminum matting. Transition zones of gravel and wood chips linked the sections. The foam withstood 1000 passes of a rubber-tired 1540-kg/axle vehicle with less than 10-mm rutting. However, it began to crumble after only 8 passes of a 2415-kg/axle vehicle.

Berg and Aitken (5) built five test sections in Fairbanks on undisturbed ice-rich silt that had a minimum active layer of 300 mm. The test sections were control asphalt concrete, white-painted asphalt, compressed peat subbase, black-painted gravel, and normal gravel. Permafrost degradation was greater beneath the asphalt-concrete section and least beneath the white asphalt, which demonstrates the profound effect of surface color on thermal regimes.

Fulwider and Aitken (6) obtained similar results with a white-painted asphalt on a runway at Thule, Greenland. They found a one-month lag and a 35 percent reduction in thaw penetration in a painted section compared with the results from an untreated asphalt surface.

Hennion and Lobacz (7) describe the use of a membrane-encapsulated soil layer constructed on Fairbanks silt. The silt was dried to 14 percent moisture content and placed between two polyurethane-cloth layers treated with cationically emulsified asphalt. After two years and 106 passes with an 8000-kg/axle vehicle, no sign of distress was visible although the silt had absorbed 40 percent of the moisture.

The Sulphur Development Institute of Canada and the Chevron Company constructed a test section insulated with sulfur foam on the Dempster Highway at Arctic Red River in the Northwest Territory in 1975; this project was based on the results from a test road in Calgary. No observations have been published, but it is expected that the sulfur will adequately insulate the road structure in this continuous-permafrost zone. Sulfur has the potential advantages over Styrofoam that it is easily transported and mixed on site and that there is a relatively good supply.

From the previous discussion, it can be seen that the major emphasis of the work on insulated embankments has been toward an understanding of the efficiency of various media for protecting the subgrade. Preliminary studies on structural behavior have been started by the Alberta Research Council (8) on sulfur foam (Furcoat) and, according to Louie of the Dow Chemical Company, on Styrofoam (H1). Both studies analyze vertical and tensile strains in the insulating layer to determine whether they exceed material strength, particularly during construction, when excessive loads are placed on the structure. Christison (8) concludes that the compressive strength of sulfur foam is not exceeded when the asphaltic wearing course is greater than 65 mm. Placement of the insulating layer directly below the wearing course results in large tensile strains at the asphalt-insulation interface, which could accelerate pavement fatigue.

Louie's study centered on the minimum lift of granular base course required over H135 and H160 Styrofoam to prevent compression of the Styrofoam during construction. He stressed that maximum protection was reached with 900 mm of gravel over H135 and 450 mm over H160. All tests were done under a 179-kN load that simulated a Caterpillar tractor.

RESEARCH STUDY

The joint Canadian-U.S. Alaska Highway project (Shakwak Project), the case study for this research, represents a real,

current, large-scale situation in which insulated pavements can be a feasible alternative.

The original proposal (1), which formed the background for this project, concluded that the following three major design alternatives were most feasible and practical at that time: (a) a sulfur-foam-insulated pavement, (b) a Styrofoam-insulated pavement, and (c) a gravel-insulated (conventional) pavement. Figure 2 illustrates these alternatives and the configurations of the component layers.

Research Approach

In order to investigate the problem efficiently and to bracket expected design situations, two environmental and four design variables were arranged in a complete factorial (Figure 3). This factorial form provides an efficient means for studying the relationships between the dependent variables of thaw depth and dynamic structural response and the independent variables of design and environment. The levels chosen for the independent variables of Figure 3 represent practical upper and lower expected design limits.

The factorial was used in two phases of the study: (a) analysis of thaw depths within the various road structures by using a one-dimensional microclimatic simulator, FROST, developed at Carleton University in Ottawa and (b) analysis of the magnitude of stresses and strains by using the bitumen-structures-analysis-in-roads (BISAR) computer program from Shell Research for elastic layers. Data used to characterize the materials were taken from the literature and are given in Table 1. [Those values for which there is no other reference are from Watson, Rowley, and Slusarchuk (12).]

The results of these two phases were used to isolate areas in which trade-offs could be investigated in detail and to derive a rough method for meeting the design constraints of thermal protection and structural response.

Figure 2. Proposed design types: Shakwak Project, Alaska Highway.

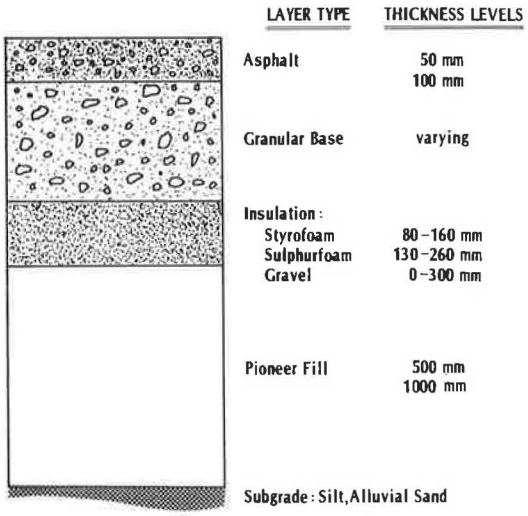

Results of the Thaw Analysis

Results of the thaw analysis, shown as the depth of thaw below the subgrade surface, are summarized in Figure 4. Because of the varying thicknesses and types of materials used, all structures have been equated to equivalent granular thickness (EGT) based on the thermal diffusivity of gravel (considered to be 1.0) relative to each material (see Table 1). The following effects are evident in Figure 4:

1. None of the designs tested was adequate in preventing subgrade thaw in discontinuous ice-rich and ice-poor permafrost soils. Therefore, either some tolerance should be required in construction scheduling (i.e., stage of construction of embankment and asphalt wearing course) or the pavement design should be built to minimize postconstruction high-level maintenance costs during the equilibration period.
2. The most significant factor in preventing subgrade thaw is the total height of gravel fill used in the design of pavements on discontinuous permafrost. That is, subgrade thaw penetration decreases as the height of fill increases.
3. There was little difference in the effect of the two synthetic insulating materials. The design of the factorial was such that insulation thicknesses were adjusted to account for differing thermal properties so that the amount of subgrade thaw was controlled. An economic analysis could be done either by comparing insulating media strictly by equality of thickness and measuring the amount of thaw or by calculating the cost per millimeter of thickness.
4. Subgrade soil type has a significant effect. The higher moisture content of silt accounts for the difference in thaw depth, since the latent heat effect of water retards thaw penetration. However, because of this higher moisture content a structure on silt can tolerate substantially less subgrade thaw than could a structure on a drier alluvial soil.
5. Asphalt thickness has little effect on subgrade thaw.

Based on the results of the simulator, a simplified model for thaw-depth prediction was developed in terms of design variables.

Figure 3. Factorial design.

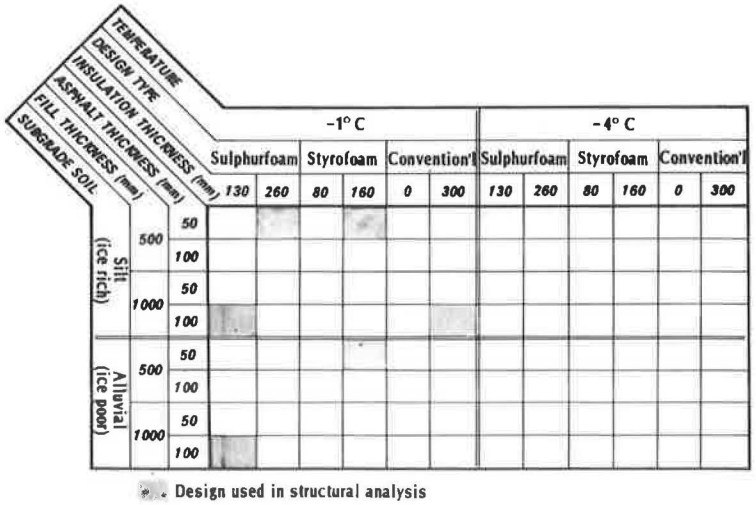

Table 1. Thermal and mechanical properties of materials used in analysis.

Material	Thermal Conductivity (W/m·K) Frozen	Thermal Conductivity (W/m·K) Unfrozen	Heat Capacity (J/kg·K 000s) Frozen	Heat Capacity (J/kg·K 000s) Unfrozen	E (MPa)	μ	λ (m/s^2)	Thermal Equivalency Based on λ[a]
Asphalt 300/400	0.926	0.926	3.02	3.02	693 (9)	0.35 (9)	0.0033	1.3
Granular base	1.383	1.88	1.55	1.72	346 (10)	0.30	0.0109	1.0
Fill	1.299	1.80	1.55	1.68	485 (10)	0.30	0.0100	1.0
	–	–	–	–	138 (wet)	–	–	–
Silt	4.19	2.18	0.251	0.502	17[b]	0.25 (11)	–	–
Alluvial	1.383	1.877	1.72	1.55	104[b]	0.27	–	–
Styrofoam	0.352	0.352	41.90	41.90	14[c]	0.25	0.0030	3.6
Sulfur foam	0.659	0.659	20.45	20.45	42 (8)	0.25	0.0010	10.9

Note: E = modulus of elasticity; μ = Poisson's ratio; λ = thermal diffusivity.
[a]Gravel = 1.0. [b]Assumed. [c]Dow Chemical Company.

Figure 4. Results of thaw analysis.

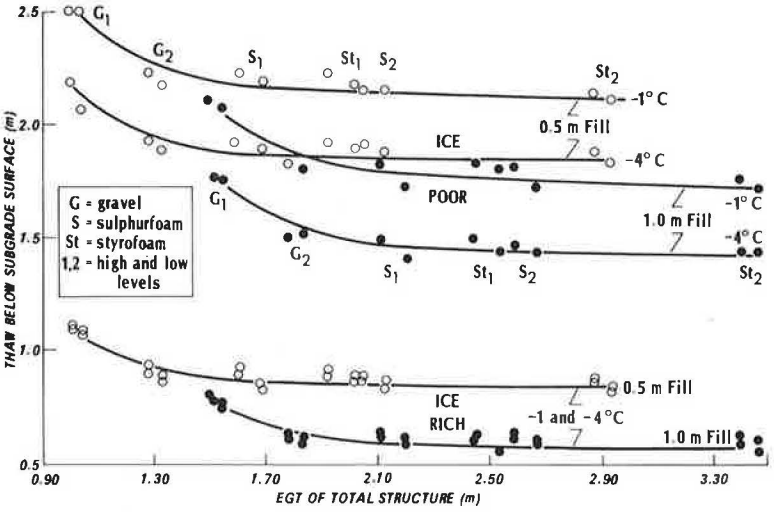

The rationale behind development of approximate simplified models based on the results of more-complex mathematical models used to calculate thaw and vertical subgrade strain lies partly in their use. Designers do not usually have either the time or the resources to rigorously evaluate all the possible combinations of alternatives. Inclusion of fundamental design variables, such as materials and thicknesses, in an approximate model permits these simple calculations to be used at least as an initial design tool; moreover, the computations can be done with a hand calculator. A simplified model, it should be stressed, is intended to be used as a guide.

The model derived is

$$m = a + b°C - c\,(\ln EGT) \quad (1)$$

where

m = thaw below subgrade surface (m),
a = 4.6118 for ice-poor soils and 3.4039 for ice-rich soils,
b = 1.0106 for ice-poor soils and 0.87 for ice-rich soils, and
c = 47.13 for ice-poor soils and 46.91 for ice-rich soils and for which $\overline{R}^2 = 0.82$.

This model may be used in two ways. First, it can give a quick evaluation of proposed alternative designs on a project basis to determine whether any will cause excessive thaw. Second, again for evaluation of alternative designs, when the allowable thaw depth is fixed (for example, in the case of massive ground ice), the model may be used to estimate the minimum EGT required.

Results of the Structural Analysis

In the design of flexible pavements, two elastic strains are usually considered critical—the horizontal or radial tensile strain at the bottom of the asphalt and the vertical compressive strain at the top of the subgrade. Excessive radial strain in the asphalt produces fatigue cracking of the surface, and excessive compressive strain at the top of the subgrade leads to permanent deformation, which is manifested by surface rutting. Fatigue cracking in arctic areas is usually of minor importance compared with thermal-shrinkage cracking and cracking caused by differential settlement of the structure. Although radial strain at the bottom of the asphalt layer was examined as part of the output, fatigue cracking was not expected to be a major problem unless it was initiated by structural settlement.

Deformation of the structure is the most commonly observed pavement distress in arctic areas. Although much of this deformation is attributed to thaw settlement of the subgrade, the degree to which excessive vertical compressive subgrade strain accelerates this process is unknown. Therefore, vertical subgrade strain was investigated in this phase of the analysis.

Prior to analysis of all the designs of Figure 3, a preliminary pilot analysis of strains and stresses for sample designs (Table 2) in the factorial was conducted to determine

1. Magnitude of vertical strain (ϵ_v) at the insulating layer-base interface,
2. Tension or compression of insulation,
3. Effect of inclusion of a soft insulating layer on excessive tension in the asphalt layer, and
4. Dead load of the thickest and thinnest structures (3 and 4, Table 2).

Material properties used in this analysis were given in Table 1. Dynamic loads were used that simulated a single-axle load (40 kN), an off-highway gravel-haulage vehicle (72 kN),

Table 2. Designs used in preliminary structural analysis for strains and stresses.

Design Number	Thickness (mm) Asphalt	Insulation	Fill	Insulation	Soil	Thaw Below Subgrade (mm)
1	100	130	1000	Sulfur foam	Ice-rich	603
					Ice-poor	1702
2	50	160	500	Styrofoam	Ice-rich	867
					Ice-poor	2160
3	50	260	500	Sulfur foam	Ice-rich	907
4	100	300	1000	Gravel	Ice-rich	608

Table 3. Results of elastic-layer analysis for sulfur-foam and for Styrofoam designs.

Design	Load (kN)	Location Below Surface (m)	ϵ_r (mm/mm)	ϵ_v (mm/mm)	σ_v (kPa)*
Sulfur Foam, Design 1					
On ice-rich soil	40	-0.10	0.000 020 89	–	–
		-0.67		–	-14.62
		-0.80		–	–
		-1.80	–	-0.000 027 7	-2.55
		-2.40	–	-0.000 010 2	-2.34
	72	-0.10	0.000 040 2	–	–
		-0.67		–	-24.27
		-0.80		–	–
		-1.80	–	-0.000 048 5	-4.50
		-2.40	–	-0.000 179	-3.71
	179	-0.10	-0.000 064 2	–	–
		-0.67		–	-40.95
		-0.80		–	–
		-1.80		-0.000 108	-10.48
		-2.40	–	-0.000 427	-8.76
On ice-poor soil	40	-0.10	0.000 021 0	–	–
		-0.67		–	-14.89
		-0.80		–	–
		-1.80	–	-0.000 025 1	-2.94
		-2.40	–	-0.000 021 2	-1.37
Styrofoam, Design 2					
On ice-rich soil	40	-0.05	0.000 018 14	–	–
		-0.59		–	-16.41
		-0.75		–	–
		-1.25	–	-0.000 061 99	-2.39
		-2.11	–	-0.000 166 7	-1.20
	72	-0.05	-0.000 132 5	–	–
		-0.59		–	-26.38
		-0.75		–	–
		-1.25	–	-0.000 107	-8.76
		-2.11	–	-0.000 294	-6.07
	179	-0.05	0.020 3	–	–
		-0.59		–	-43.02
		-0.75		–	–
		-1.25	–	-0.000 221	-19.51
		-2.11	–	-0.000 686	-14.13
On ice-poor soil	40	-0.05	0.000 023 5	–	–
		-0.59		–	-17.44
		-0.75		–	–
		-1.25	–	-0.000 051 6	-6.54
		-2.11	–	-0.000 066 5	-3.44

Note: ϵ_r = radial strain at bottom of asphalt layer (negative values indicate tension); ϵ_v = vertical strain (negative values indicate downward strain); σ_v = vertical stress (negative values indicate downward stress).

and a Caterpillar 651 bulldozer (179 kN). Results of this part of the analysis are given in Table 3 and are summarized below.

1. From the results of the structural analysis, it can be concluded that load-associated fatigue cracking will not be a problem with either the sulfur-foam or the Styrofoam design. Radial strain at the bottom of the asphalt layer is quite small in both designs for standard highway loads (40 kN), and only under construction loads (179 kN) is there any cause for alarm about fatigue cracking of either the asphalt or the insulating layer. The number of equivalent single-axle loads (40 kN/wheel) over a 20-year design life of the Alaska Highway is not expected to exceed one million applications (1); hence, dynamic loading by traffic alone will have little effect on the service life of either design.

2. In both designs, the amount of granular base course overlying the insulation is adequate and prevents excessive compressive stress. However, there is a greater potential for fatigue cracking in the Styrofoam than in the comformable sulfur foam because the Styrofoam acts like a slab.

3. The effect of varying asphalt layer thickness can be seen by comparing the vertical stresses on top of the sulfur foam and the Styrofoam. Vertical stress is 11 percent higher on top of the Styrofoam that has a 50-mm asphalt layer. From a stress-strain curve for H1-60 published by the Dow Chemical Company of Canada, the amount of compressive strain expected under the heaviest load (σ_v = 43 kPa) is less than 0.01 mm/mm.

4. The dead-load analysis involved a calculation of vertical stresses at the subgrade-base interface for the lightest and heaviest structural dead loads. The lightest dead-load is sulfur-foam design 3, which has a total load of 2.59 kPa on top of the subgrade. The heaviest load is gravel design 4, which has a load of 3.38 kPa on the subgrade. These results have been analyzed further in terms of evaluating the magnitude of the effect of static weight on subgrade settlement (13). In Figure 5 [after Luscher and Afifi (13)], the vertical subgrade stress for the thickest and thinnest structures is plotted; if we assume a frozen dry density of 1400 kg/m^3 and a moisture content of 60 percent, there is no one-dimensional thaw strain. This graph assumes that all moisture in the soil is interstitial. However, if 30-60 percent of the moisture is lenticular ice, the frozen dry density is reduced to 1200 kg/m^3 (60 percent) and the one-dimensional thaw strain ranges from 10 to 20 percent, which is quite high.

Stresses and strains in Table 3, it should be restated, are for dynamic loads. If the structure were not resting on a highly unstable, thawing, ice-rich subgrade, one could conclude that these designs were more than adequate for summer design-life traffic loads. However, the very fact that the subgrade is highly unstable and sensitive to minor changes in the environment leads to the conclusion that the greatest structural problems are brought on by thaw settlement of the structure.

Asphalt thickness was found to have little effect on the amount of subgrade thaw, but in the structural analysis it was found that under heavy construction loads a thin asphalt layer on a Styrofoam design undergoes severe tension, which

Figure 5. Frozen dry density versus one-dimensional thaw strain.

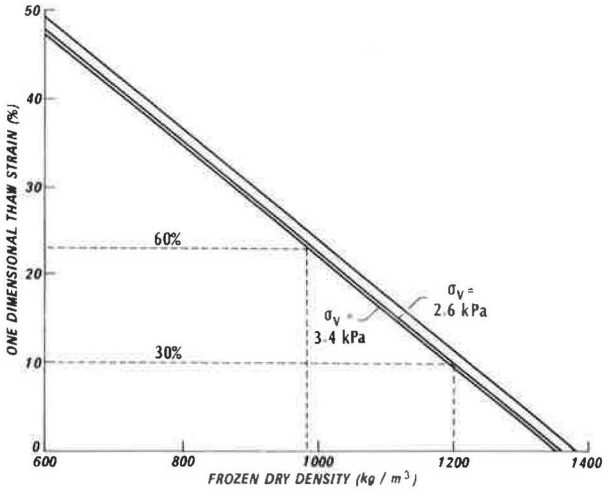

will probably result in premature cracking. This suggests that Styrofoam sections will require a thicker asphalt wearing course if the initial design service life is to be met.

The most important trade-off identified is in the total height of the embankment. Originally, insulated pavements were justified on the grounds that they minimized (a) aggregate use in areas of short supply or marginal materials and (b) structural damage by preventing thaw penetration of the subgrade.

From the results of the two analyses, it was concluded that the greatest structural damage is produced by the dead load of the structure on thawed ice-rich permafrost. Therefore, by decreasing the embankment height by inclusion of lightweight insulating materials, the dead-load effect is reduced. Reduction of the amount of gravel does not alter the structural behavior of the pavement under the range of loads that were investigated; therefore, greater benefit can be derived from a lighter structure.

CONCLUSIONS

The development of a comprehensive design technology for pavements in areas of discontinuous permafrost is a complex, large-scale problem. Moreover, fixed observations of performance in order to verify designs are a major need. The investigation reported here was directed toward developing some of the initial, fundamentally based design technology. It was primarily concerned with identifying the relative effects of design, material, and environmental factors on the thermal and structural responses of pavements on discontinuous permafrost.

The study has shown that dynamic traffic loading, for the range of conditions investigated, is not a major factor in fatigue cracking and permanent deformation of pavements in permafrost areas. However, the static dead load of the fill and pavement structure on the subgrade can be a major contributor to thaw settlement. Based on this conclusion, inclusion of a layer of low-density lightweight material in a pavement decreases the total dead load of the structure and the thaw penetration and thereby makes a double contribution to the prevention of subgrade thaw settlement.

A major problem during the investigation was determining in situ soil properties during thaw for the structural analysis. Much work has been done in the laboratory on typical soils in their frozen state, but few data have been published for ice-rich permafrost soils during or after thaw.

The investigation was essentially exploratory and theoretical, with input information acquired from various sources. The effects described need to be verified by field work, laboratory simulation, or both. Although the long-term essential requirement is to assemble data on the performance of pavements on permafrost, more immediate laboratory verification work is possible.

ACKNOWLEDGMENT

The investigation on which this paper is based was funded primarily by the National Science and Engineering Research Council (NSERC). Key information and consultative advice was provided by M. S. Cheung of Public Works Canada in Ottawa and B. P. Shields and T. Christison of the Alberta Research Council in Edmonton. Other colleagues who provided valuable advice are David Esch of the Alaska Department of Transportation, R. Vogan of Public Works Canada, and H. Johnston of NSERC. We gratefully acknowledge all this support and cooperation.

REFERENCES

1. Alaska Highway Shakwak Project Proposal. Public Works Canada Tech. Rept., Ottawa, 1976.
2. L. Cowé Falls. Structural and Thermal Response of Insulated Pavements on Permafrost. Univ. of Waterloo, Ontario, M.S. thesis, 1979.
3. D. C. Esch. Control of Permafrost Degradation Beneath a Roadway by Subgrade Insulation. In Permafrost: Second International Conference, North American Contribution, National Academy of Sciences, Washington, DC, 1973, pp. 608-622.
4. N. Smith, R. L. Berg, and L. Muller. The Use of Polyurethane Foam Plastics in the Construction of Expedient Roads on Permafrost in Central Alaska. In Permafrost: Second International Conference, North American Contribution, National Academy of Sciences, Washington, DC, 1973, pp. 736-745.
5. R. L. Berg and G. W. Aitken. Some Passive Methods of Controlling Geocryological Conditions in Roadway Construction. In Permafrost: Second International Conference, North American Contribution, National Academy of Sciences, Washington, DC, 1973, pp. 581-586.
6. C. W. Fulwider and G. W. Aitken. Effect of Surface Color on Thaw Penetration Beneath an Asphalt Surface in the Arctic. Proc., International Conference on the Structural Design of Asphalt Pavements, Univ. of Michigan, Ann Arbor, 1962, pp. 958-963.
7. F. B. Hennion and E. F. Lobacz. Corps of Engineers Technology Related to Design of Pavements in Areas of Permafrost. In Permafrost: Second International Conference, North American Contribution, National Academy of Sciences, Washington, DC, 1973, pp. 658-664.
8. J. T. Christison and B. P. Shields. Applications of Sulphur Foam for Road Insulation. Alberta Research Council, Edmonton, Project R3000 Rept., 1976.
9. F. R. P. Meyer. Permanent Deformation Prediction of Asphalt Concrete Pavement. Univ. of Waterloo, Ontario, M.S. thesis, 1974.
10. F. W. Jung and W. A. Phang. Elastic Layer Analysis Related to Performance in Flexible Pavement Design. Ontario Ministry of Transportation and Communications, Toronto, Rept. RR191, 1975.
11. H. W. Stevens. Viscoelastic Properties of Frozen Soil Under Vibratory Loads. In Permafrost: Second International Conference, North American Contribution, National Academy of Sciences, Washington, DC, pp. 400-409.
12. G. H. Watson, R. K. Rowley, and W. A. Slusarchuk. Performance of a Warm-Oil Pipeline Buried in Permafrost. In Permafrost: Second International Conference, North American Contribution, National Academy of Sciences, Washington, DC, 1973, pp. 759-766.
13. U. Luscher and S. S. Afifi. Thaw Consolidation of Alaskan Silts and Granular Soils. In Permafrost: Second International Conference, North American Contribution, National Academy of Sciences, Washington, DC, 1973, pp. 325-334.

Publication of this paper sponsored by Committee on Theory of Pavement Systems.

Laboratory Investigation of Flexible-Pavement Response by Using Transfer Functions

GALAL A. ALI, W. H. GOETZ, AND M. E. HARR

Transfer-function theory was applied to examine the behavior of flexible highway pavements. A numerical computation was used to derive pavement response functions from impulse testing of three-layer models of flexible pavements. Analytical computations formed the basis for calculating deflections that result from static and repeated loads. It was hypothesized that more-significant parameters than are commonly used could be obtained under controlled laboratory conditions. By using nonlinear regression, the response functions were approximated by a mathematical model to include these parameters. The derived model was used as the input for the analytical computations. The adequacy of the developed model was verified by comparing predicted and measured deflections. A silty-sand subgrade, a crushed-aggregate base, and an asphalt-concrete surface were the components of the three-layer systems. Model pavements of two different surface-course thicknesses were tested statically and dynamically at three different stress levels. To permit the tests to be performed inside a constant-temperature room, the maximum possible size adopted for the model pavements was 0.8 x 0.8 x 0.6 m (32.5 x 32.5 x 23.25 in). Test temperatures were 10°, 24°, and 38°C (50°, 75°, and 100°F). Deflections were measured at five locations. It was shown that time-dependent behavior of flexible pavements can be represented by response functions. The parameters in these functions are regarded as descriptors of pavement characteristics and have the capability of predicting pavement response.

The pursuit of a rational method for the design and evaluation of pavements requires considerable knowledge of pavement response behavior to realistic loadings. Current mathematical models for prediction of pavement response and evaluation of its behavior generally evolve from classical (elastic and viscoelastic) theories. These models incorporate geometric aspects and material properties within a system of equations that, in turn, are solved so as to satisfy selected boundary conditions (1). In both elastic and viscoelastic theories, mathematical expediency has led to idealization of the constitutive relations. However, any predictive model must include in situ (global) material properties. Parameters or functions capable of describing time- and temperature-dependent material properties of pavements subjected to static or dynamic loads must be obtained.

The purpose of this paper is to evaluate pavement behavior based on transfer-function theory that has been applied successfully to the solution of several problems in mechanical and electrical engineering (2-5). Swami, Goetz, and Harr (6) sought to characterize bituminous mixtures under a variety of test conditions. They concluded that an asphalt concrete at a constant temperature could be uniquely represented by a transfer function.

Boyer and Harr applied transfer functions to airfield pavements and showed that the time-dependent behavior of a flexible pavement could be represented by time-dependent transfer functions (7).

This investigation extends the transfer-function concepts to flexible highway pavements. More significant parameters, or indicators, than are usually hypothesized are defined and determined under controlled laboratory conditions.

The procedure is depicted in the flowchart of Figure 1. A known impulse load, which corresponded to the signature left by a truck tire on a pavement system, was applied to a pavement system. The resulting output deflections were measured as functions of time at several locations on the pavement surface. The time-dependent input and the corresponding outputs were analyzed by using transfer-function theory to give response functions; a computer subroutine CONVLI was used (8).

A mathematical model for the response functions was evolved by using a computer program labeled NONLINR. This model was computed analytically with step and repeated-load input functions. Computer programs STALOD and REPLOD facilitated the respective calculations. The adequacy of the developed mathematical-experimental model was evaluated by comparing predicted responses due to static and repeated loads with experimentally measured values. The effects of temperature, surface-course thickness, and spatial location on the dynamic parameters and the predictions were examined.

THEORETICAL ANALYSIS

Transfer-Function Approach

A dynamic system can be represented by a transfer function [G(s)] defined as the ratio of the Laplace transform of the output [O(t)] to the Laplace transform of the input [I(t)]. By this definition,

$$G(s) = \bar{O}(s)/\bar{I}(s) \quad (1)$$

where

$O(s) = L[O(t)]$,
$I(s) = L[I(t)]$,
s = Laplace transform parameter,
L = Laplace transformation, and
t = time variable.

Consider an impulse load input of peak value F_p that acts as a point $x = x_0 = 0$ on a pavement. The resulting deflection responses at points $x = x_1$, $x = x_2$, ..., $x = x_i$ along a line normal to the load represent the output functions.

By using the definition of Equation 1, the transfer function at a point $x = x_i$ on the pavement that is caused by the input load at $x = x_0$ can be written as

$$G_{x_i}(s) = \bar{O}_{x_i}(s)/\bar{I}_{x_0}(s) \quad (2)$$

where

$\bar{O}_{x_i}(s)$ = Laplace transform of output response at $x = x_i$,
$\bar{I}_{x_0}(s)$ = Laplace transform of input load at $x = x_0$, and
$G_{x_i}(s)$ = transfer function between an operational output response at $x = x_i$ and the operational input at $x = x_0$.

Thus, the transfer function characterizes the pavement system between points $x = x_0$ and $x = x_i$ and provides a body concept for the pavement. This is in contrast to the point concept inherent in classical elastic and viscoelastic theories.

After Equation 2 has been rewritten, it follows that

$$\bar{O}_{x_i}(s) = G_{x_i}(s)\bar{I}_{x_0}(s) \quad (3)$$

Equation 3 can be expressed in the time domain by using the computation of two functions (5):

$$O_{x_i}(t) = \int_0^t G_{x_i}(\tau) I_{x_0}(t - \tau)\, d\tau \quad (4)$$

where τ is the dummy time variable. The function $G_{x_i}(t)$ is the inverse transform of the transfer function $G_{x_i}(s)$ and is called the impulse response or the response function of the system.

Figure 1. Procedure for pavement evaluation.

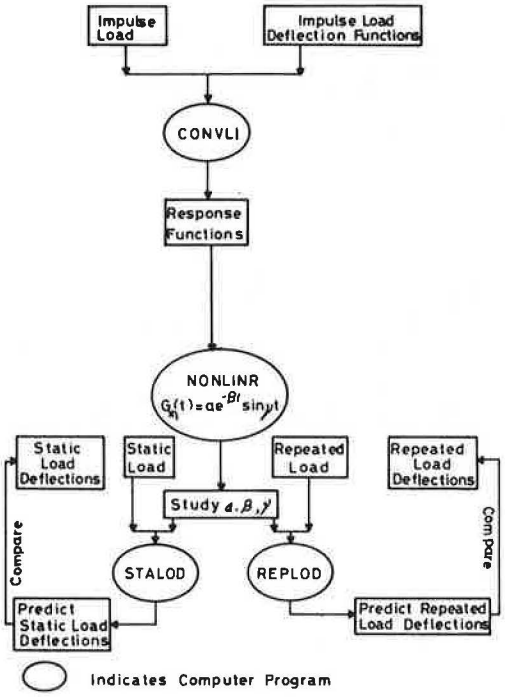

The finite-difference solution (7) of Equation 4 to yield $G_{x_i}(t)$ gives Equation 5, provided that $I_{x_0}(t)$ and $O_{x_i}(t)$ are available as discrete values:

$$G_{x_i}(k) = \left[O_{x_i}(k) - \sum_{j=1}^{k-1} G_{x_i}(j) I_{x_0}(k - j + 1)\Delta t_{x_i}\right] \Big/ I_{x_0}(l)\Delta t_{x_i} \quad (5)$$

where j, k = dummy variables that represent discretized units and Δt = time interval.

Form of Response Function

The experimental basis discussed here to obtain the response function is the impulse test. An impulse-load input of known peak value was applied for a short time to the system for which the response function was sought. Both the impulse input force and the output deflections were recorded as functions of time. By using a modified version of the computer program CONVLI (8), the computation of response functions in conjunction with Equation 5 resulted in vector quantities of the response functions. These values were then approximated by a mathematical function that employed a nonlinear least-squares curve-fitting method (computer code NONLINR). A study of the response functions suggested the equation

$$G_{x_i}(t) = \alpha \exp(-\beta t) \sin\gamma t \quad (6)$$

where

$G_{x_i}(t)$ = response function,
t = time, and
α, β, and γ = parameters of the response function.

Prediction of Step-Load Response

Consider the step-function input $F_{x_0}(t)$ applied at a point x_0 on the pavement:

$$F_{x_0}(t) = 0 \quad \text{for} \quad t = 0$$
$$F_{x_0}(t) = F_0 \quad \text{for} \quad t > 0 \quad (7)$$

where F_0 = magnitude of the static compressive force. If the corresponding output time function at $x = x_i$ is $y_{x_i}(t)$, substitution of Equations 6 and 7 into Equation 4 yields

$$y_{x_i}(t) = \int_0^t F_{x_0}(t - \tau)\, \alpha \exp(-\beta\tau) \sin\gamma\tau \, d\tau \quad (8)$$

Prediction of Repeated-Load Response

A haversine repeated load applied at $x = x_0$ is defined as

$$F_{x_0}(t) = 0 \quad \text{for } t = 0$$
$$F_{x_0}(t) = (F_0/2)[1 - \cos(2\pi/p)t] \quad \text{for } t > 0 \quad (9)$$

where p = period of loading.

Substitution of Equations 6 and 9 into Equation 4 gives the repeated-load response $Y_{x_i}(t)$ at $x = x_i$:

$$Y_{x_i}(t) = (F_0/2) \int_0^t \alpha \exp(-\beta\tau) \sin\gamma\tau [1 - \cos(2\pi/p)(t - \tau)] \, d\tau \quad (10)$$

The detailed solutions of Equations 8 and 10 and the computer programs STALOD and REPLOD, respectively, may be found elsewhere (9).

EXPERIMENTAL METHOD

To investigate the developed theory of pavement behavior, controlled laboratory testing of three-layer models of flexible pavements was conducted.

Scope of Testing

A silty-sand subgrade, a crushed-aggregate base 88.9 mm (3.5 in) thick, and an asphalt-concrete surface course were the components of the three-layer systems. Surface-course thicknesses of 25.4 and 50.8 mm (1 and 2 in) were used. Static, impulse, and cyclic loadings were considered. Contact pressures of 103, 206, and 412 kPa (14.93, 29.86, and 59.72 lbf/in^2) were applied over a circular loading plate of 101.6-mm (4-in) diameter at the center of the pavements. The tests were carried out in a constant-temperature room at 10°, 23.9°, and 37.8°C (50°, 75°, and 100°F).

Materials and Preparation of Pavements

The model pavements were contained in a wooden box reinforced with steel angles. To conduct the tests inside the constant-temperature room, the maximum possible size of the box had to be 0.8 x 0.8 x 0.6 m (32.5 x 32.5 x 23.25 in) deep. The silty-sand subgrade was compacted into 20 lifts by using an air hammer. The average dry density as determined by the sand-cone method (AASHTO T191) was 1848 kN/m^3 (115.5 lbf/ft^3), which was 101 percent of the standard AASHTO T99. The moisture content averaged 13.9 percent, which was close to the optimum moisture of 13.7 percent.

The base-course material was crushed-limestone aggregate conforming to Indiana specifications size 53. Tests performed according to T99 and T193 gave, respectively, an optimum density of 2022.4 kN/m^3 (126.4 lbf/ft^3) at an optimum moisture of 6.2 percent and a soaked California bearing ratio of 51.3 percent. The aggregate was compacted to a total thickness of 88.9 mm in three lifts by means of the air hammer. The surface was leveled with a vibrator.

The bituminous mixture used for the surface course was prepared from crushed limestone and sand blended according to Indiana type-B gradations. Asphalt cement was used that had a 6 percent (by weight of aggregate) penetration value of 60-70. The surface course was compacted and leveled by the air hammer and vibrator for a predetermined time. The density obtained for the 25.4-mm asphalt concrete was 2396.8 kN/m^3 (149.8 lbf/ft^3). The in-place void

Figure 2. Generation of impulse.

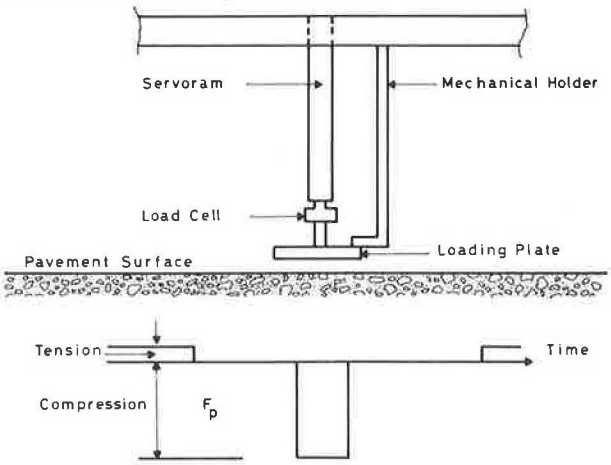

Figure 3. Overall view of test setup.

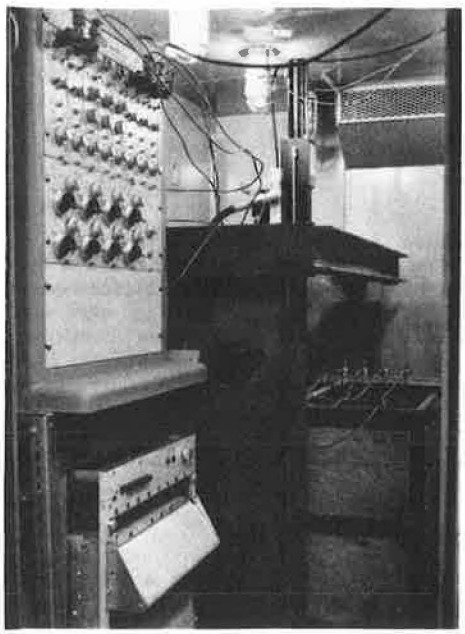

content corresponding to this density was calculated to be 4.6 percent. Hveem tests on laboratory-mix specimens yielded a unit weight of 2408 kN/m³ (150 lbf/ft³), Hveem stability of 48.1, and air voids of 4.2 percent.

On completion of the tests on the pavement that had 25.4-mm surfacing, the surface-course thickness was increased to 50.8 mm.

Instrumentation

Instrumentation was devised that would record the time-dependent input and output functions. A crucial part of the instrumentation technique was to devise a system capable of applying an impulse force of desired magnitude and duration and of detecting the surface motion at any required location on the pavement surface.

The equipment consisted of a steel loading frame coupled to a Material Testing System (MTS) electrohydraulic actuator. A mechanical holder was devised to hold the Servoram while the MTS console was being programmed in tension prior to application of a compressive square wave. The generation of an impulse by this technique is illustrated schematically in Figure 2.

Figure 4. Closeup view of test setup.

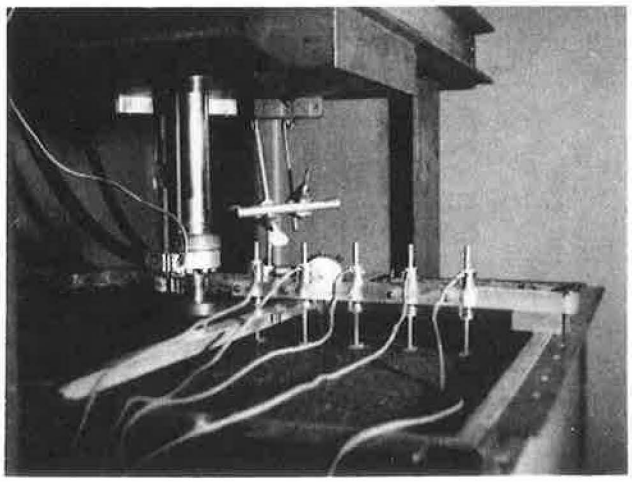

Table 1. Summary of data coding.

Surface-Course Thickness		Test Temperature		Input Function		Load Intensity[a]	
Code	mm	Code	°C	Code	Loading	Code	kPa
1	25.4	L	10	I	Impulse	1	103
2	50.8	M	23.9	S	Static	2	206
		H	37.8	R	Repeated	3	412

Note: 1 mm = 0.04 in; $t°C = (t°F - 32)/1.8$; 1 kPa = 0.145 lbf/in².

[a]Applied to a plate 101.6 mm (4 in) in diameter, these pressures amount, respectively, to 0.8, 1.7, and 3.3 kN.

Loads were applied by the MTS machine and measured with a FLIU 4.4-kN (1000-lbf) capacity Strainsert load cell mounted between the hydraulic actuator and the loading plate. The output of the load cell was recorded with a Brush Mark 280 two-channel recorder.

Five Sanborn Linearsyn linear variable differential transformers (LVDTs) were used to sense the deflections. One LVDT was located 82.6 mm (3.25 in) from the center of the loading plate. The other four were spaced 63.5 mm (2.5 in) apart along the same radial line. The outputs were amplified and recorded by an eight-channel Sanborn recorder.

The LVDTs were fixed to the pavement surface by screwing one end of a brass extension rod into the LVDT core and the other end into a brass plate 19 x 12.7 x 3.2 mm (0.75 x 0.5 x 0.125 in) thick. The plate was then glued to the appropriate location on the pavement surface by using Eastman 910 adhesive. The LVDTs were supported by aluminum channels and Plexiglas beams connected to the top angles of the box. Figure 3 shows the overall view of the test setup inside the constant-temperature room; a closeup of the LVDTs is show in Figure 4.

Test Procedures

Impulse-load magnitudes of 0.8, 1.7, and 3.3 kN (187.5, 375.0, and 750.0 lbf) were applied for about 0.16 s. The load input and the output responses formed the data for determination of the response functions. Static compressive forces of the same magnitudes were applied and held until the deflections were almost constant with time. This was found to be of the order of a few minutes. The repeated-load tests were conducted at a rate of 15 cycles/min for 250 cycles. The data coding shown in Table 1 summarizes the tests that were performed. For example, one series of tests might be represented by the code "series 1LI1".

Figure 5. Input-load and output-deflection functions: data for series 1HI1.

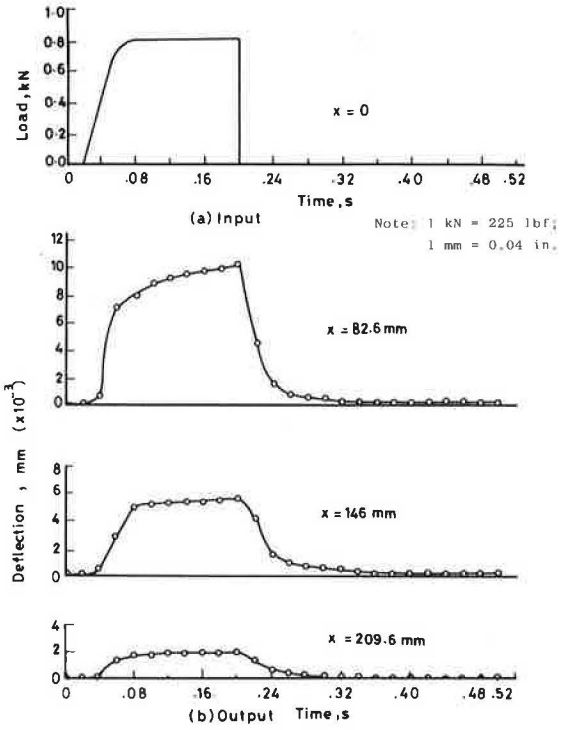

Figure 6. Input-load and output-deflection functions: data for series 1HI3.

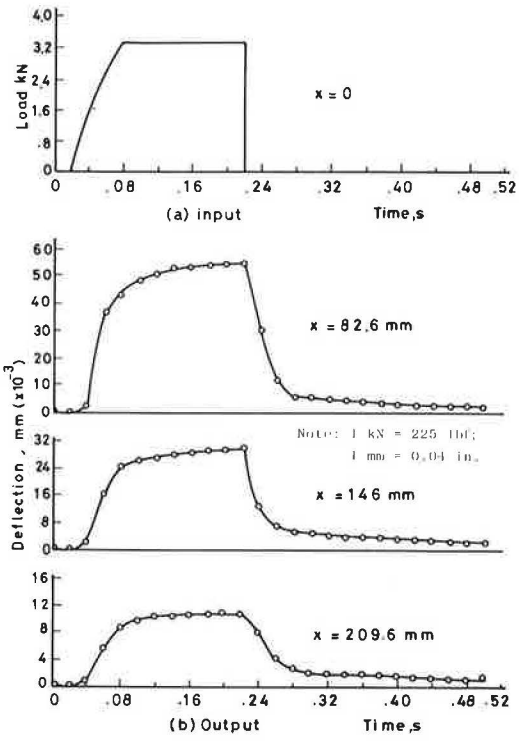

Figure 7. Response functions: data from series 1HI1.

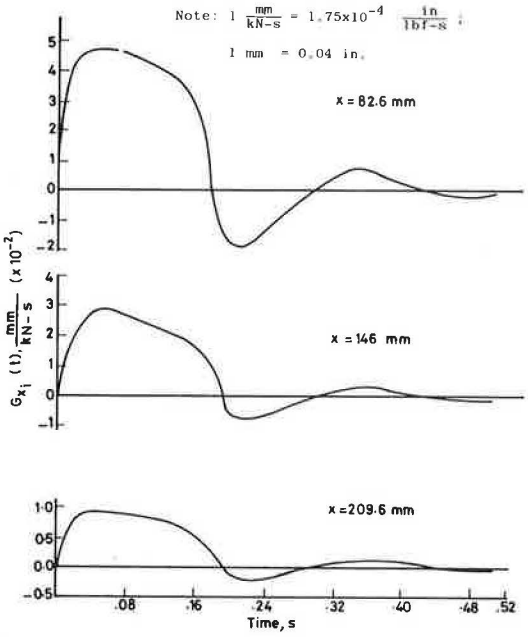

Figure 8. Response functions: data from series 1HI3.

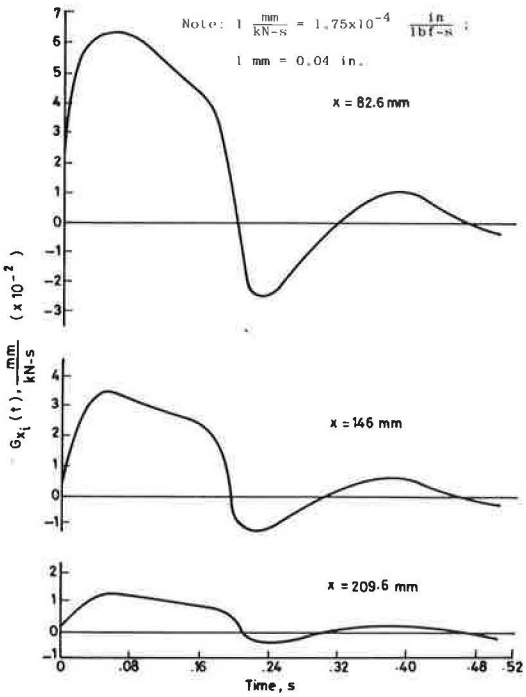

RESULTS

Response-Function Parameters

Typical plots of the inputs and outputs from impulse tests are shown in Figures 5 and 6, and the corresponding response functions are illustrated, respectively, in Figures 7 and 8. It is seen that the response functions reach a peak and then oscillate with time. In general, the peak occurred in the time band of 0.04-0.08 s. The general shape of the response functions and the corresponding results agreed with those obtained from mechanical models (10-12). However, when mechanical models are used to describe pavement behavior, the parameters must first be defined, usually in the form of differential equations, and no reliable method now exists by which to determine them. The consistency of the response functions obtained in this study appears to validate the hypothesis that a determinable relationship exists between input and output of a pavement system.

Table 2 summarizes four response-function parameters for a surface-course thickness of 25.4 mm and a test temperature of 37.8°C (100°F). It is evident from this table that these parameters do not change significantly as the peak impulse load is changed. These results are quite similar to those found by Boyer and Harr in prototype testing of an airfield pavement (7).

Typical values of the α-, β-, and γ-parameters of Equation 6 are shown in Table 3, in which it is indicated that, in general, the parameters for a given test combination do not vary appreciably as the magnitude of load changes. In a few cases, distinct variability was evident in the α-values. It is possible that this discrepancy may be reduced if more parameters are included in the response-function model. Continuation of this research is already under way by using the following proposed equation:

$$G_{x_i}(t) = \alpha \exp(-\beta t) \sin\gamma t + \delta \cos\epsilon t \quad (11)$$

where α, β, γ, δ, and ε are parameters. Preliminary analysis indicated that the squared correlation coefficient (R^2) was improved.

Parameters α, β, and γ are measures of the peak of the response function $G_{x_i}(t)$ and the variability of $G_{x_i}(t)$ with time. As such, α can be regarded as representing the stiffness characteristics of a pavement system, whereas β and γ reflect the damping characteristics of the system. Pavement materials that have large α-values will provide less resistance to imposed loads.

From the plots of α versus temperature shown in Figure 9, it is observed that temperature plays an important role in the response function of pavement systems. Since flexible-pavement components (asphalt concrete in particular) are thermoplastic, they yield increased response for increases in temperature and hence increased α-values.

Figure 9 indicates that when x = 82.6 mm (3.25 in) and 146 mm (5.75 in) the value of α decreases with increases in surface-course thickness at all temperatures. However, at x = 209.6 mm (8.25 in) α increases slightly with increase in thickness. This trend reflects the slablike action of the system in which a thicker pavement responds more at remote locations than does a thinner one. The value of α decreases with increasing values of x; thus the attenuation of the magnitude of α with spatial location is depicted.

The interaction between surface-course thickness and temperature is exhibited by the shape of the curves in Figure 9. For the 25.4-mm surface, the bottom layers (the response of which constitutes most of the total deflection) are less affected by temperature changes than is the surface course, and hence the rate of increase in α decreases with increasing temperature (convex curves). In the case of the thicker pavement, increasing temperature raises the rate of increase in α (concave curves) due to the temperature susceptibility of asphalt concrete. Note that this trend is practically negligible at x = 209.6 mm, at which the effect of load is small.

Table 2. Comparison of response functions.

x (mm)	F_p (kN)	First Positive Peak		First Negative Peak	
		Magnitude (mm/kN·s)	Time (s)	Magnitude (mm/kN·s)	Time (s)
82.6	0.8	0.0480	0.06	-0.0190	0.20
	1.7	0.0713	0.06	-0.0300	0.22
	3.3	0.0634	0.06	-0.0250	0.22
146.0	0.8	0.0297	0.04	-0.0075	0.22
	1.7	0.0369	0.04	-0.0094	0.24
	3.3	0.0343	0.04	-0.0118	0.22
209.6	0.8	0.0094	0.06	-0.0022	0.22
	1.7	0.0125	0.06	-0.0043	0.22
	3.3	0.0128	0.06	-0.0031	0.24

Note: 1 mm = 0.04 in; 1 kN = 225 lbf; 1 mm/kN·s = 1.75 x 10^{-4} in/lbf·s.

Table 3. Descriptive parameters in the response functions at 10 and 37.8°C.

Thickness (mm)	x (mm)	F_p (kN)	α (mm/kN·s)	β (1/s)	γ (1/s)	R^2 (%)
Response Functions at 10°C						
25.4	82.6	1.7	0.035 9	10.764	13.382	85.73
		3.3	0.059 4	10.551	15.848	87.48
		Avg	0.047 6	10.658	14.615	
	146.0	1.7	0.007 8	7.127	14.593	78.09
		3.3	0.020 6	8.784	17.285	86.79
		Avg	0.014 2	7.956	15.939	
	209.6	1.7	0.002 7	6.140	14.470	75.86
		3.3	0.004 1	8.195	15.716	86.32
		Avg	0.003 4	7.168	15.093	
50.8	82.6	0.8	0.030 8	12.879	12.336	92.39
		1.7	0.020 4	9.847	12.709	87.60
		3.3	0.030 8	8.785	16.018	84.34
		Avg	0.027 3	10.504	13.688	
	146.0	0.8	0.013 8	11.302	14.222	83.88
		1.7	0.009 7	7.517	12.988	83.16
		3.3	0.020 0	7.540	16.406	84.82
		Avg	0.014 5	8.786	14.539	
	209.6	0.8	0.004 0	9.610	12.598	65.68
		1.7	0.002 9	7.409	12.996	73.44
		3.3	0.008 9	8.792	16.824	83.86
		Avg	0.005 3	8.604	14.139	
Response Functions at 37.8°C						
25.4	82.6	0.8	0.011 05	8.953	16.968	84.62
		1.7	0.014 88	7.950	15.353	83.28
		3.3	0.015 03	8.633	15.334	84.30
		Avg	0.013 65	8.512	15.885	
	146.0	0.8	0.070 6	10.044	15.383	88.75
		1.7	0.012 65	12.506	12.335	82.95
		3.3	0.085 3	9.478	14.911	81.78
		Avg	0.094 1	10.676	14.210	
	209.6	0.8	0.025 2	10.523	15.061	88.57
		1.7	0.035 1	10.951	14.452	78.24
		3.3	0.036 9	10.659	12.977	85.20
		Avg	0.032 4	10.711	14.163	
50.8	82.6	0.8	0.010 02	11.273	14.046	83.11
		1.7	0.013 29	13.187	13.870	86.90
		3.3	0.011 05	12.960	12.700	80.87
		Avg	0.011 45	12.473	13.539	
	146.0	0.8	0.062 2	9.051	14.274	87.87
		1.7	0.063 3	8.779	12.825	89.93
		3.3	0.089 5	12.068	13.983	89.15
		Avg	0.071 7	9.966	13.694	
	209.6	0.8	0.026 1	8.202	13.798	84.81
		1.7	0.042 6	11.846	11.680	92.34
		3.3	0.038 2	11.081	13.015	93.19
		Avg	0.035 6	10.376	12.831	

Note: 1 mm = 0.04 in; 1 kN = 225 lbf; 1 mm/kN·s = 1.75 x 10^{-4} in/lbf·s.

Figure 9. Curves of α-parameter versus temperature.

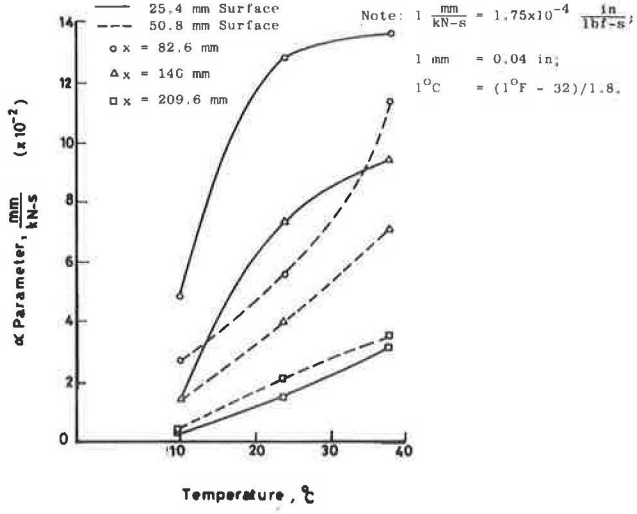

Figure 10. Typical predicted and measured static-load deflections, 25.4-mm surface, 37.8°C.

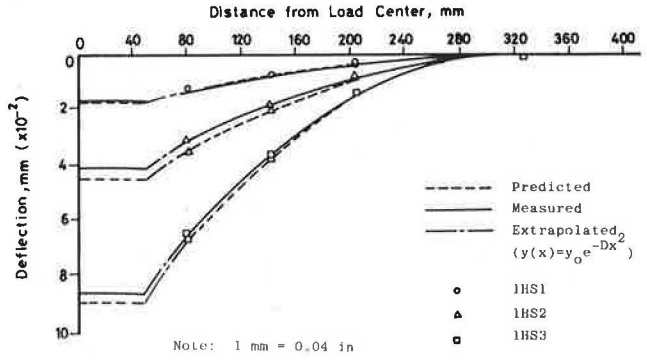

Figure 11. Typical predicted and measured static-load deflections, 50.8-mm surface, 10°C.

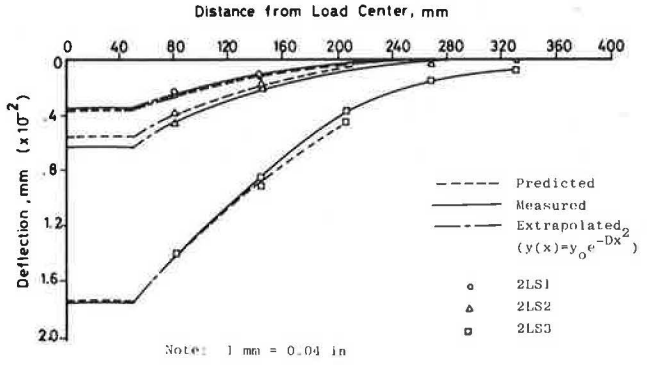

Examination of Table 3 reveals that changes in β and γ are small when temperature, thickness, or location change. This is possibly due to the fact that no significant change is observed in the shapes of the response-function curves. Furthermore, the slight variations in the values of these parameters are not critical, since they appear as exponential and sinusoidal functions, respectively, in the response-function model (Equation 6).

Pavement Response

Typical plots of predicted and measured deflections are shown in Figures 10 and 11 for static loads and in Figures 12 and 13 for repeated loads (total deformation). Close agreement is observed in almost all cases. The results indicate that static and repeated-load responses can be predicted by using the theory developed in this investigation.

For the application of the procedure to prototype flexible highway pavements, catalogs of response functions and pavement systems must be obtained by using, for example, a standard (or test) vehicle. Once sufficient information has been gathered, responses due to any stationary or moving vehicle can be computed by using computer programs STALOD and REPLOD, respectively.

When the deflection profiles of Figures 10-13 are plotted, the section from the innermost LVDT to the edge of the loaded plate was extrapolated by using the following equation (9, 13):

$$y(x) = y_0 \exp(-Dx^2) \quad (12)$$

where

y(x) = deflection at a distance x from the load center,
y_0 = maximum deflection of the deflected basin, and
D = a constant that reflects the attenuation of the deflected basin with x.

Figure 12. Typical predicted and measured repeated-load deflections, 25.4-mm surface, 23.9°C.

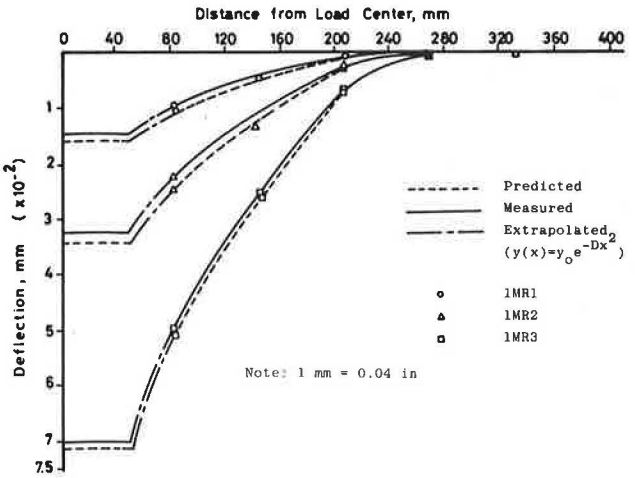

Figure 13. Typical predicted and measured repeated-load deflections, 50.8-mm surface, 10°C.

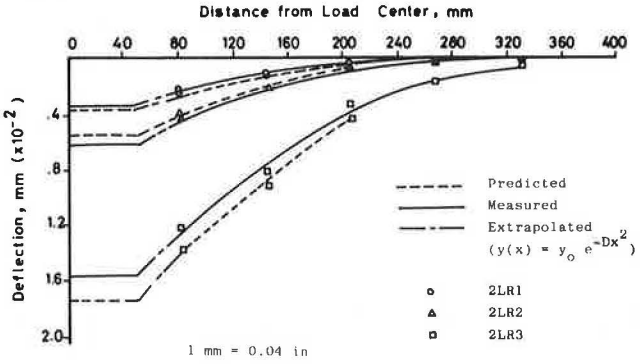

It may be observed in Figures 10-13 that the portion of the pavement surface under the loading plate was considered to have experienced constant displacement. This was a consequence of using a rigid loading plate, which was chosen to obtain a distinct trace of load duration during impulse tests.

SUMMARY AND CONCLUSIONS

Pavement parameters were determined from impulse-load tests and by using transfer functions. The derived parameters were used in conjunction with a formulated theory to predict static- and repeated-load deflections for various test conditions. Close agreement was observed between predicted and measured values.

From the results and analyses of the data and within the scope of this investigation, the following conclusions can be drawn:

1. The time-dependent behavior of a flexible pavement can be represented by a set of response functions $G_{x_i}(t)$, which are functions of time (Equation 6). It is possible to obtain these functions from impulse tests on the pavement.
2. Parameters in the response functions are believed to be descriptors of pavement behavior. These parameters are generally independent of type or magnitude of input load.
3. Temperature, surface-course thickness, and spatial location have their respective influences on the response functions. Increases in temperature increase the value of the α-parameter in the response functions, whereas

increases in surface-course thickness or in the distance from the load center decrease the α-value. The β- and γ-parameters do not seem to be affected appreciably by the above factors.

4. It is believed from the favorable agreement between calculated and measured responses that transfer-function theory appears to be capable of predicting static- or repeated-load deflections of flexible pavements.

ACKNOWLEDGMENT

We extend our sincere thanks to the authorities of the Joint Highway Research Project of Purdue University for financial support of this research. The opinions and conclusions expressed are ours and do not necessarily reflect those of the sponsoring agency.

REFERENCES

1. C.B. Drennon and W.J. Kenis. Response of a Flexible Pavement to Repetitive and Static Loads. HRB, Highway Research Record 337, 1970, pp. 40-54.
2. T.M. Eggleston and C.W. Mathews. Application of Several Methods for Determining Transfer Functions and Frequency Response of Aircraft from Flight Data. National Advisory Committee for Aeronautics, TR-Rept. 1204, 1954, pp. 1-24. NTIS: NACA-TR-1204.
3. P.A. Crafton. Shock and Vibration in Linear Systems. Harper, New York, 1961.
4. J.H. Goldberg. Automatic Controls: Principles of Systems Dynamics. Allyn and Bacon, Boston, 1964.
5. T.K. Puchalka and A. Wozniak. Elements and Circuits for Automatic Control. Boston Technical Publishers, Cambridge, MA, 1968.
6. S.A. Swami, W.H. Goetz, and M.E. Harr. Time and Load Independent Properties of Bituminous Mixtures. HRB, Highway Research Record 313, 1970, pp. 63-78.
7. R.E. Boyer and M.E. Harr. Predicting Pavement Performance. Transportation Engineering Journal of ASCE, Vol. 100, No. TE2, May 1974, pp. 431-442.
8. R.E. Boyer. Predicting Pavement Performance Using Time-Dependent Transfer Functions. Purdue Univ. and Indiana State Highway Commission, Lafayette, IN, Joint Highway Research Proj. 32, Sept. 1972.
9. G.A. Ali. A Laboratory Investigation of the Application of Transfer Functions to Flexible Pavements. Purdue Univ., Lafayette, IN, Ph.D. thesis, Aug. 1972.
10. W. Heukelom. Analysis of Dynamic Deflections of Soils and Pavements. Geotechnique, Vol. 11, No. 3, Sept. 1961, pp. 224-243.
11. N.M. Isada. Detecting Variations in Load-Carrying Capacity of Flexible Pavements. NCHRP, Rept. 21, 1966.
12. N.M. Isada. Impulsive Load Stiffness of Flexible Pavements. Journal of the Soil Mechanics and Foundations Division of ASCE, Vol. 96, No. SM 2, March 1970, pp. 639-648.
13. G.Y. Baladi and M.E. Harr. Nondestructive Pavement Evaluation: The Deflection Beam. TRB, Transportation Research Record 666, 1978, pp. 19-26.

Publication of this paper sponsored by Committee on Flexible Pavement Design.

Evaluation of Pavement in Florida by Using the Falling-Weight Deflectometer

JATINDER SHARMA AND R. N. STUBSTAD

A method is presented by which mechanical properties of a pavement system can be determined by using nondestructive test methods that are now available. The ultimate goal is the establishment of rehabilitation criteria for existing flexible pavements that use purely analytical (as opposed to empirical) relationships. More specifically, the use of the falling-weight deflectometer (FWD) is discussed. Several sections of Interstate 75 in Florida were chosen in order to determine material characteristics of the pavement layers. These sections were also tested with the Dynaflect apparatus. Data developed from the FWD and Dynaflect deflections were accumulated and elastic moduli for the typical section were determined by using a computer program developed at the Florida Department of Transportation: in situ stress-dependent elastic moduli, four layers (ISSEM4). The elastic moduli were then compared with other test results, and a good correlation was indicated. How such mechanical properties may be used in an appropriate structural analysis to better locate and control distress parameters in the pavement system is outlined. Such analysis is possible from the knowledge obtained in situ of the various structural layers involved.

For many years the Florida Department of Transportation (FDOT) has used various deflection concepts to monitor both local and Interstate road networks. Generally, it has been found that deflection alone is not an adequate indicator of pavement performance or loss of serviceability. For example, many situations have been observed in which deflections remained low, even though significant load-associated pavement deterioration was visibly taking place.

Surface deflection may be interpreted as the sum of the vertical strains throughout each structural layer below. If a weakness should develop in one or more of these layers, it may not necessarily change the total deflection significantly; e.g., a relatively thin layer might contribute little change to the center measurement of a deflection-measuring device. A more-indicative measure of distress is thus necessary.

In order to further understand and evaluate pavement deterioration and ultimately recommend corrective rehabilitation and management strategies, it was decided to try to isolate problem areas in terms of which layer or layers were instrumental in the deterioration of Interstate 75 in northern Florida. Also, it was hoped that performance criteria based on derived material properties could be developed.

On the basis of work done in Europe, the falling-weight deflectometer (FWD) was chosen to carry out a layered-system (mechanistic) analysis of the pavement structure. Approximately 180 lane-km (110 lane-miles) of Interstate were tested and analyzed (see Figure 1).

FWD AND ASSOCIATED EQUIPMENT

Use of the FWD has been well documented elsewhere (1-3). Briefly, the basic idea behind the development of the FWD

Figure 1. Falling-weight deflectometer (FWD) on I-75 near Gainesville, Florida.

Figure 2. Dynatest 7800 registration equipment for FWD testing.

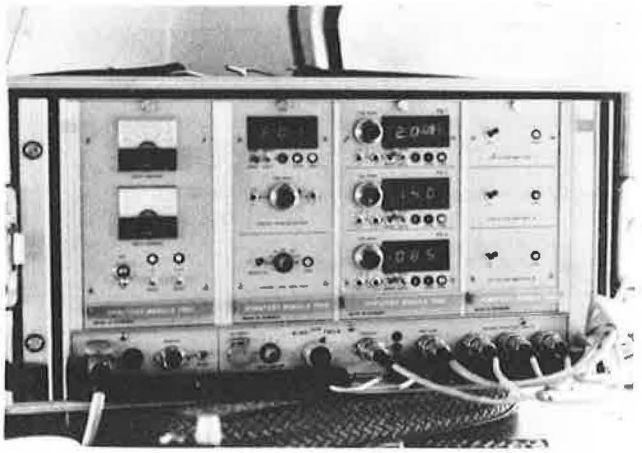

was attractive, i.e., to simulate the effect of a moving-wheel load with a nondestructive test apparatus. This is accomplished in terms of both stress and load and, to a lesser degree, in terms of duration of load. Not simulated is the rotation of principal stresses as they occur under a moving-wheel load. Although the FWD satisfactorily simulates the duration of load near the surface, when the moving-wheel load is measured at greater depths, there is a somewhat longer duration than that measured by the FWD.

Nevertheless, the possible shortcomings of the wheel-load-simulating FWD loading system have been largely dispelled by several research projects (4,5). In these projects the deflections, stresses, and strains throughout the pavement systems were compared for similar moving-wheel-load and FWD-imposed forces. The correspondence of the two was remarkably satisfactory for all three parameters (within 10 percent). Therefore, it was felt that the FWD system would be beneficial to the state of the art. Features of the FWD are (a) a capable load range of about 13-50 kN (3000-11 000 lbf), (b) an associated loading time (approximately half-sine-formed) of 26 ms, and (c) vertical deflections that may be taken at any desired position from the center of the loading plate outward along the deflection basin. The peak value of the stress level under the loading plate and the corresponding peak values of deflection are digitized and recorded on the Dynatest 7800 registration equipment (Figure 2).

On the assumption that the elastic moduli of materials may be derived from deflection tests, it was felt that the FWD would correspond better to conditions that would be appropriate for properties relevant to the wheel (axle) load than would the several available steady-state loading systems now in use in the United States, provided that an appropriate structural analysis based on surface deflections could be carried out.

MULTILAYERED REVERSE-ITERATIVE COMPUTER PROGRAM

Although approximate methods that can be performed on a calculator have been devised and documented for deriving stiffness values based on deflection measurements (6), it was felt that a quicker and more foolproof method would be the development of a reverse elastic-system computer program. Such an approach was attractive because the derived parameters, due to the similarity between FWD and moving-wheel-load effects, would be relevant for direct measurement of performance criteria of traffic-associated loadings.

Although a finite-element program, in which each element would have been modeled by using the best information available for each respective structural material, would have been best suited to derive values of stiffness of modulus, such an approach would have required too much computer time per analysis to ascertain these stiffness relationships from each set of FWD deflection data. At the same time, it should be pointed out that most road-building materials do not respond linearly; i.e., different states of stress result in different apparent stiffnesses (secant moduli) for the same material. If a linear-elastic program, in which calculated versus measured deflections are matched by juggling E-values, is used to model the pavement system, gross errors will result even if the stress-dependent nature of the materials (especially the semi-infinite subgrade) are comparatively minimal.

These factors predicted that the linear-elastic ELSYM5 program (7) could nevertheless be employed, although it would have to be modified so that variable stiffnesses that depended on the state of stress under each corresponding deflection sensor could be used for calculating the total deflection. The individual solution is valid for that particular deflection position only. A separate calculation is necessary for each measured deflection along the deflection basin.

By using principles of the method of equivalent thicknesses as well as Boussinesq's equations, the iteration procedure was streamlined and implemented so that a unique solution could be quickly obtained. The program is known as in situ stress-dependent elastic moduli, four layers (ISSEM4), documented elsewhere (8).

The only additional input quantities needed, other than those normally used in the ELSYM5 input format, are the measured deflections at the design or FWD load, the load magnitude and radius, and the K_2-values for the second (base), third (subbase), and fourth (subgrade) layers, where the stiffness or resilient modulus (E) assumes the form

$$E(\text{or } E_0) = K_1 \sigma_x^{K_2} \quad (1)$$

where

σ_x = some selected dynamic stress parameter in the modeled material,

E = element (cylindrical column the height of the structural layer) modulus,

E_0 = surface (i.e., subgrade surface) or composite modulus, and

K_1 and K_2 = material characterization constants.

The K_2-values can be obtained through FWD tests that are conducted at different stress levels.

Finally, the iterative ISSEM4 program is seeded with a set of E-values to start the iteration process. The results are output in the form of derived variable stiffnesses for the three unbound structural layers and an E_1-value for the

centerline; all of these are characterized by the corresponding measured versus derived deflections at several distances r from the load (up to seven positions). The derived K_1-values for each structural material (layer) are also listed in the output.

The most useful and interesting aspect of the results of these calculations is, of course, the centerline stiffnesses, which can be used in the calculation of critical stresses and strains for a given design-load configuration. If the design load is significantly different from the imposed FWD load level used in the analysis, the centerline E-values may be altered according to the Equation 1 relationship(s) mentioned above.

BASIC APPROACH TO ISSEM4 PROGRAM

As the ISSEM4 program now exists, it is necessary to assign certain stiffness model parameters (K_2-values) for layers 2, 3, and 4 in the pavement structure. Again, a model of the form specified by Equation 1 was chosen. This model may be used to assist in the optimal use of the ISSEM4 program as follows.

Generally speaking, the farther a deflection reading is from the load, the deeper the materials in the structure affect that deflection. In fact, as Ullidtz (6) has shown, if the equivalent thickness (h_e) of the pavement structure above the subgrade is defined as

$$h_{e,m} = 0.85\left[h_1\sqrt[3]{E_1/E_m} + h_2\sqrt[3]{E_2/E_m} + \ldots h_{m-1}\sqrt[3]{(E_{m-1})/E_m}\right] \quad (2)$$

which is equal to or less than the distance r from the center of the FWD load to a deflection sensor, the surface modulus (E_0) of the subgrade will be very close to

$$E_{0,m} = [\sigma_0 a^2(1 - \nu^2)]/(rS_{0,r}) \quad (3)$$

where

σ_0 = the loading-plate stress level,
a = radius of the plate,
ν = Poisson's ratio, and
$S_{0,r}$ = deflection reading at position r.

Since the falling weight may be used over a wide range of stress levels, the K_2-value associated with the subgrade may now be easily calculated from FWD test results alone by calculating the $E_{0,m}$-values for a series of stress levels σ_0.

Since σ_x in Equation 1 is approximately proportional to σ_0, a regression analysis (in a log-log form) between the variables σ_0 and $E_{0,m}$ will yield the subgrade slope K_2.

By selecting proper deflection sensor positions, the K_2-values associated with other areas of the pavement structure can be deduced, and this process generally results in a better-than-educated-guess estimate of the three K_2-values needed for the ISSEM4 input format. Furthermore, since the effective layer stiffnesses that correspond to the various distances r from the actual load associated with the FWD or other deflection-testing devices vary significantly, even for very small values of K_2, an educated guess at these values will produce far more reliable centerline stiffness results than if no stress sensitivity were considered. This illustrates a fundamental error normally inherent in most nondestructive-testing analysis techniques, namely, that the layered-system E-values are typically modeled as constant in a horizontal direction. This assumption, especially with regard to the subgrade, will result in gross errors when the deflection basin is used to derive centerline stiffness.

SAMPLE RUNS OF ISSEM4

The structural dimensions and materials of one of the areas of I-75 that was investigated are as follows (1 mm = 0.039 in):

Material	Thickness (mm)
Asphalt concrete, h_1	178
Limerock base, h_2	265
Subbase, h_3	310
Subgrade, h_4	∞

FWD test results at a typical point in the inner-wheel path of the traffic lane gave the set of measured deflections shown below for a plate diameter of 300 mm (11.7 in) (1 mm = 0.039 in; 1 kPa = 0.145 lbf/in²):

Distance from Load, r (mm)	Deflection, $S_{0,r}$ (μm) σ_0 = 695 kPa	(μm) σ_0 = 354 kPa
0	205	93
300	150	66
450	118	51
750	77	32
1200	41	18

By using Equation 3, the values of $E_{0,m}$ that correspond to the subgrade at two stress levels may be calculated with the deflections at r = 1200 mm (47 in). For σ_0-values of 695 and 354 kPa (100.8 and 51.3 lbf/in²), $E_{0,m}$ = 279 and 324 MPa (40 455 and 46 980 lbf/in²), respectively. By using the model depicted in Equation 1, the K_2-exponent of σ_0 versus $E_{0,m}$ then becomes $K_2 = -0.22$. This value is rounded to -0.20.

If we keep in mind that the determination of a K_2-value that corresponds to a distance $r \sim h_e$ above layers 2 or 3 will produce a composite slope, which includes the materials below the layer in question, the K_2-values may nevertheless be estimated by considering the superposition nature of the E_0-values thus obtained. Initially, this is carried out in a qualitative manner, but finally the whole deflection basin can be compared with the final calculated deflection values to obtain the best solution.

In this case, the final K_2-values and the estimates of Poisson's ratio were

Layer	ν	K_2
1	0.35	-
2	0.25	-0.20
3	0.35	-0.40
4	0.35	-0.20

Figure 3 shows how the layered-system E-values vary according to the $E = K_1\sigma_0^{K_2}$ relationship for all r's $\leq h_e$ above the layer in question. The results are quite reasonable; the average asphalt temperature was about 18°C (64°F) (tested in January 1979). Interestingly, the same series of FWD tests was run about seven months later, during the summer of 1979. The average asphalt temperature was then about 27°C (80°F), an increase of 9°C (16°F).

By using the method outlined above, the K_2-values were fixed, and the resulting ISSEM4 output is shown in Figure 4.

It is significant to note that even though the asphalt modulus E_1 was lower during the summer, as expected, the center FWD deflection actually decreased, which indicates a stiffer overall surface modulus (composite stiffness). A comparison of the two ISSEM4 outputs reveals why: The stiffnesses of the unbound materials increased during the summer, whereas the stiffness of the asphalt concrete (AC) decreased. The overall effect at this test point and most others on I-75 was a lower deflection; this is quite the opposite of what one would expect by regarding changes in asphalt stiffness due to temperature variation alone. This was the general tendency for all sections that were investigated along I-75.

Thus, it was possible to see clearly what was happening seasonally on this Florida section of Interstate roadway, which enabled a more rational use of critical stresses and strains relative to performance criteria through what is now

Figure 3. ISSEM4 outputs that depict derived stiffnesses for a four-layer system from FWD tests: winter analysis.

ELASTIC SYSTEM 2 - I-75 ALACHUA COUNTY SBT STA 3A, WINTER FWD ANALYSIS

	R1	R2	R3	R4	R5	R8
MEASURED DEFLECTIONS: MICRO-METERS	205.00000	150.00000	118.00000	(not used)	77.00000	41.00000
CALCULATED DEFLECTIONS: MICRO-METERS	206.25656	150.06708	121.14775	96.80402	77.14532	40.96275
MEASURED DEFLECTIONS: MILS	8.07085	5.90550	4.64566	0.0	3.03149	1.61417
CALCULATED DEFLECTIONS: MILS	8.12032	5.90814	4.76959	3.81117	3.03721	1.61270
SIG12, MAX PRIN, CENTER LAYER 2, MPA	-0.06465	-0.04620	-0.03283	-0.02300	-0.01604	-0.00543
SIG12, MAX PRIN, CENTER LAYER 2, PSI	-9.37737	-6.70052	-4.76113	-3.33518	-2.32585	-0.78771
SIG13, MAX PRIN, CENTER LAYER 3, MPA	-0.02559	-0.02235	-0.01900	-0.01561	-0.01253	-0.00602
SIG13, MAX PRIN, CENTER LAYER 3, PSI	-3.71122	-3.24114	-2.75626	-2.26336	-1.81660	-0.87314
SIGZZ4, VERTICAL, TOP OF SUBGRADE MPA	-0.01855	-0.01581	-0.01297	-0.01007	-0.00749	-0.00264
SIGZZ4, VERTICAL, TOP OF SUBGRADE PSI	-2.69113	-2.29343	-1.88047	-1.45987	-1.08562	-0.38249
E1, MPA	7080.953	6573.000	6573.000	6573.000	6573.000	6573.000
E1, PSI	1027005.063	953332.688	953332.688	953332.688	953332.688	953332.688
E2, MPA	466.953	505.624	504.000	504.000	504.000	504.000
E2, PSI	67725.688	73334.438	73098.938	73098.938	73098.938	73098.938
E3, MPA	203.698	215.804	230.120	249.089	273.972	351.000
E3, PSI	29543.840	31299.742	33376.059	36127.344	39736.254	50908.227
E4, MPA	195.188	201.737	209.933	221.027	234.335	284.363
E4, PSI	28309.563	29259.527	30448.125	32057.297	33987.344	41243.391
K1	0.0	273.37109	0.0	0.0	47.51357	88.24374
K2	0.0	-0.20000	0.0	0.0	-0.40000	-0.20000

Figure 4. ISSEM4 outputs that depict derived stiffnesses for a four-layer system from FWD tests: summer analysis.

ELASTIC SYSTEM 2 - I-75 ALACHUA COUNTY SBT STA 3A, SUMMER FWD ANALYSIS

	R1	R2	R3	R4	R5	R8
MEASURED DEFLECTIONS: MICRO-METERS	179.00000	106.00000	80.00000	(not used)	51.50000	30.00000
CALCULATED DEFLECTIONS: MICRO-METERS	178.13080	106.07993	83.79709	64.86893	51.30841	29.98637
MEASURED DEFLECTIONS: MILS	7.04723	4.17322	3.14960	0.0	2.02755	1.18110
CALCULATED DEFLECTIONS: MILS	7.01301	4.17637	3.29909	2.55389	2.02001	1.18056
SIG12, MAX PRIN, CENTER LAYER 2, MPA	-0.09798	-0.05942	-0.03792	-0.02420	-0.01546	-0.00462
SIG12, MAX PRIN, CENTER LAYER 2, PSI	-14.21110	-8.61764	-5.49914	-3.51018	-2.24263	-0.67034
SIG13, MAX PRIN, CENTER LAYER 3, MPA	-0.03472	-0.02778	-0.02315	-0.01813	-0.01388	-0.00601
SIG13, MAX PRIN, CENTER LAYER 3, PSI	-5.03517	-4.02954	-3.35733	-2.62971	-2.01253	-0.87237
SIGZZ4, VERTICAL, TOP OF SUBGRADE MPA	-0.02399	-0.01871	-0.01487	-0.01085	-0.00757	-0.00243
SIGZZ4, VERTICAL, TOP OF SUBGRADE PSI	-3.48009	-2.71427	-2.15716	-1.57306	-1.09823	-0.35287
E1, MPA	4043.707	4414.000	4414.000	4414.000	4414.000	4414.000
E1, PSI	586489.813	640196.313	640196.313	640196.313	640196.313	640196.313
E2, MPA	627.082	692.286	601.000	601.000	601.000	601.000
E2, PSI	90950.438	100407.563	87167.625	87167.625	87167.625	87167.625
E3, MPS	342.268	365.723	396.537	437.514	489.461	518.000
E3, PSI	49641.625	53043.602	57512.859	63456.004	70990.188	75129.500
E4, MPS	316.127	322.367	330.644	341.415	353.473	389.366
E4, PSI	45850.355	46755.355	47955.883	49518.012	51266.855	56472.738
K1	0.0	393.61084	0.0	0.0	88.43462	217.11929
K2	0.0	-0.20000	0.0	0.0	-0.40000	-0.10000

viewed as a relevant mechanistic analysis at the proper time, i.e., the season.

It must be emphasized here that, on the assumption that (a) elastic (linear or nonlinear) theory holds, (b) the material characterization models employed are valid, and (c) the FWD force and deflections are accurate, the solution derived through this iterative technique is unique to the accuracy allowed in the iterative process. The criterion for uniqueness is that there must be one or more deflection readings per structural layer and that these must be fairly strategically placed, approximately as outlined in the preceding discussion.

COMPARISON OF FWD WITH OTHER AVAILABLE TEST RESULTS

The temperature-modulus curve for the unaged asphalt mix that was used on the section of I-75 in the preceding sample run may be seen in Figure 5. A plot of the two E_1-values from the FWD tests shown in Figure 4 is also shown in

Figure 5. Relationship between temperature and complex modulus for the I-75 asphalt-concrete mix.

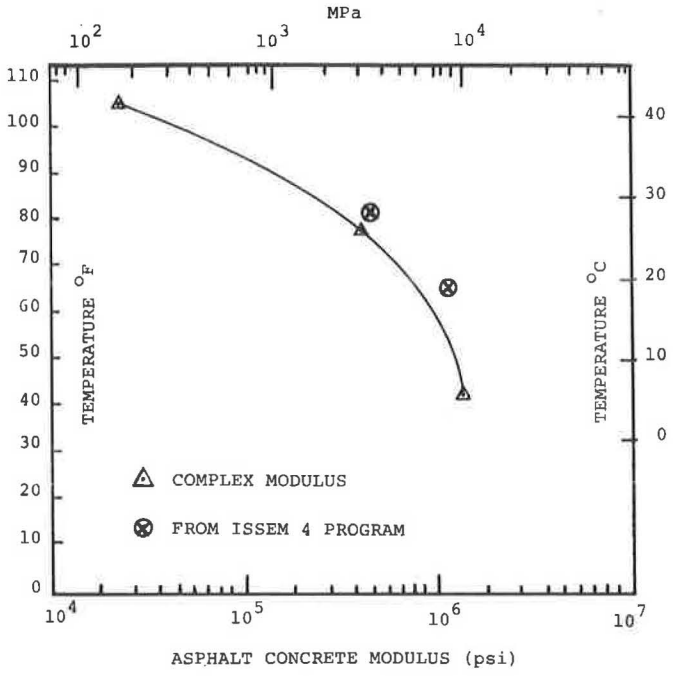

Figure 5. As expected, the mix is harder now, and the points fit the shape of the curve remarkably well.

A few static plate-bearing tests run on the trenches of I-75 subgrade compared favorably with the results derived from the FWD surface tests, although only when the change in stiffness according to Equation 1 was considered. This is in fact very important, because static plate-bearing tests are usually run at stress levels that are much higher, i.e., 10-100 times as high as those that actually occur under the completed pavement structure. The resulting difference in subgrade stiffness (depending on the magnitude of the K_2-value) may be of the order of a factor of 2 or 3.

On selected sections, the Dynaflect and FWD deflection basins were compared. Several of these sections are shown in Figure 6. The FWD deflections are normalized to units per 1000 lbf (units per 4.45 kN) to make the comparison clearer. In some cases, it may be seen that the comparison is reasonable in view of the lesser applied-load magnitude of the Dynaflect apparatus; in others, the comparison is poor.

Even though in principle the same approach may be used for evaluating Dynaflect data by using the ISSEM4 program (provided that some means of assigning K_2-values can be found), even a moderately different deflection basin will yield appreciably different stiffness values. An analysis of this sort was attempted that used the K_2-values derived from FWD tests. In accordance with the indications in Figure 5, it was found that the results often compared favorably with the FWD-derived values at a low stress level. In other cases, the derived values diverged from the FWD counterparts, most often on the high side for E_1, E_2, and E_3 and on both sides for $E_{0,4}$.

Figure 6. FWD and Dynaflect deflection basins.

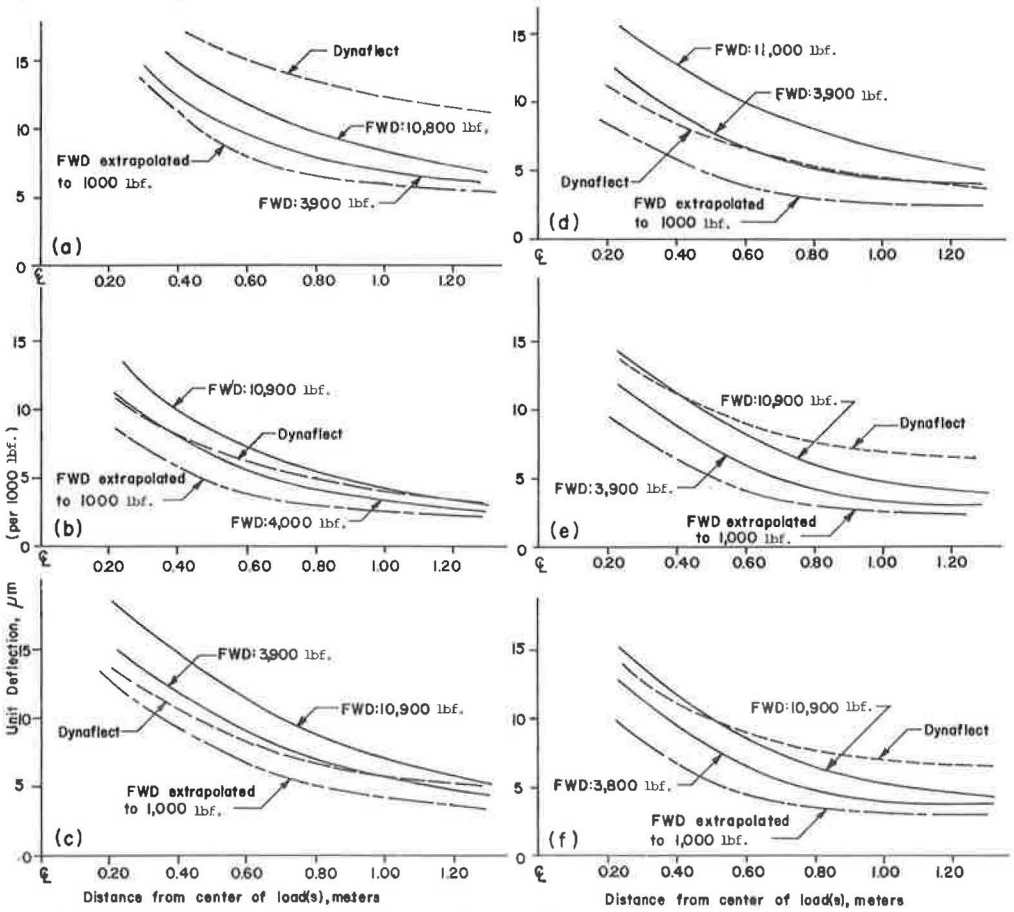

Note: Sections from I-75 northbound, outer wheel path, at Alachua, as follows: (a) FWD station 9.0 (extra-thickness test section), longitudinal cracking under plate; (b) FWD station 10c, longitudinal cracking under plate (strongest embankment encountered); (c) FWD station 13b, longitudinal and transverse cracking under plate; (d) FWD station 13c, no cracking under plate, longitudinal cracking; (e) FWD station 14b, longitudinal cracking 50 mm (2 in) from plate; (f) FWD station 14b + 40 ft (12 m), longitudinal cracking under plate.

Figure 7. Stiffness values for four layers as a function of distance from FWD-ISSEM4 analysis.

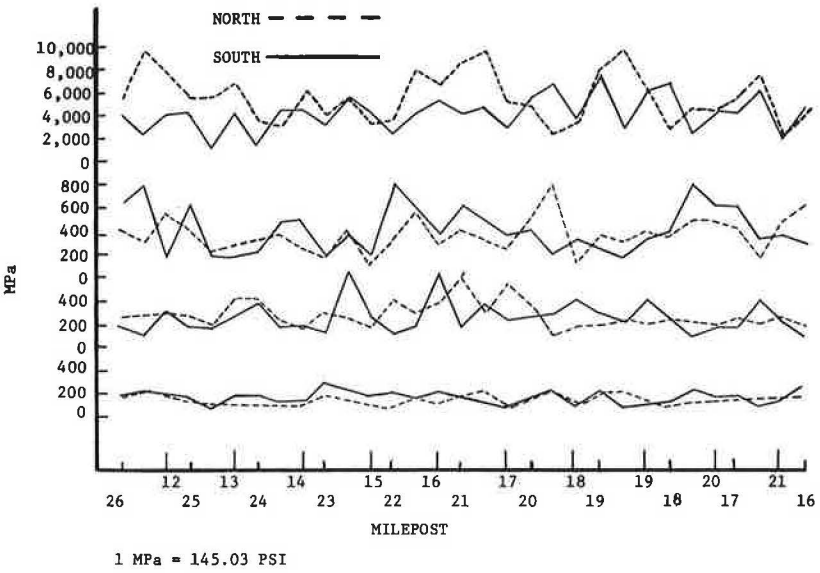

Table 1. Observed surface cracking for 24 test sections at Chiefland, Florida.

Section	Cracking (%/1000 ft²) 50-mm AC Layer	Cracking (%/1000 ft²) 75-mm AC Layer	Limerock Base Thickness (mm)	Subbase LBR[a]	Subgrade LBR
1B, 1A	0	0	225	32	18
10B, 10A	4	49	150	55	18
11B, 11A	8	33	225	18	18
12A, 12B	1	90	300	32	18
2A, 2B	1	0	300	55	18
3B, 3A	3	1	150	32	18
4B, 4A	6	7	300	18	18
5A, 5B	3	112	150	55	18
6B, 6A	5	118	225	32	18
7A, 7B	7	93	300	18	18
8B, 8A	139	28	150	18	18
9A, 9B	1	28	225	55	18

Note: 1 mm = 0.04 in; 1 ft² = 0.09 m².
[a]LBR = limerock bearing ratio.

At this time it is not exactly clear why this happens or which factors are causing these differences. However, stress sensitivity does not appear to be the only factor.

USE OF FWD-DERIVED STRUCTURAL PARAMETERS

The derived FWD E-values (centerline) are plotted for part of the roadway tested (Figure 7). It can be seen here that the embankment subgrade is fairly uniform; there is a subgrade surface stiffness of about 200 MPa (29 000 lbf/in²) under the maximum FWD load of 50 kN (≈11 000 lbf) imposed at the surface of the pavement. Both directions of traffic were tested independently and plotted so that the longtitudinal locations of points match up. A significant correlation between trends in $E_{0.4}$ for both directions may be shown, which indicates that this procedure is able to detect variations in E-values that are caused by moisture content or suction variations as a function of the natural landscape and geophysical conditions.

The E_1 (asphalt) values correlate well with the magnitude of cracking; low values generally had class 2 fatigue cracking, and high values had either class 1 or no cracking. In some cases, the E_1-value was high in spite of class 2 surface cracking that was associated with non-load-associated cracking. In those cases, cores revealed that the cracks appeared to extend only about 25 mm (1 in) downward from the surface.

CONCLUSIONS

Determining in situ elastic moduli from FWD deflections by using the ISSEM4 program is of great significance and interest to the highway designer from several viewpoints:

1. The need for triaxial testing, which is required in the procedures developed by Austin Research Engineers (9) or Resource International (10), would be eliminated. For triaxial testing one has to use destructive techniques, obtain enough laboratory samples, and recompact the specimens for testing. In Florida, limerock material is widely used, and our experience and a considerable amount of testing during the past 15 years have shown that limerock gains strength with time. Plate-bearing E-values have often increased by 100 percent after construction. During the recompaction and testing for triaxial tests, we feel that the added stiffness due to cementing action is not taken into account; hence the idea of extensive destruction testing that has been suggested by other researchers becomes fruitless.
2. It is imperative that we begin to shift our design technique from purely empirically based models (AASHTO) to mechanistically based models that may help explain several distress phenomena such as the one illustrated in Table 1. In this table, the magnitude of the cracking--percentage/1000 ft² [percentage/90 m²]--is shown for sections with 50 mm (2 in) and 75 mm (3 in) of asphalt concrete over 150, 225, and 300 mm (6, 9, and 12 in) of limerock base, and 300 mm of three different strengths of subbase. It is clear that in 90 percent of the cases, the 50-mm sections have cracking that is less than or equal to that of the 75-mm sections, contrary to what the AASHTO model would predict. Such phenomena can only be explained by a critical stress-and-strain type of analysis and, as can be shown for a given stiffness, the tensile strains at the bottom of asphalt concrete are higher for 75 mm than for 50 mm; hence the cracking is greater (Figure 8).
3. Once we know the proper E-values of all the layers and can attribute the variations in E-values to the known causal variables, it will help the designer to make better decisions about choice of rehabilitation alternatives, which may extend from doing nothing to resurfacing or recycling or both. The designer can then calibrate the fatigue and rut-depth criteria by knowing the history of traffic on the facility and by incorporating the stiffness values in the

Figure 8. Tensile strain at the bottom of the asphalt-concrete layer as a function of thickness.

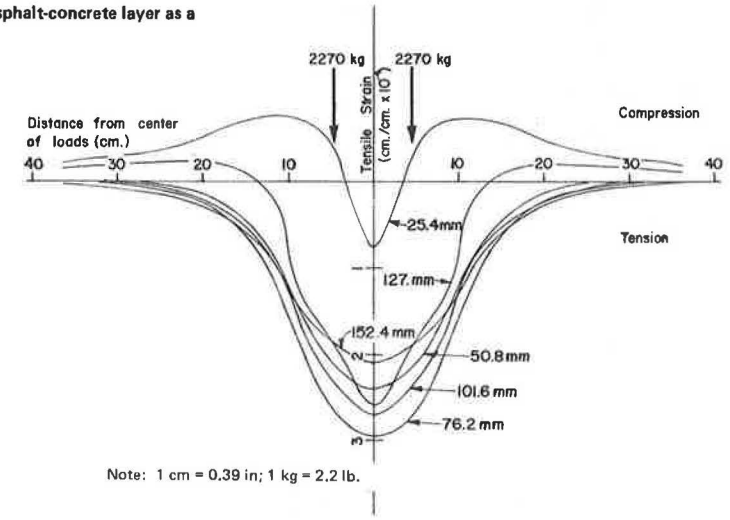

Note: 1 cm = 0.39 in; 1 kg = 2.2 lb.

known pavement-design models like PDMAP and VESYS. Once the model has been calibrated at that location of the roadway, the designer can calculate a thickness of overlay or recommend recycling with a greater degree of certainty.

ACKNOWLEDGMENT

This study was conducted at the Office of Materials and Research of the Florida Department of Transportation. Our special thanks go to P.E. Carpenter of the Federal Highway Administration for approving the funding of the project through preliminary engineering funds. We also wish to thank Dick Wheeler and Jerry Moxley, who carried out the entire testing program; Gary Fitzpatrick and Frank Sullivan, who helped us in reducing data, doing computer analyses, and drafting figures; and C.F. Potts and L.L. Smith for technical assistance. Dynatest Consulting, Inc., of California was retained by FDOT to furnish the falling-weight deflectometer and associated equipment, to coordinate and establish the testing program, and to initiate the ISSEM4 computer program. To this end, the Engineering Systems Design Section of FDOT furnished Fortran programming assistance in order to optimize the basic ISSEM system for wide-scale use. Warren Clary was responsible for this work, without which this project would not have been possible.

REFERENCES

1. A. A. Bohn, P. Ullidtz, R. Stubstad, and A. Sorensen. Danish Experiments with the French Falling Weight Deflectometer. Proc., 3rd International Conference on the Structural Design of Asphalt Pavements, London, 1972, Vol. 1, pp. 1119-1128.
2. A. Claessen, C. Valkering, and R. Ditmarsch. Pavement Evaluation with the Falling Weight Deflectometer. Proc., AAPT, Vol. 45, 1975.
3. A. Claessen and R. Ditmarsch. Pavement Evaluation and Overlay Design--The Shell Method. Proc., 4th International Conference on the Structural Design of Asphalt Pavements, Univ. of Michigan, Ann Arbor, 1977.
4. P. Ullidtz. The Use of Dynamic Plate Loading Tests in Design of Overlays. Presented at Conference on Road Engineering in Asia and Australasia, Kuala Lumpur, 1973.
5. C. Busch and P. Ullidtz. Laboratory Testing of a Full-Scale Pavement. Tech. Univ. of Denmark, Lyngby, IVTB Rept. 19, 1978.
6. P. Ullidtz. Overlay and Stage-by-Stage Design. Proc., 4th International Conference on the Structural Design of Asphalt Pavements, Univ. of Michigan, Ann Arbor, 1977.
7. G. Ahlborn. Elastic-Layered System with Normal Loads. Institution of Transportation and Traffic Engineering, Univ. of California, Berkeley, 1972.
8. R. Stubstad and J. Sharma. Deriving Mechanistic Properties of Pavements from Surface Deflections. Presented at International Conference on Computer Applications in Civil Engineering, Roorkee, India, 1979.
9. Austin Research Engineers, Inc. Asphalt Concrete Overlays of Flexible Pavements. Federal Highway Administration, June 1975.
10. Resource International, Inc. Development of an Overlay Design Procedure Based on Dynaflect Deflections. Federal Highway Administration, Oct. 1979.

Publication of this paper sponsored by Committee on Pavement Condition Evaluation.

Reinforcement of Transportation Support Systems Through Fabric Prestressing

LUTFI RAAD

This paper investigates the mechanism of fabric reinforcement of transportation support systems in which significant rutting during the service life of the system is unacceptable, in particular, the concept of fabric prestressing. An analysis is used that incorporates the finite-element method, the nonlinear stress-strain properties of granular and subgrade soils, and stiffness (i.e., tension modulus), creep, and frictional properties of the fabric. Results of such an analysis performed on a two-layer system that consists of a granular base over a soft-clay subgrade indicate that prestressed fabrics would reduce resilient deformations or vertical stresses in the subgrade. Fabric prestressing can be applied to improve the shear strength and load-deformation behavior of granular layers in transportation support systems. The allowable prestressing tension in the fabric is limited by fabric slippage relative to adjacent soil layers or passive failure in the granular layer. Although more experimental work is required to verify analytical predictions of the beneficial effects of fabric prestressing, it appears that this concept will improve the performance of transportation support systems under applied traffic loads.

Engineering fabrics (i.e., geotextiles) have been used to improve the performance of transportation support systems under repeated traffic loads. Although a fabric could act as a separation medium between the subgrade soil and the granular layer, it could also improve the load-bearing capacity of the systems. The reinforcing effect of fabrics in high-deformation systems, such as haul roads and temporary-access roads, where significant rutting is acceptable has been demonstrated by many investigators (1,2).

In low-deformation systems such as pavements and railroads, where significant rutting during the service life of the system is unacceptable, fabric prestressing can be applied to enhance structural capacity and improve performance under applied traffic loads. Here the fabric is placed over the subgrade, stretched, and then released after construction of the granular base so that the tension in the fabric helps increase the confinement of the base. Model tests performed by Barvashov and others (3) show that fabric prestressing could reduce surface deflections by as much as 40 percent.

In this paper the mechanisms of fabric reinforcement in low-deformation systems through prestressing will be studied. Analysis that incorporates the finite-element method, the nonlinear stress-strain behavior of subgrade and granular soils, and stiffness, creep, and frictional properties of the fabric will be used.

METHOD OF ANALYSIS

The analytical procedure summarized in the following can be used to investigate the prestressing reinforcement of fabrics in low-deformation systems.

A two-layer system that consists of a granular base over a subgrade is considered in this case. The fabric, which is assumed to have been stretched before placement of the base, is placed at the interface of the subgrade and the granular layers. After construction of the granular base, the applied tension is released and transferred to the soil layers adjacent to the fabric as shear stresses. This mechanism is illustrated in Figure 1.

Consider the forces that act on an element of fabric (dx) of unit width at equilibrium (Figure 2a); then

$$(T + dT) - T = -(\tau_u + \tau_L)dx \quad (1)$$

$$dT/dx = -(\tau_u + \tau_L) = -\tau_r \quad (2)$$

where

τ_u = shear stress at upper interface of fabric,
τ_L = shear stress at lower interface of fabric, and
T = tension in fabric due to prestressing.

If we assume that τ_r varies linearly from zero at the center of the section (because of symmetry) to a maximum of τ_f at the ends of the fabric, as shown in Figure 2b, then for $0 \leq x \leq L$,

$$T = -\int \tau_r dx = -\int \tau_f (x/L)dx \quad (3)$$

If $T = 0$ at $x = L$,

$$T = (\tau_f L/2) - (\tau_f x^2/2L) \quad (4)$$

If T_p is equal to the applied prestressing force,

$$T_p = \tau_f L/2 \quad (5)$$

$$T = T_p[1 - (x^2/L^2)] \quad (6)$$

$$\tau_r = 2T_p x/L^2 \quad (7)$$

The finite-element analysis is used to predict the response of the system that uses prestressed fabric. In the analysis, the prestressing effect for a given prestressing force (T_p) is determined before application of traffic loads. Shear stresses transmitted by the fabric to adjacent soil layers are replaced by equivalent nodal forces that act at the interface of these layers. The magnitude of each nodal force is determined by using Equation 7. The hyperbolic stress-strain model suggested by Duncan and Chang (4) is used to define the constitutive relation for the granular and subgrade layers. The load is applied in increments, and a tangential modulus (E_t) and Poisson's ratio (ν_t) for each increment are given by

$$E_t = K\bar{P}(\sigma_3/\bar{P})^{\beta}\left[1 - \{[R_f(1 - \sin\phi)(\sigma_1 - \sigma_3)]/(2c\cos\phi + 2\sigma_3\sin\phi)\}\right]^2 \quad (8)$$

$$\nu_t = \frac{G - F\log(\sigma_3 - \bar{P})}{\left[1 - \left\{\frac{d(\sigma_1 - \sigma_3)}{K\bar{P}(\sigma_3/\bar{P})^{\beta}\left[1 - \frac{R_f(1 - \sin\phi)(\sigma_1 - \sigma_3)}{2c\cos\phi + 2\sigma_3\sin\phi}\right]}\right\}\right]^2} \quad (9)$$

where

β, K, G, R_f, F, d = material constants,
c, ϕ = total stress parameters corresponding to cohesion and angle of friction, respectively,
$\bar{P}$ = atmospheric pressure, and
σ_1, σ_3 = major and minor principal stresses, respectively.

Stresses induced by fabric prestressing are then used as initial stresses to predict the response of the system under repeated loads. The stress-deformation characteristics of base and subgrade in this case are expressed in terms of the resilient modulus (M_R), which is defined as the ratio of repeated deviator stress ($\sigma_1 - \sigma_3$) to the recoverable strain.

For granular soils (5),

$$M_R = k(\theta)^n \quad (10)$$

Figure 1. Mechanism of fabric prestressing.

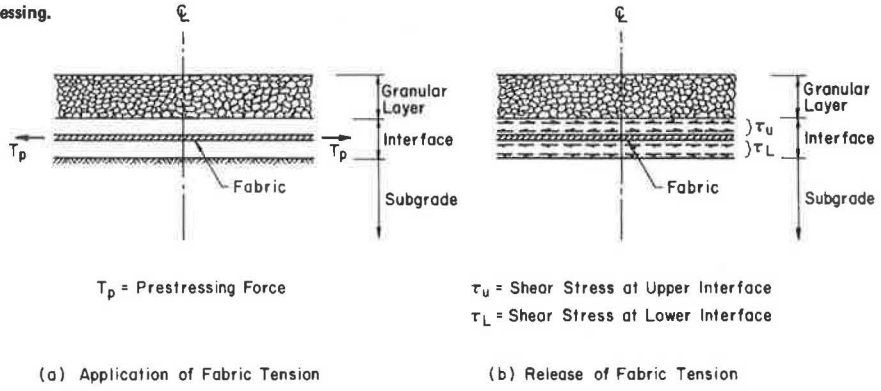

Figure 2. Shear and tensile forces that act on prestressed fabric.

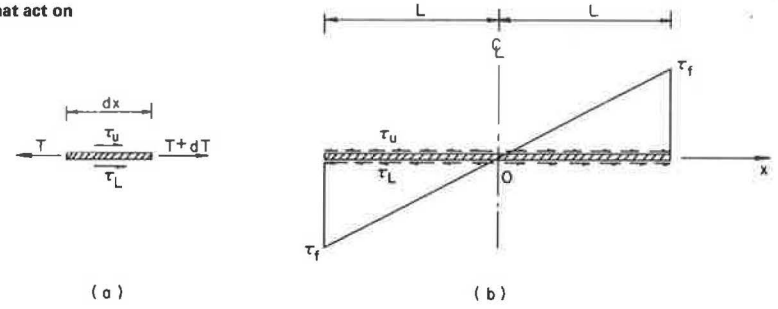

where

k, n = material constants,
$\theta = \sigma_1 + \sigma_2 + \sigma_3$, and
$\sigma_1, \sigma_2, \sigma_3$ = principal stresses.

For fine-grained soils (6),

$$M_R = K_2 - K_3 [K_1 - (\sigma_1 - \sigma_3)] \quad K_1 > (\sigma_1 - \sigma_3) \tag{11a}$$

$$M_R = K_2 + K_4 [(\sigma_1 - \sigma_3) - K_1] \quad K_1 < (\sigma_1 - \sigma_3) \tag{11b}$$

where K_1, K_2, K_3, and K_4 are material constants. K_3 and K_4 are equal to the rate of change of M_R with repeated deviator stress.

The base and subgrade are divided into sublayers, and the system is discretized into a set of elements that are connected at their joints or nodal points. A modulus of elasticity in compression is determined for each sublayer from Equations 10, 11a, and 11b. The granular and subgrade soils are assumed to be unable to accommodate tensile stresses and are therefore assigned low values of modulus in tension. The fabric is modeled as a series of truss elements that can carry tension but not compression. Plane strain conditions are assumed in the analysis. An iterative technique is used by which the load is applied in one increment and the modulus in compression is used for all elements on the first iteration. On successive iterations, the state of stress at the center of each sublayer is used to calculate a new modulus in compression and the modulus in tension is substituted in directions of principal tension. Three or four iterations are usually sufficient to attain a reasonable degree of convergence.

LIMITING CRITERIA

The maximum fabric prestressing force (T_p) corresponds to the tensile force that could be retained by the fabric if it did not slip relative to the base and subgrade or induce passive failure in the granular layer.

Slippage of fabric is assumed to occur when the maximum shear stress (τ_f) that acts on the fabric exceeds the frictional resistance between the fabric and adjacent soil layers, i.e.,

$$\tau_f > \sigma_v \tan\delta + \alpha c \tag{12}$$

where

σ_v = overburden pressure on fabric,
δ = angle of friction between fabric and granular layer,
α = adhesion factor between fabric and subgrade, and
c = cohesion of subgrade soil.

On the other hand, passive failure in the granular base would occur when

$$\sigma_1 = \sigma_3 \tan^2 [45 + (\phi/2)] \tag{13}$$

where σ_1 and σ_3 are major and minor principal stresses, respectively, induced by the prestressed fabric.

The beneficial effects obtained are maintained as long as the fabric is capable of retaining the tensile force applied during prestressing. Since fabrics in general exhibit creep behavior under sustained loads, it is possible that they cannot retain the prestressing force after a certain time. Results of creep test published by Kinney (1) show that the tested fabrics could retain 67 percent of the initial tension for loading periods greater than 30 min. Based on these results, a creep factor (C_f) can be defined such that

$$T_f C_f = T_p \tag{14}$$

where T_f = initially applied fabric tension and T_p = prestressing force retained by fabric.

The prestressing effect of the fabric is a function of T_p. For a given system, higher values of T_p can be attained if frictional properties of the fabric relative to adjacent soil layers are improved. However, if the value of T_p is limited by the passive failure in the granular base, further improvement of frictional properties will not increase the allowable value of T_p.

Figure 3. Finite-element representation of sample problem.

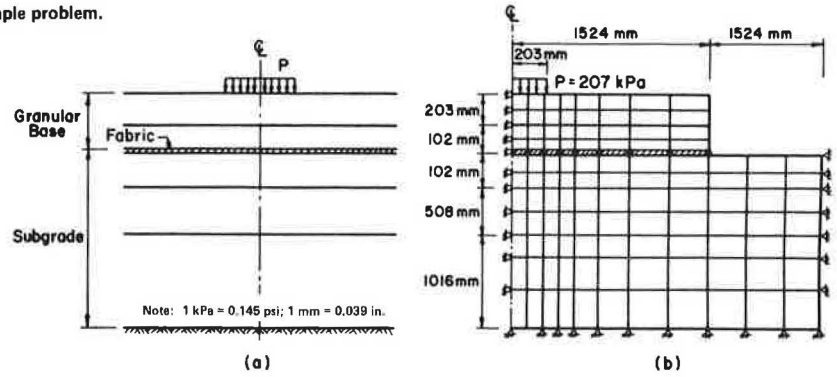

Table 1. Material properties used in finite-element analysis.

Soil Properties Under Static Loading			Soil Properties Under Repeated Loading		
Parameter	Soft-Clay Subgrade	Granular Base	Soft-Clay Subgrade (MPa)	Granular Base	Fabric Properties
β	0	0.30	K_1 = 0.041	k = 876	t_f = 0.63 mm
K	200	3000	K_2 = 41.3	n = 0.65	E_f = 207 MPa
R_f	0.90	0.70	K_3 = 1170		$\delta = 45°$
F	0.10	0.10	K_4 = -143		α = 0.40
G	0.35	0.20			C_f = 0.67
d	5.0	6.40			T_p = 13.2 kN/m
c (MPa)	0.069	0			
ϕ (°)	0	45			
P (MPa)	0.10	0.10			
γ (kN/m^3)	15.8	20.4			
K_0	0.5	0.5			

Notes: 1 MPa = 145 psi; 1 kN/m^3 = 6.37 lbf/ft^3; 1 mm = 0.039 in; 1 kN/m = 0.69 lbf/ft. γ = density; K_0 = coefficient of at-rest pressure; E_f = fabric stiffness; t_f = fabric thickness.

Figure 4. Response of two-layer system under repeated loads.

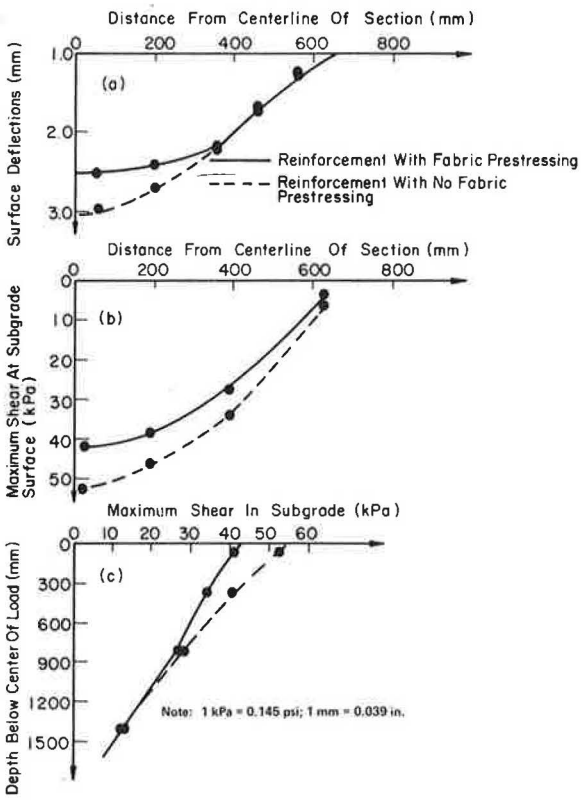

SAMPLE PROBLEM

The analytical procedure that has been presented is applied to investigate the reinforcing effect of a two-layer system that consists of a granular base over a soft-clay subgrade, as shown in Figure 3. Material properties are summarized in Table 1.

Results of the analysis (Figure 4) indicate that fabric prestressing would reduce resilient surface deflections and maximum shear stresses in the subgrade. Consequently, it will improve the performance of the system under applied traffic loads.

CONCLUSION

The mechanism of fabric prestressing in low-deformation systems has been studied by using the finite-element method of analysis. Fabric prestressing seems to increase the confining stresses in granular layers; their shear-strength and load-deformation characteristics are thereby improved. The maximum allowable prestressing tension is limited by fabric slippage relative to adjacent soil layers or passive failure in the granular layer. Additional experimental work is required to verify analytical predictions of the beneficial effects of fabric prestressing.

REFERENCES

1. T. C. Kinney. Fabric-Induced Changes in High-Deformation Soil-Fabric-Aggregate Systems. Univ. of Illinois at Urbana-Champaign, Ph. D. dissertation, 1978.
2. D. A. Bender and E. J. Barenberg. Design and Behavior of Soil-Fabric-Aggregate Systems. TRB, Transportation Research Record 671, 1978, pp. 64-75.
3. V. A. Barvashov and others. Deformations of Soil Foundation Reinforced with Prestressed Synthetic Fabrics. Proc., International Conference on the Use of Fabrics in Geotechnics, Volume 1, Paris, April 20-22, 1977.
4. J. M. Duncan and C. Y. Chang. Nonlinear Analysis of Stress and Strain in Soils. Proc., ASCE, Vol. 96, No. SM5, Sept. 1970.
5. J. J. Allen. The Effects of Non-Constant Lateral Pressures on the Resilient Response of Granular Materials. Univ. of Illinois at Urbana-Champaign, Ph. D. dissertation, 1973.
6. M. R. Thompson and Q. L. Robnett. Resilient Properties of Subgrade Soils. Transportation Engineering Journal, ASCE, Vol. 105, No. TE1, Jan. 1979, pp. 71-89.

Publication of this paper sponsored by Committee on Strength and Deformation Characteristics of Pavement Sections.